Aus der Klinik und Poliklinik für Neurochirurgie
Klinikum der Universität München Ludwig-Maximilians-Universität München

DISSERTATION

Cannabidiol for glioblastoma therapy: models, molecular pathways, and predictive markers

Zum Erwerb des Doctor of Philosophy (PhD) in medical research
an der Medizinischen Fakultät der Ludwig-Maximilians-Universität zu München

vorgelegt von
Marie Nhery Murielle Volmar

aus
Port-au-Prince, Haïti

am
10/04/2019

Supervisor:	Prof. Dr. rer. nat. Rainer Glass
Second expert:	Prof. Dr. rer. nat. Reinhard Zeidler
Dean:	Prof. Dr. med. dent. Reinhard Hickel
Date of oral defense:	15. 10. 2019

Contents

II. Abbreviations

ARE	Antioxidant response element
BSA	Bovine Serum Albumin
β-3 tub.	Class III Beta tubulin
CBD	Cannabidiol
Cdkn2a	Cyclin-dependent Kinase inhibitor 2a
Cl. PARP1	Cleaved Poly (ADP-ribose) polymerase 1
CM	Conditioned medium
CNPase	2',3'-cyclic nucleotide 3'-phosphodiesterase
CRE	Cyclization Recombination Enzyme
DCF	2',7'-dichlorofluorescein
DMEM	Dubelcco's Modified Eagle's Medium
DMEM/F-12	DMEM/Nutrient mixture F-12
DMF	Dimethyl fumarate
DMSO	Dimethyl sulfoxide
DsRed	Discomona sp. Red
E. coli	Escherichia coli
EGF	Epidermal Growth factor
EGFR	Epidermal growth factor Receptor
EGFRvIII	EGFR transcript variant 3
eIF2α	Eukaryotic translation initiation factor 2A
ER	Endoplasmic reticulum
FACS	Fluorescence activated cell sorting
fcs	Flow cytometry standard
FGF	Fibroblast growth factor
FVD	Fixable viability dye
GBM	Glioblastoma
GFP	Green Fluorescent Protein
GFAP	Glial Fibrillary Acidic Protein
hs	Homo Sapiens
H&E	Hematoxylin & Eosin
H2-DCFDA	2',7'- dichlorodihydrofluorescein diacetate
KO	Knock-out
IDH	Isocitrate dehydrogenase
IkB	Inhibitor of kappa B
i.p	Intraperitoneal
LSL	Lox-STOP-Lox
MGMT	O6-methyguanine-DNA methyltransferase
Mm	Mus musculus
MRI	Magnetic resonance imaging
MMP	Mitochondrial membrane potential
Mu/mut	Mutant
Nes	Nestin
NeuN	Neuronal Nuclei
NG2	Neural/Glial antigen 2
NF1	Neurofibromatosis Type1
NSC	Neural stem cell
NFkB	Nuclear factor kappa-light-chain-enhancer of activated B cells
NMR	Nuclear Magnetic Resonance
NPC	Neural stem and precursor cell
NRF2	Nuclear respirator factor 2
NSC	Neural stem cell
PBS	Phosphate Buffered Saline
Pen-Strep	Penicillin-Streptomycin
PFA	Paraformaldehyde
PTEN	Phosphatase and Tensin homolog
PDGFB	Platelet derived growth factor, Beta polypeptide
p65	Transcription factor polypeptide 65 Kda
RCP	Rainbow Calibration Particles
Rel-a	v-rel avian reticuloendotheliosis viral oncogene homolog a
RNA	Ribonucleic acid
ROS	Reactive oxygen species
SOX	Superoxide
SOX2	Sex-determining region Y-box2
SVZ	Subventricular zone
TDP-43	TAR DNA-binding protein 43
TF	Transcription factor
TMZ	Temozolomide
TNF-α	Tumor Necrosis Factor alpha
TNFR	TNF-α receptor
TP53	Tumor protein 53
Wt	Wild-Type
ZsGreen1	Zoanthus sp. Green fluorescent protein 1

1. Introduction

1.1. Adult subventricular zone and neural stem and precursor cells

In adulthood, pools of neural stem cells persist in at least two brain regions: the sub-granular zone (SGZ) of the hippocampus and the sub-ventricular zone (SVZ) of the lateral ventricles. The SVZ is extensively investigated for the understanding of neurogenesis [Llorens-Bobadilla E., et al. (2017)] and its implications in hyperproliferative diseases such as brain tumors [Gollapalli K., et al. (2017)]. Indeed, Neural stem cells (NSCs) maintain their self-renewal capacity along with the ability to differentiate into neuronal and glial precursors depending on microenvironmental signals. In the developing brain, these precursors cells can give rise to neurons, astrocytes, and oligodendrocytes [Bergström T., et al. (2012)]. Neurons are the key impulse generating and propagating brain cells. They classically, arise from asymmetric division of NSCs, followed by lineage commitment through several stages of differentiation. Other possible sources, such as reprogramming of astrocytes, have also been described [Pino A. et al. (2017)]. Astrocytes are star-shaped components of the central nervous system (CNS) that represent about 50% of all brain cells. They participate in homeostatic distribution and clearance of metabolites [Villa G.R. et al., (2016)] and [Dossi, E. et al. (2017)], and control exchange at the blood brain barrier. In collaboration with Schwann cells and astrocytes, oligodendrocytes synthesize and integrate large amounts of lipids necessary to generate the myelin sheath of axons without which rapid propagation of neuronal impulses could not be carried out [Camargo N. et al. (2017)] and [Hofmann K. et al. (2017)]. In the adult CNS, small pools of NSCs are perpetuated. Under physiological and pathological conditions, they maintain neurogenic functions but also regulate brain homeostasis, express phagocytic functions towards microglia, and sense and dampen inflammatory signals [Martino G., et al. (2014)].

1.2. Cells of origin of gliomas

Neural stem and precursor cells guarantee a backup pool of new neuronal and astroglial cells in the brain. Their function is capital to maintain CNS plasticity and rescue from potential neurodegenerative threats [Yamaguchi M. et al. (2016)]. However, failure to tightly control the mechanisms of their proliferation and/or differentiation can lead to accumulation of genetic alterations that promote malignant transformation and initiate glioma development. Gliomas and glioblastoma maintain many stem cell characteristics and a hypothesis of glioblastoma-cancer stem cell (GBM-CSC) has been proposed [Yuan X. et al. (2004)]. Pools of GBM-CSC share embryonic and NPC stem cell markers such as nestin, sex determining region Y-box2 (SOX2), Krüppel-like factor 4 (KLF-4), myelocytomatosis cellular oncogene (c-Myc), CD44, CD133, and the astrocytic marker Glial fibrillary acidic protein (GFAP). Inhibition or silencing of these genes has shown positive effects against GBM growth *in vitro* and *in vivo* [Bradshaw A. et al. (2016)]. The role of GBM-CSC (GSCs) is actively being investigated for therapeutic purposes to understand the genesis and maintenance of GBM aggressiveness and its resistance to therapy. Upon therapy, pools of GSCs may alter gene expression levels and metabolic features not targeted by an initial treatment. After therapy schedule, non-drug-sensitized cells, could generate new populations of GBM resistant to standard therapy [Liebelt B. D. et al. (2016)].

1.3. Glioblastoma: clinical presentation and diagnostics

1.3.1. Clinical presentation of glioblastoma

Patients with glioblastoma present a variety of neurological symptoms ranging from headache, nausea, vomiting, dizziness, seizures. The presented symptoms vary according to the location of the glioblastoma and the neurological centers that might be affected. [Hanif F. et al. (2017)].

1.3.2. Diagnosing glioblastoma

Often, glioblastoma is diagnosed after the detection of the first neurological symptoms. The diagnosis of glioblastoma is a multi-step process. Neurological examination, brain imaging and biopsy are performed to confirm brain neoplasms. Multiple imaging techniques are available to diagnose glioblastoma. They include but are not limited to gadolinium-enhanced MRI, magnetic resonance spectroscopy, functional magnetic resonance imaging, FDG-PET [Szopa W. et al (2017)]. After diagnosis, multi-disciplinary decision will be taken for the coordination of maximal surgical resection and the schedule of chemo-radiotherapy. Many of the diagnostic techniques, such as functional fMRI and FDG-PET are also used to monitor the outcome of therapy on the GBM [Louis D. N. et al. (2016)].

1.4. Genetic diversity of glioblastoma

Glioblastoma present multiple genetic alterations and have been classified into different subtypes: proneural, classical, mesenchymal [Brennan C. et al. (2013)] and [Figure 1.1]. Primary glioblastoma generally arises without an identified pre-existent lesion. A first level of classification is based on the isocitrate dehydrogenate (IDH) status segregating between IDH^{wt} and IDH^{mu} GBMs [Olar A. et al. (2014)] and [Louis D. N. et al. (2016)]. Heterogeneity of glioblastoma has always been a concern in the handling of patients and it has been associated with therapy failure and GBM recurrence. Inter-tumoral heterogeneity exists when comparing GBM in young (less than 18 years old) to older patients (more than 45 years old). Alterations in tumor protein 53 (TP53), platelet derived growth factor receptor alpha (PDGFRA), v-RAF murine sarcoma viral oncogene homolog B (BRAF) tended to be dominant in young patients whereas in older patients more frequent alterations were found in O (6)-methylguanine-DNA methyltransferase (MGMT) methylation status and phosphatase and tensin homolog (PTEN) [Ferguson S. D. et al. (2016)]. On top of this first level of heterogeneity, coexists a second level of intra-tumoral heterogeneity. For gliomas, intra-tumoral heterogeneity is associated with poor clinical outcome [Andor N. et al. (2016)]. Indeed, clones of a same tumor showing different genetic alterations can also show differential sensitivity to drug treatment and trigger resistance to therapy [Meyer M. et al. (2015)]. GBM intra-tumoral heterogeneity is not a fixed stage of the tumor as it evolves under therapy and phenomena of genetic subtype switches are commonly described along with some driver genes experiencing switches in codon point mutations of a same protein encoded gene such as epidermal growth factor receptor (EGFR), PDGFRA, TP53 [Wang J. et al. (2016)].

GBM subtype	Loss/mutation	Overexpression
Proneural	$IDH1_{(30\%)}$,$PTEN_{(16\%)}$,cdkn2a, $TP53_{(54\%)}$	MYC,$PDGFR_{(11\%)}$,cdk4
Classical	Cdkn2a	EGFR/EGFRvIII,CCNE1
Mesenchymal	$NF1_{(37\%)}$, $TP53_{(32\%)}$,$PTEN_{(32\%)}$	EGFR

Figure 1.1 Genetic diversity of glioblastoma. GBMs are classified into three main genetic subtypes based on the loss or mutation of tumor suppressors and overexpression of oncogenes. The most common proneural GBMs often have loss or mutation in TP53 or cdkn2a, associated with overexpression of PDGFR. EGFR is one of the most amplified genes. 57% of GBMs show rearrangements, alternative splicing, mutation, or amplification in EGFR, associated with homozygous deletion of cdkn2a (Classical GBM) or dual

loss/mutation in TP53-PTEN (Mesenchymal GBMs). Another group of mesenchymal GBMs is enriched in concomitant alterations in NF1 and TP53. Adapted from [Brennan C. et al. (2013)].

1.5. The brain tumor microenvironment

GBMs are highly proliferative tumors that need a supportive microenvironment. Therefore, GBMs secrete factors that can modify and re-program surrounding brain cells [Treps L. et al. (2017)]. Microglia, which are resident brain macrophages, represent 5 to 20% of the total glial cells [Zhou W. et al. (2014)] and can account for up to 30% of the tumor mass. However, they are de-programmed from their M1-polarization and re-programmed to be M2-polarized [Arcuri C. et al. (2017)]. This functional phenotype is characterized by a panel of immunosuppressive/tumor-promotive cytokines (IL4, IL10, IL13) and decreased MHC-II expression leading to poor tumor antigen-presentation to dendritic cells [Gieryng A. et al. (2017)]. Tumor secreted reactive oxygen species (ROS) induce increased nuclear respiratory factor 2 (NRF2) expression in tumor associated dendritic cells leading to lack of maturation and impaired antigen presentation [Wang J. et al. (2017)]. Nuclear factor kappa-light-chain-enhancer of activated B cells (NFkB), which balances NRF2 responses, is also altered in myeloid derived suppressor cells (MDSCs). In the micro-milieu of GBMs, canonical NFkB signaling of p50-p65, has been shown to be anti-inflammatory in MDSCs, and knocking out p65 in myeloid cells resulted in increased secretion of proinflammatory cytokines (IFNγ, TNFα), Th1 polarization, and proliferation of CD8+ cytotoxic T cells [Achyut B. R. et al. (2017)]. Astrocytes are particularly enriched around GBM masses, where they secrete interleukin 6 (IL6), increase matrix metalloproteinase 14 (MMP14), and contribute to glioma migration [Chen et al. (2016)]. Knocking down connexin 43 in reactive astrocytes abolishes channel communication between GBM and astrocytes and significantly reduced GBM invasion in a syngeneic model of GL261 glioma [Sin W. C. et al (2016)].

1.6. Glioblastoma metabolism

1.6.1. “Non-oncogene addiction” in cancer

It is well accepted that oncogenesis occurs by progressive accumulation of a range of genetic alterations inducing hyperactivation of oncogenes often accompanied by inactivation of tumor suppressors [Tsatsanis C. et al. (2000)]. During these genetic changes, cells transitioning to a malignant lesion also experience changes in their metabolism to adapt to various levels of stress. Therefore, genetic, and epigenetic changes in genes not inherently tumorigenic also occur [Vivanco I. (2014)]. These modifications are defined as non-oncogene addiction, where growing tumor cells learn to control metabolic pathways promoting their survival: Stress response transcription factors and their pathways, metabolite uptake, drug efflux, inhibition of death pathways [Nagel R. et al. (2016)].

1.6.2. Oxidative stress in glioblastoma

High proliferative and metabolic rates in glioblastoma require increased mobilization of all cellular compartments especially those involved in energy production, *de novo* protein synthesis, and catabolism. Metabolic pathway by-products accumulate in the form of reactive oxygen and nitrogen species (ROS/NOS) [Salazar-Ramiro A. et al. (2016)]. Sites of ROS generation include mitochondria (mt), endoplasmic reticulum (ER), and peroxisomes [Holzerová E. et al. (2015)]. GBM-mitochondria preferentially generate adenosine triphosphate (ATP) using glycolysis over oxidative phosphorylation [Agnihotri S. et al. (2016)]. Modifications in the electron transport chain contribute to increased mitochondrial oxidative stress. One of the most important by-products of mitochondrial ATP production is ROS [Tan Q. et al. (2017)]. Increased

GBM metabolism requires increased protein synthesis and folding by the endoplasmic reticulum (ER). ER activity generates ROS itself, and in the context of heavy mitochondrial ROS and Ca^{2+}, the ER faces exhaustion, and proper protein folding cannot be guaranteed [Sevier C. S. et al. (2008)]. This state of exhaustion is called ER stress and, in an effort to restore ER homeostasis, the unfolded protein response of the ER (UPR^{ER}) is engaged [Bhat T. A. et al. (2017)] and [Hempel N. et al. (2017)]. Depending on the nature of the stressor, its duration, and the timing of expression of sensor proteins, the UPR^{ER} can promote survival or death. Under ER stress, ER-resident nuclear respiratory factor 1 (NRF1) translocates to the nucleus and directs the expression of proteins of proteolytic cascades and antioxidant responses [Peñaranda Fajardo N. M. et al 2016)] and [Lindholm D. et al. (2017)]. As mitochondrial DNA (mtDNA) only encodes 1% of mitochondrial proteins, alterations in ER-dependent protein folding during ER stress directly impact proteins destined to mitochondria. As in the ER, mtDNA encoded-proteins are subjected to quality control by mitochondrial chaperones [Raza M. H. et al. (2017)]. Sustained oxidative stress, mtDNA damage and increased misfolded proteins induce mitochondrial unfolded protein response (UPR^{mt}) and mitochondrial retrograde signaling to the nucleus to mobilize the expression of quality control genes [Kenny T. C. et al. (2017)]. UPR^{mt} is directly linked to UPR^{ER} as most of the requested quality control proteins are also ER stress dependent transcription factors such as activating transcription factor 5 (ATF5) and C/EBP homologous protein (CHOP) [Qureshi M. A. et al. (2017)]. Chronic and unbalanced ROS exposes to genetic and epigenetic alterations such as DNA damage, oxidation of lipids and proteins, all leading to the state called oxidative stress, where, oxidant-induced modifications alter the homeostatic function of cellular organelles and affect multiple networks. Targets of ROS include key signaling pathways such as Kelch-like ECH-associated protein1 (Keap1) / Nuclear factor erythroid 2-related factor 2 (NRF2), nuclear factor kappa-light-chain-enhancer of activated B cells (NFkB), mitogen activated protein kinase (MAPK), phosphatidylinositol-4,5-bisphosphate 3 kinase (PI3K) / protein kinase B (AKT). ROS also interfere with ion homeostasis and thus impact multiple cellular reactions they run including receptor transporter functions in endo- and exocytosis [Zhang J. et al. (2016)] and [Prasad S. et al (2017)].

1.7. Antioxidant responses in GBM

In cancer cells and glioblastoma, ROS levels have been described as high, and cellular antioxidant systems are mobilized but ineffective [Moloney J. N. et al. (2017)]. The master regulator of cellular antioxidant responses is NRF2 [Rinaldi M. et al. (2016)]. Under physiological conditions, NRF2 is mostly in the cytoplasm, where it is sequestered by Keap1 and regularly ubiquitinylated for proteasomal degradation [Zhu J. et al. (2014)]. Sustained oxidative insults induce NRF2 phosphorylation and its nuclear translocation where it binds ARE-DNA sequences to modulate the expression of antioxidant effectors and detoxification enzymes [Suzuki T., et al. (2017)]. However, in cancer cells, homeostatic regulation of ROS by NRF2 is disrupted. Indeed, oxidative stress repurposed proteins destabilize the Keap1-NRF2 complex either by competing with Keap1 for binding with NRF2 (p21) or competing with NRF2 for binding with Keap1 (p62, iASPP). Free NRF2 translocates in the nucleus and constitutively stimulates the transcription of genes encoding for proteins with cytoprotective functions. This explains why high NRF2 activity has been described in several cancers [Ge W. et al. (2017)].

Under physiological conditions, the signaling of NRF2 pathway is balanced by multiple factors including NFkB [Figure 1.3]. NFkB represents a family of transcription factors with 5 subunits: 3 proteins with Rel homology domains Rel-a (p65), Rel-b, c-Rel, and 2 pre-proteins p100 and p105 which are cleaved to generate p50 and p52. These subunits form homo- and heterodimers, with the most common form being p50-p65 [Zhang Q. et al. (2017)]. In many cancers and in glioblastoma, NFkB is highly expressed and described as pro-inflammatory and pro-proliferative with the capacity to reprogram multiple cellular pathways [Cahill K. E. et al. (2016)] and [Friedmann-Morvinski D. et al. (2016)]. In GBMs, NFkB signaling

is modulated by multiple tumor associated proto-oncogenes and regulates major pathways promoting GBM survival by inhibiting Notch signaling, increasing B-cell lymphoma extra-large (Bcl-xL) and survivin, promoting angiogenesis and inflammation via pro-inflammatory cytokine secretion [Cahill K. E. et al. (2016)].

1.8. Standard therapy for glioblastoma

Currently, multimodal therapy including surgery, radiotherapy and chemotherapy is the standard of care for glioblastoma patients. If the patient would not withstand a surgical intervention, stereotactic needle biopsy is performed to collect tumor specimens. Otherwise, surgery with craniotomy (standard or awake) is carried out [Hervey-Jumper S. L. et al. (2015)]. Using current imaging techniques, the surgeon can locate the tumor and perform maximal safe resection of the tumor mass [Li Y. M. et al. (2017)]. The extent of resection of GBM has been associated with increased patient survival in multiple studies, thus the importance to use all available tools (iMRI, fMRI, functional mapping…) to maximize tumor removal before chemo-radiotherapy [Brown T. J. et al. (2016)]. Radiotherapy is based on the ability of ionizing radiation to generate double strand breaks in DNA and promote cell death. Currently, common approaches for radiotherapy include, volumetric modulated arc therapy, hypofractionation, and intensity modulated radiotherapy coupled with image-guided radiotherapy. The aim is to deliver beamlets of different intensities to different regions of the tumor mass, while sparing unaffected brain [Aktan M. et al. (2015)] and [Macchia G. et al. (2017)]. More recently, hypofractionation radiation therapy, has gained more interest especially in elderly GBM patients with poor prognosis [Mak K. S. et al. (2017)]. It uses lower irradiation intensities while dividing the radiation schedule. Doing so, normal cells would have time to recover from therapy effects (less side-effects), while irradiated tumor cells that could be escaping radiation induced death, could be re-targeted with another round of radiation [Glaser S. M. et al. (2017] and [Gzell C. et al. (2017)]. Because of better survival outcomes, combination of radiotherapy with adjuvant chemotherapy is the standard of care after surgical resection [Davis M. E. (2016)] and [Kole A. J. et al. (2017)]. Temozolomide (TMZ) is the first-line chemotherapeutics prescribed in GBMs. It is an alkylating molecule introducing methyl groups in nucleic acids guanine (N^7, O^6) and adenine (N^3). These modifications are detected by base excision repair and mismatch repair pathways that will induce cell cycle arrest and try to repair the DNA, but failure of repair will signal to death [Anjum K. et al. (2017)]. While TMZ therapy prolongs the survival of some GBM patients, more than half of them do not respond to the treatment. This is mainly due to hyperactivation of MGMT, which antagonizes TMZ action, by removing TMZ introduced O6-methyl groups on guanines. Indeed, GBM patient survival treated with TMZ, inversely correlates with MGMT activation levels, and methylation of MGMT promoter is considered a favorable biomarker to TMZ therapy [Stupp R. et al. (2005)] and [Taylor J. W. et al. (2015)]. Bevacizumab is usually used as second line of treatment. It is a monoclonal antibody against vascular endothelial growth factor (VEGF), and it acts by blocking VEGF-induced angiogenic cascades that would be triggered in GBMs upon VEGF binding to its receptor (VEGFR) [Wang Y. et al. (2016)]. Bevacizumab is often combined with irinotecan, leading to important reported side-effects (hypertension, anemia, deterioration of liver functions, pulmonary toxicity) [Kim J. H. et al. (2017)]. Since GBMs are highly heterogenous and adaptable tumors, they resist to standard multimodal therapy, re-occur and are ultimately fatal. Development of new therapeutic strategies are urgently needed, targeting genetic and metabolic GBM addictions.

1.9. Vanilloids, cannabinoids and cannabidiol

Vanilloids were first discovered in *capsicum annuum* (chili pepper), a native plant of the Americas domesticated since 7500 B.C. and described in pre-columbian Aztec manuscripts [Perry L. et al. (2007)].

The active ingredient capsaicin was isolated by Tresh in 1846, its chemical structure published in 1919, and the capsaicin induced vanilloid receptor VR1 described by Holzer in 1991. VR1 has been later renamed transient receptor potential vanilloid type 1 receptor (TRPV1) because of its structural similarity with members of the TRP channel superfamily [Nilius B. et al. (2007)]. In 1975, resiniferatoxin (RTX), a potent capsaicin analog, was isolated. Because they share a homo-vanillin group allowing their biological effects, capsaicin, RTX and their analogs are called vanilloids [Szallasi A. et al. (1999)]. Cannabinoids were originally so-called because of their first discovery as components of *cannabis sativa* plant [Figure 1.2]. Today, we understand that cannabinoids include the endocannabinoids (physiologically produced in the CNS), synthetic cannabinoids (chemically produced to mimic cannabinoid effects) and the phytocannabinoids (natural substances mainly from the *cannabis sativa* plant) [Russo E. B. (2016)], [Hanuš L. O. et al. (2016)], and [Turner S. E. et al. (2017)]. Endogenous cannabinoids have been shown to stimulate vanilloid receptors, and vice-versa. This led to the understanding that vanilloid- and cannabinoid receptors are part of a same G protein coupled receptor family [Zygmunt P. M. et al. (1999)]. Delta-9-tetra-hydrocannabinol (Δ9-THC) and cannabidiol (CBD) are the two most studied substances of *cannabis sativa*. To the contrary of Δ9-THC, CBD is a non-psychoactive substance with poor affinity to cannabinoid receptors [Falenski K. W. et al. (2009)]. Phytovanilloids as with endovanilloids are fatty acid-based molecules with capacity to modulate TRPV channels [Starowicz K. et al. (2007)]. CBD, as a lipophilic compound crosses the cellular plasma membrane and accesses a plethora of intracellular targets influencing mitochondrial calcium stores, glycine receptors, fatty amide hydrolase [Zhornitsky S. et al. (2012)]. The high lipophilicity of CBD allows it to cross the blood brain barrier giving it access to targets in the central nervous system [Cabral G. A. et al. (2014)]. Cannabidiol is being considered for the treatment of several disorders including epileptic seizures [Jones N. A. et al. (2010)], multiple sclerosis, chronic pain [Iskedjian M. et al. (2007)] and is an orphan drug for glioblastoma therapy [Dumitru C. A. et al. (2018)].

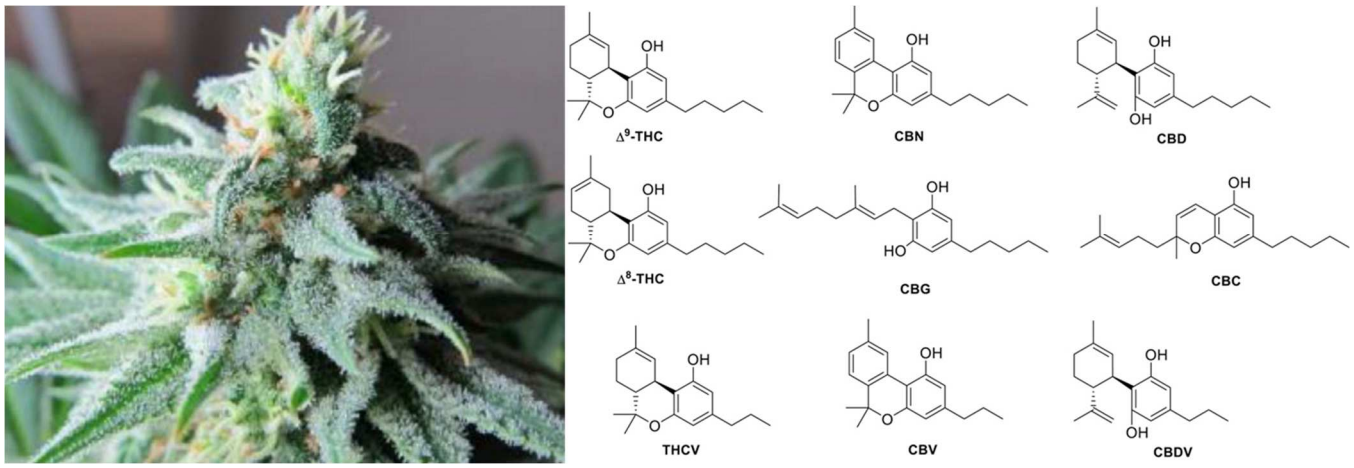

Figure 1.2 Cannabinoids as therapeutic agents. Illustration of the *cannabis sativa L.* plant and the chemical structures of extracts with medicinal interest: Δ^9-tetrahydrocannabinol (Δ^9THC), cannabinol (CBN), cannabidiol (CBD), Δ^8-tetrahydrocannabinol (Δ^8 THC), cannabigerol (CBG), cannabichromene (CBC), tetrahydrocannabivarin (THCV), cannabivarin (CBV), cannabidivarin (CBDV). Adapted from [Russo E. B. (2016)], [Morales P. et al. (2017)].

1.10. Aim of the thesis

Cannabidiol has been reported to have significant cytotoxicity effects in cultured GBM cells [Singer E. et al. (2015)]. Promising *in vitro* and pre-clinical studies have propelled this phyto-therapeutics to clinical trials for the treatment of GBMs [Massi P. et al. (2004)]. However, a reliable patient stratification scheme for beneficial CBD therapy is still missing.
This PhD work aims to study the genetic diversity of human GBM in mouse and uncover potential genetic and metabolic alterations that could be used as predictive biomarkers of CBD sensitivity.

Scientific questions are:

1. Which cell death mode is induced in CBD sensitive GBMs?
2. What is the impact of GBM genetic diversity on CBD induced therapy?
3. Which molecular pathways are triggered in GBMs upon CBD treatment?
4. Can patients be stratified for beneficial CBD therapy?

2. Materials

2.1. Table 2.1 Laboratory equipment.

Name	Cat.No	Company
Autoclave	Dx23/8485333	Systec
Automated cell counter	Countess II FL	Life Technologies
Balance	AG204	Mettler Toledo
Biophotometer	613120751 (8,5mm)	Eppendorf
Cell culture incubator	CB (E6)	Binder
Centrifuge	Multifuge 1S	Heraeus
Dry incubator	Hera hybrid	Heraeus
Flow cytometer	LSR Fortessa	BD
Freezing container, Nalgene® Mr. Frosty	C1562-1EA	Sigma-Nalgene
Fume hood	2-428-N	Kottermann
Inverted microscope	Axiovert25	Zeiss
Laminar flow hood	HeraSafe KS12	Heraeus
Magnetic hot plate stirrer	RCT basic	VWR International
Microtome	Slide 2003	PFM Medical
Microwave	3850WRA011A	Siemens
Perfusion system	Dose-IT P910	Integra Biosciences
pH meter	Multi-cal	WTW
Pipettor Accujet Pro	04L27051	Brandt
PCR machine	Mastercycler Pro S	Eppendorf
Stepper	Multipette-Plus	Eppendorf
Table top centrifuge	5415R	Eppendorf
TECAN plate reader	Infinite F2000 PRO	TECAN
Vortex mixer	12-620-856	VWR
Waterbath	WB14	Memert

2.2. Table 2.2 Consumables.

Name	Cat.No	Company
Bacillol AF	973380	BODE Chemie Gmbh
Bepanthen Augen und Nasensalbe	82290583	Bayer
Cell culture dish (10cm)	4520005	Brand
Cell culture flask, T25	90026	TPP
Cell culture flask, T75	909760	TPP
Cell culture flask, T150	909151	TPP
Cell scraper 240mm, 13mm	99002	TPP
Cell scraper 300mm, 20mm	99003	TPP
Cell strainer 40µm (blue)	352340	BD
Cell strainer 70µm (white)	352350	BD
Cell strainer 100µm (yellow)	352360	BD
Combitips advanced®, 0.1 mL, Biopur®	30089405	Eppendorf
Combitips advanced®, 0.5 mL, Biopur®	30089421	Eppendorf
Combitips advanced®, 1.0 mL, Biopur®	30089642	Eppendorf
Combitips advanced®, 5.0 mL, Biopur®	30089456	Eppendorf
Coverslip 24x50mm	631-0146	Gerhard Menzel
Cryomatrix	6769006	ThermoFischer
Cryomold cassette	4566	Vogel
Cryotube	CV11-2	Kischer Biotech
Culture slides, 8-well, glass	354118	BD
Distilled water DNAse/RNAse-free	10977-035	Gibco
epT.I.P.S. Reloads 0-10µl	30 073.746	Eppendorf
epT.I.P.S. Reloads 2-200µl	30 073.800	Eppendorf
epT.I.P.S. Reloads 50-1000µl	30 073.843	Eppendorf
FACS tubes-1,1ml	15086	ThermoFischer
Gloves-Nitril Blue Vasco	9209825	Braun
Microscope slide	J3800AMNZ	ThermoScientific
Needle 30G	3054000	BD Microlance
Pipette, 5ml	CLS4051-200EA	Costar
Pipette, 10ml	CLS4488-200EA	Costar
Pipette, 25ml	P7865-200EA	Greiner
Scalpel sterile	#11/#15/#20/#23	Feather
Surgical mask	42280	Mölnlcke healthcare
Syringe, 1ml Injekt-F	9166017V	Braun
Tubes-0,5ml	0030 121.023	Eppendorf
Tubes-1,5ml	0030 121.694	Eppendorf
Tubes-2ml	0030 120.094	Eppendorf
Tubes-15ml	91015	TPP

Name	Cat.No	Company
Tubes- 50ml	352070	Corning
UV microcuvettes	759200	Brandt
Wypall	2061349	Kimberly Clark
6 well-plate	92406	TPP
12 well-plate	92412	TPP
24 well-plate	92424	TPP
96 well-plate	92096	TPP
384 well-plate, Black, Flat Bottom	3573	Corning

2.3. Table 2.3 Chemicals and reagents.

Name	Cat.No	Company
Accutase	A1110501	Gibco
Agar	A5306-250G	Sigma
Ampicillin	A9518-5G	Sigma
Antibody diluent	S3022	Dako
BSA	A7906	Sigma
Collagenase/ Dispase	11097113	Serva
DMSO	D8418	Sigma
DNase I	11284932	Sigma
EDTA	E7889-100ML	Sigma
Ethanol 70%	-	Apotheke/Innenstadt
Ethanol 96%	-	Apotheke/Innenstadt
Ethanol 100%	-	Apotheke/Innenstadt
Fluorescence mounting medium	S3023	Dako
G418	A12167.0001	Applichem
Hygromycin	H3274-50MG	Sigma
Isopropanol	9866.1	Roth
Kanamycin	K1377-5G	Sigma
Laminin	L2020-1MG	Sigma
LB broth	L3152-1KG	Sigma
L-Lysine hydrate	282677-25G	Sigma
PFA	P6148-500G	Sigma
Poly-L-Ornithine	P3655-50MG	Sigma
TissueTek OCT	4583	Sakura-Finetek
Tween 20	P9416-100ML	Sigma
Tween 80	P4780-100ML	Sigma
Triton x100	T8787	Sigma
Trypan blue solution 0,4%	T8154	Sigma
Trypsin/EDTA	T 4299	Sigma

2.4. Table 2.4 Small molecules.

Name	Cat.No	Company
Cannabidiol	-	GW pharmaceuticals
Dimethyl fumarate	242926-100G	Sigma
Digitonin	19551.01	Serva
EGCG	E4143-50MG	Sigma
H2O2	H1009	Sigma
N-Acetyl-L-cysteine	A7250-5G	Sigma
Q-VD-OPH	15260	Cayman
TNFa	300-01A-50UG	PeproTech

2.5. Table 2.5 Collection of human GBMs

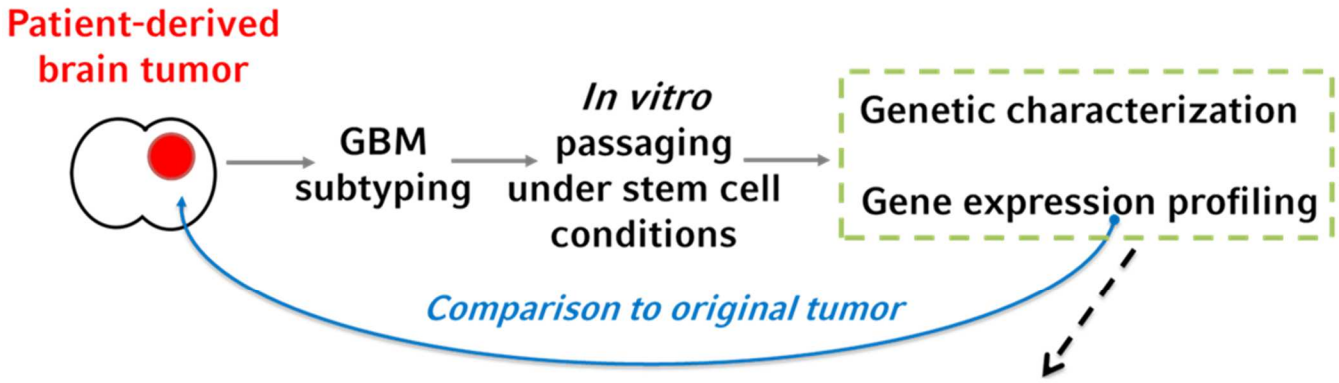

Proneural	Undefined	Classical	Mesenchymal
Line#7	GBM10	Line#2	GBM20
Line#8	GBM14	BT112	Line#6
Line#9	NCH441	BT423	Line#10
GBM13	NCH588J*		Line#11
NCH421k	NCH592B*		
NCH644	NCH684*		
	BT172		

* Recurrent GBM

Human primary GBMs were obtained by surgical resection of brain tumors after informed consent and following recommendations of respective institutional review boards of the operating hospitals. GBM cells labeled as "NCH" were obtained from a collaborating laboratory in Heidelberg [Campos B. et al. 2010]. GBM cells labeled as Line# were obtained from a collaborating laboratory in Italy [Galli R. et al. 2004]. In both cases primary cells were obtained after enzymatic dissolution of tissues and by seeding in floating

neurosphere conditions. Primary tumor samples were classified as glioblastoma following the World Health Organization guidelines.
The human cell line HEK-293T was obtained from ATCC.

2.6. Cell culture media and supplements

DMEM-10%FBS: DMEM (Biochrom, # FG0415), 10% FBS, 1% Pen/Strep
NPC culture medium: DMEM-F12 (Gibco 11320-074 or 21041-033), 1% Pen/Strep, 10ng/ml EGF, 10ng/ml FGF, 1x B27 (Invitrogen-17504-044)
NSC medium: NeuroCult™ Basal Medium-Mouse (STEMCELL technologies cat#05700), NeuroCult™ proliferation supplement-Mouse (STEMCELL technologies cat#05701), 1% Pen/Strep, 10ng/ml EGF, 10ng/ml FGF, heparin.

2.7. Buffers and solutions

- 1x PBS: Apotheke, Klinikum Grosshadern
- TBST permeabilization buffer: 3% donkey serum, 150mM Nacl, 1% Tween20,100mM Tris in 1xPBS.
- FACS buffer: 1% BSA, 2mM EDTA in 1x PBS (sterile filtered)
- 5x TBE buffer: 54g trisbase, 27.5g borate, 20ml of 500mM EDTA (pH 8) in1L demineralized H_2O.
- 4% PFA: 40g paraformaldehyde (PFA) in 1000ml
- Drug vehicle for *in vivo* i.p. injections: 2% EtOH, 2% tween80, 96% saline
- Total protein isolation buffer: 96% RIPA buffer, 2% protease inhinitor (P8340-Sigma), 1% phosphatase inhibitor cocktail-1 (P5726-Sigma), 1% phosphatase inhibitor cocktail-3 (P0044-Sigma)

2.8. Table 2.6 List of kits for cell- and molecular biology

Name	Cat.No	Company
CellTiter 96® AQueous One	G3582	Promega
Cell Titer 96 Non-Radioactive Cell Proliferation Assay	G4000	Promega
CytotoxFluor	G9262	Promega
Dual-glo Luciferase® reporter assay system	E2920	Promega
ER stress transcription factor array	FA-10006	Signosis
Lipofectamine®2000 LTX + PLUS™	15338030	Life Technologies
Lipofectamine®3000 + P3000™	L3000008	Life Technologies
Nuclear extraction kit	SK-0001	Signosis
QIAGEN Plasmid Mini Kit (25)	12123	Qiagen
QIAGEN Plasmid Maxi Kit (25)	12163	Qiagen
Quick Start™ Bradford Protein Assay kit	5000203	Biorad
Shield1	632189	Takara- Clontech

2.9. Table 2.7 List of plasmids

Name	Cat.No	Company
EGFR-neo	BC094761	Transomic
GFP-tagged Mouse Trp53	MG206086	Origene
pCMV-Neo-Bam p53 R175H	16436	Addgene
pCMV-Neo-Bam p53 R273H	16439	Addgene
pCMV-Neo-Bam p53 R248W	16437	Addgene
pCMV-Neo-Bam p53 R249S	16438	Addgene
pCMV-Neo-Bam p53 V143A	16435	Addgene
pGL4 27 [luc2P minP Hygro]	E8451	Promega
pGL4.37[luc2P/ARE/Hygro]	E3641	Promega
pGL4 74[hRluc TK] Vector	E6921	Promega
pIRES2-ZsGreen1-IRES2-GFP-mP53R270H	MR29-Korr1-2Maxi	Eurofins
pIRES2-ZsGreen1-IRES2-GFP-mP53WT	MR27-2-2Maxi	Eurofins
pIRES2-ZsGreen1-IRES2-GFP-mP53R172H	MR28-Korr3-0Maxi	Eurofins
pNFkB-DD-ZsGreen1 Reporter	631080	ClonTech

2.10. Immunolabeling

2.10.1. Table 2.8 Antibodies for flow cytometry

Marker	Cat.No	Company
HLA-A, B, C- Alexa Fluor® 647	311414	Biolegend
PARP1 (Cleaved) eFluor® 450	48-6668-42	eBioscience
p62/SQSTM1 Antibody (5H7E2) [AF 647]	NBP2-23490AF647	Novus Biologicals
LYNX Rapid RPE-Cy7 Antibody Conjugation	LNK111PECY7	AbD serotec
LYNX Rapid RPE Antibody Conjugation Kit	LNK021RPE	AbD serotec
MLKL/ MLKL-P	17-10400	EMD Millipore

2.10.2. Table 2.9 Primary & secondary antibodies for immunofluorescence

Marker	Cat.No	Company
p65	653002	Biolegend
Donkey anti Rabbit-AlexaFluor488	711-545-152	Jackson ImmunoResearch

2.10.3. Table 2.10 Dyes

Name	Cat.No	Company
CellROX® Deep Red Reagent	C10422	Molecular probes
Fixable Viability Dye eFluor® 506	65-0866-14	eBioscience
H2-DCFDA	D399	Molecular probes
Hoechst 33342	H3570	Molecular probes
Image-iT® Lipid Peroxidation Kit	C10445	Molecular probes
MAK-142	MAK142-1KT	Sigma
MitoSOX-red	M36008	Molecular probes
MitoLite(TM) Blue FX490	ABD-22674	AAT Bioquest
MitoSpy™ green	424805	Biolegend
Propidium iodide	P4864-100ML	Sigma
Rainbow calibration particles, 8 peaks	422903	Biolegend

2.10.4. Table 2.11 Software

Name	Usage	Company
Axiovision Rel 4.8	Microscopic image acqisition	Zeiss
BD coherent connection	Flow cytometry acquisition	BD Bioscience
BD FACSDIVA™	Flow cytometry acquisition	BD Bioscience
FCS Express 5	Flow cytometry analysis	DeNovo Software
GraphPad Prism 5	Graph generation	GraphPad Software Inc.
Serial Cloner 2.6.1	Primer design	Serial Basics
SoftMax Pro	Absorbance plate reading	Molecular devices
TECAN i-control™	Fluorescence/Luminescence reading	TECAN

3. Methodology

3.1. Cell culture

3.1.1. Patient-derived cells and culture

Human primary and recurrent GBMs were cultured in T75 or T150 flasks under neurosphere conditions at 37°C in a humidified atmosphere of 5% CO2 in NPC culture medium. Cells were passaged 3 times per week every 2 days using a seeding density of 0,3-0,5x 10^6 cells/10ml [Campos B. et al. (2010)]. Human GBMs labeled as "Line#..." were also cultured under neurosphere conditions but in NSC medium [Galli R. et al. (2004)] and [Binda E. et al. (2012)].

3.1.2. Mouse primary cells

3.1.2.1. Subventricular zone NPC isolation

Subventricular zone NPCs were isolated as previousy described [Talaverón R. et al. (2015)]. In brief, the mouse was sacrificed using cervical dislocation, and its body thoroughly sprayed with bacillol to prevent bacterial contamination. All dissection materials were previously washed and autoclaved. The neck was

sharply cut, and the brain excised and immediately placed in a 15ml tube filled with 1x sterile PBS. Under a microscope the subventricular zone was collected and placed in a 15ml tube filled with 3ml of DMEM-F12 medium. When multiple brains were being processed, all samples were placed on ice as they were collected. To generate original mouse NPC cultures, pieces of SVZ were incubated in 3ml of trypsin for 15 min at 37°C, homogenized with a sterile glass pipette, and further incubated 10 min at 37°C with 55,6µl of collagenase. Cell suspension was washed once with DMEM-10% FCS and twice NPC culture medium. The cells were then plated in a 6 well-plate by dividing the cells into 2 wells of 2ml each. The cells were subsequently checked every other day and 200µl of NPC culture medium was added until spheroid formation (approximately 5 days). Once spheroid formation was noticed and the center of the spheroids started to darken, they were gently disrupted, and the culture was up-scaled in 10-cm dish for expansion [Campos B. et al. (2010)] and [Ferrari D. et al. (2010)].

3.1.2.2. Generation of mouse GBM models

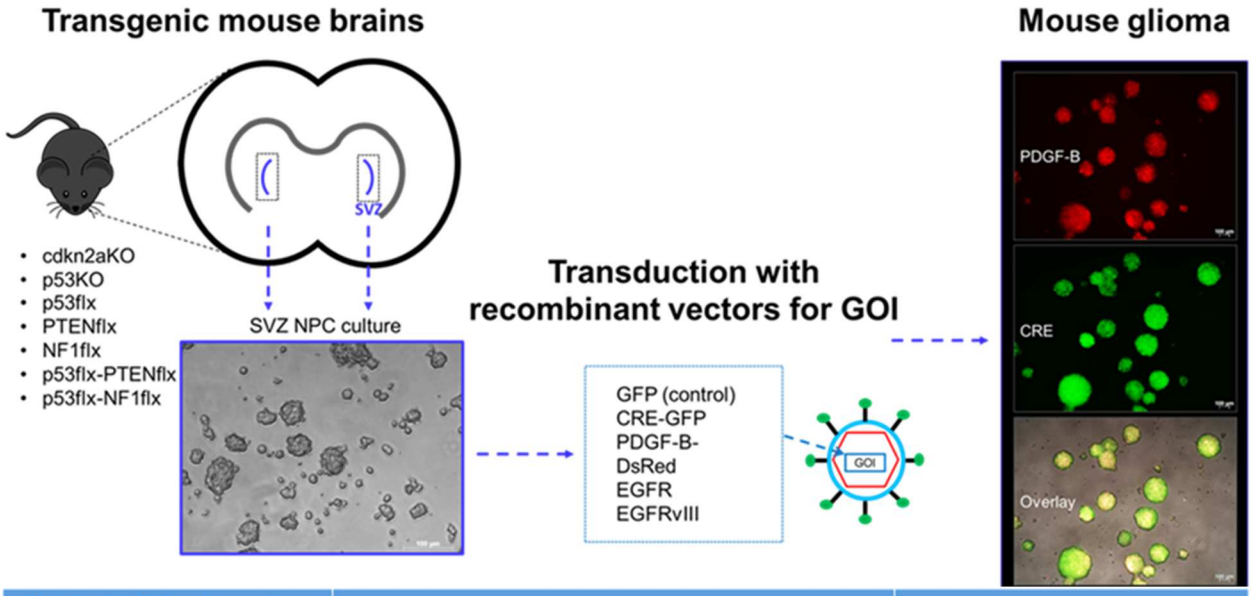

Original NPC culture from mouse brains	Recombinant vectors		Mouse glioma model
	Plasmid	Lentivirus	
p53KO	-	PDGFB-IRES-GFP	p53KO-PDGFB-GFP
p53KO	EGFR-neo	-	p53KO-EGFR-neo
p53KO	$p53^{mut}$-neo	PDGFB-IRES-GFP	$p53^{mut}$-PDGFB-GFP-neo
cdkn2aKO	-	PDGFB-IRES-DsRed	cdkn2aKO-PDGFB-DsRed
cdkn2aKO	EGFR-neo	-	cdkn2aKO-EGFR-neo
cdkn2aKO	EGFRvIII-blast	GFP	cdkn2aKO-EGFRvIII-GFP
p53flx-PTENflx	EGFR-neo	CRE-IRES-GFP	$p53^{\Delta/\Delta}PTEN^{\Delta/\Delta}$-EGFR-neo
p53flx-PTENflx	-	PDGFB-CRE-IRES-GFP	$p53^{\Delta/\Delta}PTEN^{\Delta/\Delta}$-PDGFB-GFP
p53flx-NF1flx	-	CRE-IRES-GFP	$p53^{\Delta/\Delta}NF1^{\Delta/\Delta}$-GFP
LSLp53R172H,p65wt/wt	-	PDGFB-CRE-IRES-GFP	p53R172H-PDGFB-GFP
2408 (LSLp53R172H,p65L/L)	-	PDGFB-CRE-IRES-GFP	p53R172H,$p65^{\Delta/\Delta}$-PDGFB-GFP
2412 (LSLp53R172H,p65L/L)	-	PDGFB-CRE-IRES-GFP	p53R172H,$p65^{\Delta/\Delta}$-PDGFB-GFP
2414 (LSLp53R172H,p65wt/L)	-	PDGFB-CRE-IRES-GFP	p53R172H,$p65^{wt/\Delta}$-PDGFB-GFP

Mouse glioma models by genetic subtypes

Proneural	Undefined	Classical	Mesenchymal
$p53^{-/-}$ PDGF-B $p53^{mut}$ PDGF-B $p53^{\Delta/\Delta}$ $PTEN^{\Delta/\Delta}$ PDGF-B $p53^{mut}$ $PTEN^{\Delta/\Delta}$ PDGF-B $cdkn2a^{-/-}$ PDGF-B	$p53^{-/-}$ EGFR $p53^{mut}$ EGFR $cdkn2a^{-/-}$EGFR	$cdkn2a^{-/-}$ EGFRvIII $cdkn2a^{-/-}$ EGFRvIII-EGFR	$p53^{\Delta/\Delta}$ $NF1^{\Delta/\Delta}$ $p53^{mut}$ $NF1^{\Delta/\Delta}$ $p53^{\Delta/\Delta}$ $NF1^{\Delta/\Delta}$ EGFR $p53^{mut}$ $NF1^{\Delta/\Delta}$ EGFR $p53^{mut}$ $PTEN^{\Delta/\Delta}$ $p53^{\Delta/\Delta}$ $PTEN^{\Delta/\Delta}$ EGFR $p53^{mut}$ $PTEN^{\Delta/\Delta}$ EGFR

$p53^{mut}$ human: R175H, R248W, R249S, R273H, V143A, p53wt / $p53^{mut}$ mouse: R172H, R270H, p53wt

Figure 3.1 Generation of mouse glioma models from isolated pre-malignant SVZ NPCs. To generate mouse models of human glioblastoma, we used mice bearing a selection of genetic alterations of key tumor suppressors described in different human GBMs subtypes (p53, cdkn2a, PTEN, NF1) alone or in combination. After isolation and culture of SVZ NPCs, glioma models were obtained by inducing overexpression of proto-oncogenes (EGFR, EGFRvIII, PDGFB). Engineered cells were put back in culture for expansion. The first table summarizes how the different mouse glioma models were obtained showing the original NPC culture, the recombinant vectors (plasmid for transfection or lentivirus for transduction), and the name of the mouse glioma model. The second table indicates the different mouse gliomas organized by genetic subtypes.

3.1.2.3. *In vitro* proliferation capacity and generation of NPC conditioned medium

Mouse glioma models were evaluated for their *in vitro* proliferation capacity under basal cell culture conditions using microscopic evaluation and the MTS assay. To generate NPC conditioned medium, $0{,}5x10^6$ Wild type NPC / ml were cultured under neurosphere conditions in DMEM F-12. The conditioned medium was collected after 48h by centrifugation (800g, 30 minutes) and filtration though a 0,45µm pore membrane [Ma et al. (2011)]. The collected medium was then aliquoted, stored at -80°C and thawed on the day of experimentation.

3.1.2.4. *In vivo* tumorigenicity

All animal experiments were conducted following animal welfare regulations of the Bavarian government, Munich, Germany. To evaluate the capacity of the generated mouse gliomas to induce tumors *in vivo*, mice were anesthetized and immobilized in flat-skull position in a stereotactic head holder. $0{,}1x\ 10^6$ cells/1 µl/mouse were inoculated using a 30-gauge Hamilton syringe approximately 1,5mm posterior and 1,5 mm lateral to the bregma [Glass R. et al. (2005)]. After operation, the skin was sutured, and mice placed back in their cage for recovery. The animals were inspected twice a day until humane end-point. They were then anesthetized, perfused with PFA and their brain collected. Brains were placed in 30% sucrose for dehydration, then cryopreserved in tissueTek O.C.T solution. Tumorigenesis was evaluated by hematoxylin-eosin staining and/or FET-PET imaging.

3.1.2.5. Fluorescence immunocytochemistry

Permeabilized cells were washed 3 times in 1x PBS. The primary antibodies incubated overnight at 4°C. The cells were washed 3 times with 1x PBS and incubated in the dark for 2 hours at room temperature with a mixture of fluorescently labeled secondary antibody and Hoechst 33342 for nuclear counter staining. Secondary antibody control staining was also carried out to exclude unspecific fluorescent staining. All wells were washed 3 times 5 min with 1x PBS. The chambers were dislocated from the wells and the excess PBS removed. One drop of fluorescence mounting medium was added on each well, the slide covered with

a coverslip and sealed with clear nail polish. Mounted slides were stored at 4°C in an opaque box until image acquisition.

3.2. Routine molecular biology

3.2.1. Protein extraction

3.2.1.1. Total protein and nuclear protein

$5x10^6$ cells were washed once with 1x PBS, and pelleted at 2500g, 5min at 4°C. Pellets were resuspended and vortexed in 500µl of RIPA buffer mix (480µl RIPA buffer, 5µl Phosphatase inhibitor cocktail 1, 5µl Phosphatase inhibitor cocktail 3, 10µl Protease inhibitor cocktail). The mixture was incubated on ice for 10 minutes at 4°C, then vortexed and centrifuged 14000g, 20 min, 4°C. The protein supernatant was transferred to a new 1,5ml tube and stored at -80°C until use. For the study of transcription factors, the Signosis nuclear extraction kit was used. Nuclear proteins were extracted from at least 10^7 cells in two rounds of incubation in lysis buffer (1ml 1x Buffer I/BufferII, 10µl di-thio-threitol solution, 10µl protease inhibitor) at 4°C.

3.2.2. Protein quantification

Protein concentration was evaluated using the Bradford assay following manufacturer's instructions. In brief, 1 µl of protein extract was mixed with 100 µl of assay buffer in triplicates. In parallel 1 µl of protein standards of known concentration (ranging from 0 to 2000µg/ml) were mixed with 100 µl assay buffer. The plate was incubated at 37°C for 10 minutes. Absorbance was recorded in a Versa Max microplate reader using the SoftMax Pro software. Blank was subtracted from all wells and protein concentrations were calculated by interpolating the sample protein values set as unknowns from the known protein concentration of the standard curve using the GraphPad Prism software.

3.2.3. NMR profiling

To identify metabolic alterations induced in CBD-sensitive GBMs upon treatment, $40x10^6$ cells per condition were cultured in T150 flasks with 0,01% DMSO or 10µM CBD for 20 hours. The cell pellets were collected in 1,5ml tubes, flash frozen in liquid nitrogen, and stored at -80°C. Methanol-chloroform protocol [Lindon et al. (2005)] was used to isolate the polar extracts, and the water/methanol top phase containing the polar extracts was transferred to glass vials to remove the methanol using a stream of dry nitrogen. To evaluate differences between DMSO and CBD treated samples, a multivariate statistical data analysis using PCA and PLS-DA projection methods.

3.3. Microbiology

3.3.1. Chemo-transformation of bacteria for plasmid amplification

50µl of chemo-competent E. coli were slowly thawed and incubated 30 minutes with 10µl (1µg) of plasmid on ice. The temperature was rapidly raised to 42°C for 45sec and the mixture quickly transferred on ice for 2 minutes. Each tube received 500 µl of LB medium without antibiotics and taped in a 37°C shaking incubator for 60 minutes. Distant drops (10µl) of bacteria were seeded in LB-agar plates with the appropriate antibiotics and spread using an ethanol sterilized glass rod. Dishes were then closed, inverted, and placed in a 37°C dry incubator for 16- 24 hours.

3.3.2. Plasmid amplification and glycerol stocks, and DNA purification

To generate suspension bacterial cultures, three to six single colonies were picked per plate using the tip of a 200µl pipette and inoculated in 3ml LB medium supplemented with the appropriate antibiotics. The tubes were placed in a 37°C shaking incubator for 16- 24 hours. When a maxiprep was needed, 1,5-3 ml of

bacterial culture was inoculated in 250ml LB medium with the appropriate antibiotics. Bacterial glycerol stock was generated using 500µl of a single colony culture. The suspension was transferred to a cryotube containing 500µl of 50% glycerol, and immediately stored at -80°C. Plasmids were amplified from glycerol stocks by scraping the icy glycerol stock with a 200µl pipette tip and inoculating it in 3ml LB medium with the appropriate antibiotics.

3.3.3. Plasmid DNA purification and quantification

Transfection grade plasmids were purified using Quiagen Plasmid Mini or Maxi kits with Quiagen-tip 20 or Quiagen-tip 500 respectively. Manufacturer´s protocol was followed without any modification. To quantify the purified plasmid DNA, a biophotometer was used. Background was set with a water containing cuvette. 2µl of purified DNA was mixed with 98µl of DNAse/RNAse-free water and absorbance at 260/280nm was recorded.

3.4. Plasmid transfection into mammalian cells

10^6 cells/well in serum-free/antibiotic-free medium was seeded in a 6 well-plate and placed back in the incubator awaiting transfection. 3µg of plasmid was mixed and incubated 15 minutes at RT with 150µl of Optimem medium and 3µl of Plus-reagent. Then, 159µl of lipofectamine dilution (150µl Optimem + 9µl lipofectamine 2000) was transferred to each plasmid containing tube, incubated 30 min. at RT, before being added drop-wise to the plated cells. The day after transfection, the cells were collected from the wells, centrifuged, and plated in complete culture medium.

3.5. Pantropic virus production and transduction

PDGFB-GFP and PDGFB-DsRed viruses were a gift from Magdalena Goetz [Calzolari F. et al. (2008)]. Otherwise, lentiviruses were generated using the MISSION® third generation lentiviral packaging system in a BSL-2 setting, following manufacturer's recommendations with minor changes. One day before packaging, HEK293T were plated in T75 flasks. The next day, they were co-transfected with packaging mix and transfer vector containing the gene of interest. 24 hours later, the cells were re-fed with fresh medium. Lentiviral particles were harvested on day 2 and 3 post-transfection, filtered, aliquoted and stored at -80°C until use. Pantropic viral transductions were carried out under BSL-2 conditions. On the day of transduction, $0{,}2x10^6$ cells in 5µl culture medium were transduced with 1,6µl of purified virus (500 µl of raw viral supernatant for unpurified virus). The mixture was incubated 37°C incubator for 1 hour, then received 500µl of culture medium. At 24-, 48-, and 72 hours the culture medium was changed and replaced with virus-free compete medium. After the last medium change, fluorescence expression of transduced recombinant viruses was checked using a fluorescence microscope.

3.6. Flow cytometry

3.6.1. Surface antigen staining for flow cytometry

10^6 cells were cultured for the desired amount of time with or without treatment. The day of acquisition, the cells were collected, centrifuged, and washed once with 1xPBS. In 1,5 ml tubes, the cells were stained with fluorescently labeled surface antibody in FACS buffer (1µg/10^6cells/100µl) for 30 minutes on ice in the dark. Afterwards, the cells were washed twice with FACS buffer, and transferred to 1ml FACS tubes for acquisition in a BD LSR Fortessa.

3.6.2. Intracellular staining and quantitative flow cytometry

Cells were fixed with 100µl of IC fixation buffer for 20 minutes at RT. Without washing, 500µl of 1x Permeabilization buffer was added to each tube and centrifuged at 400g, 2 minutes at 4°C. The supernatant was discarded, and pellet resuspended and incubated in 500µl 1x permeabilization for 5 minutes.

Centrifuged pellets were resuspended in 50µl of 1x permeabilization buffer and 50µl of intracellular staining cocktail (1µg of each antibody) in FACS buffer. After 30 min. of incubation on ice in the dark, 500µl of 1x permeabilization buffer was added to each tube before centrifugation. The supernatant was discarded, and pellets washed twice with 500µl 1x permeabilization buffer. The cells were resuspended in 500µl FACS buffer and transferred to 1ml FACS tubes. The cells were kept on ice in the dark until flow cytometric acquisition.
To quantify the relative amount of fluorescence molecules that corresponds to the acquired median fluorescence intensity (MFI), rainbow calibration particles (RCP) where acquired the same day and using the same laser settings as the samples. Exported fcs files were analyzed in FCS express5 for their MFI and their MEFL calculated using the standard curve of known RCP MEFL concentrations. The normalized median fluorescence intensity (nMFI) was also calculated by dividing the MFI by the number of events (MFI/number of events).

3.7. Automated plate assays

3.7.1. *In vitro* cytotoxicity assay

Cytotoxicity was detected using the CytoTox-Fluor™ cytotoxicity assay from Promega. In 96 well-plates, 3 x10^3 in 50µl (5 replicates per condition) were treated for 24 hours with 50µl of vehicle/drug in NPC medium without phenol red. 40µl of cells and diluted bis-AAF-R110 substrate (1:1 ratio) incubated for 2 hours before measuring fluorescence intensity in the Tecan InfiniteF200 fluorescence plate reader (485nmEx/520nmEm). Blank was substracted from all wells and the fluorescence read-out for untreated cells (vehicle control) was normalized to 1. Read-outs from treated cells were normalized to those of untreated cells and fold change of relative cytotoxicity calculated for each well. Outliers were detected and omitted, if any, using the Grubbs test. Graphs were generated using the GraphPad Prism software version 5.01.

3.7.2. *In vitro* viability assay (MTT)

The CellTiter 96® Non-radioactive Cell Proliferation Assay was used according to manufacturer´s instructions. Cells were seeded and treated as in the cytotoxicity assay. After 72 hours of incubation at 37°C in a humidified atmosphere, each well incubated with 15µl of dye solution for 4 h at 37°C. During this incubation period, living cells with active metabolism convert the MTT tetrazolium component of the dye solution into a formazan product. To solubilize the formazan product, 100µl of solubilization/stop solution was added to each well and incubated 1 hour at 37°C. The absorbance was then recorded using an absorbance plate reader set at 570nm using the SoftmaxPro software. Blank was subtracted from all wells and fold change to vehicle control was calculated.

3.7.3. *In vitro* viability assay (MTS)

The CellTiter 96® AQueous Non-Radioactive Cell Proliferation Assay was used according to manufacturer´s instructions. Cells were seeded and treated as in the MTT assay. After 72 hours of incubation at 37°C in a humidified atmosphere, each well incubated with 20µl of MTS/PMS solution for 4 h at 37°C. To stop the reaction, 25µl of 10% SDS solution was added to each well and incubated 1 hour at 37°C. The absorbance was then recorded using an absorbance plate reader set at 490nm using the SoftmaxPro software. Blank was substracted from all wells and fold change to vehicle control was calculated.

3.7.4. Activated ER stress transcription factor array

The Signosis ER stress activation profiling plate array was used to simultaneously detect alterations in 16 ER related transcription factors: XBP-1, ATF4, ATF6, GADD153/CHOP, CBF/NFY, SREBP1, YY1, ERR, ATF3, AP-1, FOXO1, IRF, p53, NFkB, NRF2/ARE, HNF4 [Jiang S. et al. (2016)]. Samples were treated with DMSO or CBD for 20h. Nuclear proteins were extracted using the Signosis kit SK0001 and quantified

using the Bradford assay. For each sample, 10µg of nuclear extract were mixed with probe mix and transcription factor bound probes were retained on a separation column. After removing free probes, bound probes were eluted, denatured and hybridized to the pre-coated array plate overnight at 42˚C. Biotinylated probes were detected with streptavidin-HRP using the luminescence filters of a TECAN plate reader.

3.7.5. ARE-luciferase promoter reporter assay

GBM cells were co-transfected with 4.74-hRluc and 4.27-luc2P (minimal promoter) or 3.37-luc2P(ARE). [Schagat T. et al. (2007)]. After weeks of hygromycin selection, 0.1 x 10^6 cells were treated with DMSO or CBD for 24 hours. 96 well plates were removed from incubator and each well received 75µl of Dual-glo luciferase assay reagent, and firefly luciferase activity measured 10 minutes later in TECAN reader. 75µl of Dual-glo stop & glo was added and renilla luminescence measured. The ratio of ARE reporter luminescence to control reporter was calculated and compared in DMSO / CBD treated wells.

3.8. ProteoTuner, NFkB promoter fluorescence reporter assay

Patient-derived Glioblastoma cells were transfected using lipofectamine as previously described. Stable transfectants were used in four experimental conditions: Shield alone (detection of GBM cells basal promoter activity), Shield+CBD, and Shield + TNFα (positive control for NFkB promoter activity). Green fluorescence of treated cells (active NFkB promoter) was examined by fluorescent microscopy or flow cytometry.

3.9. *In vivo* experiments: tumor implantation, *in vivo* therapy, and tissue processing

Athymic nude mice were anesthetized and inoculated with 0.1 x 10^6 cells in the right hemisphere. The wound was cauterized, and mice placed back in their cages for awakening before being brought back to animal housing. The mice were followed and inspected twice a day in the morning and late afternoon. For *in vivo* therapy, treatment was prepared daily by mixing vehicle (0) or CBD (15mg/kg) EtOH aliquots (-20˚C) to room temperature vehicle solution. Mice were transported to operation room, weighed, and received 10 µl/g of freshly mixed vehicle or CBD i.p.
At humane end-point, the animals were anesthetized and perfused with 4% PFA via cardiac puncture. Brains were collected in 4% PFA, transferred in sucrose for 3 days and embedded in cryomatrix. Liquid nitrogen frozen brains were sliced in dry ice and floating sections stored at -20˚C until use.

3.10. *Ex vivo* experiments

3.10.1. Tumor biopsy dissection and processing

Athymic nude mice bearing patient-derived GBM xenografts were sacrificed and brains collected. The tumor was dissected, tumor biopsy cut into 10mg pieces, and mashed through cell strainer. One part of cell suspension was stained with human HLA A, B, C-AlexaFluor647 and 20µM H2DCFDA in 1x PBS for 30 minutes at 37˚C. The rest was stained with H2-DCFDA for glass capillary detection in the IOS [Gorpas D. et al. (2017)] and [van Dam G. M. et al. (2011)].

3.10.2. *Ex vivo* labeling of live tumor biopsies

For *ex vivo* imaging of GBM ROS levels, suspensions of filtered mashed brains (0.5x10^6 cells) were either unstained or stained with Hoechst 33342 (1:1000 dilution), 30µM H2DCFDA (intracellular ROS) or Hoechst 33342 and H2DCFDA. After 30 minutes at 37˚C, the dyes were washed away, and tumor soup loaded in glass capillaries for imaging.

4. Results

4.1.Human and mouse GBMs and their characterization

4.1.1. Characterization of human GBMs

4.1.1.1. Patient derived human GBMs proliferate *in vitro* under stem cell conditions

Patient derived GBMs were cultured under spheroid conditions in their respective culture media. Three times per week, the spheroids were passaged by gentle disaggregation, splitting, and re-plating in fresh culture medium. Figure 4.1 illustrates a microscopic evaluation of the cultured spheroids before passaging and shows the variety of growth pattern observed for different GBMs.

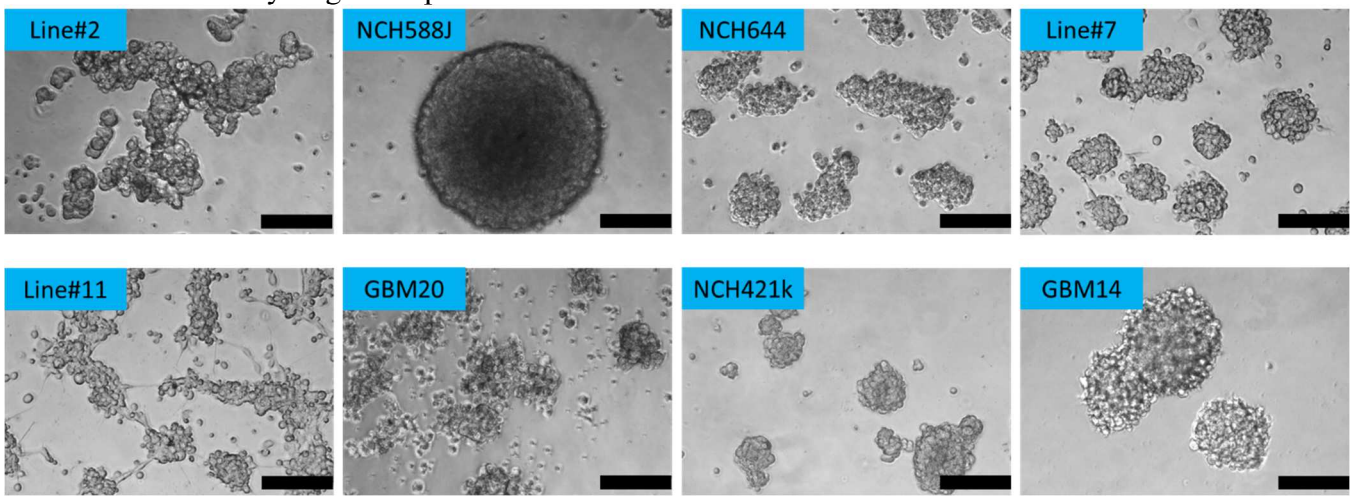

Figure 4.1 Microscopic visualization of patient derived GBM spheroid cultures. GBM cells were cultured under spheroid conditions and the cultures were monitored using a light microscope at 20x magnification. The name of cells used is on the left-hand corner of each picture and the black scale bar indicates 100µm.

4.1.1.2. Patient derived GBMs retain the capacity to induce glioblastoma *in vivo*

After successful culture *in vitro*, we evaluated the ability of a selection of GBM cells to induce tumors in athymic nude mice brains.

We found that different GBM cells have different time-course of tumorigenicity and that the generated tumors are not alike. Some tumors are very solid and compact with well-defined borders (Line#2, NCH644, GBM14), whereas others present a gel-like appearance and are difficult to demarkate (NCH421k) [Figure 4.2].

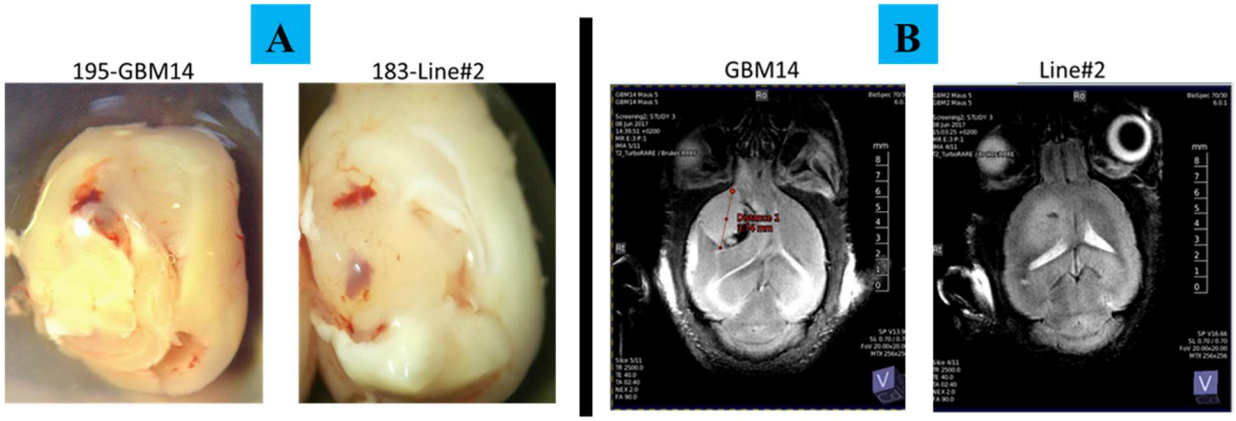

Figure 4.2 *In vivo* tumorigenicity of patient derived glioblastoma after implantation in athymic nude mouse brain. Picture of dissected mouse brain showing the tumor in the right hemisphere (A) and MRI scans for GBM14 and Line#2 (B).

4.1.2. Generation of mouse models of GBMs

NPCs bearing floxed or knock-out genes (TRP53 wt/mutant, NF1, PTEN, or cdkn2a), alone or in combination, were isolated from mouse subventricular zone, cultured under neurosphere conditions, and transduced with lentiviral vector expressing CRE recombinase. These pre-malignant cells were further virally transduced or transfected to overexpress PDGFB or EGFR/EGFRvIII in order to obtain fully malignant glioma cells. Spheroids of mouse gliomas are illustrated in Figure 4.3.

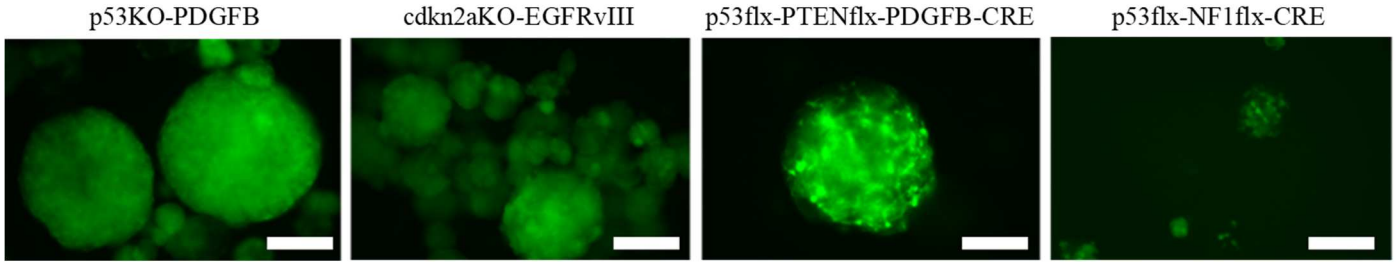

Figure 4.3 Spheroids of generated mouse gliomas. Microscopic evaluation of transduction efficiency for the generation of mouse gliomas. Fluorescence imaging for transduction efficiency at 40x magnification after viral transduction of SVZ-NPCs. Mouse cells were floxed or knock-out for cdkn2a, p53, PTEN, NF1 and transduced with viral particles CRE, PDGFB, or EGFRvIII concomitantly with a fluorescence tag (GFP). The scale bar is at the lower-right-hand corner of each picture and indicates100µm.

4.1.3. Characterization of mouse glioma models

4.1.3.1. Glioma mouse models differentially proliferate *in vitro* under stem cell conditions

Visual inspection of the cells during culture suggested that they had different proliferation rates. Indeed, we found that at comparable seeding density, mouse glioma cells tend to form bigger spheres and grow faster than NPC-wt. [Figure 4.4].

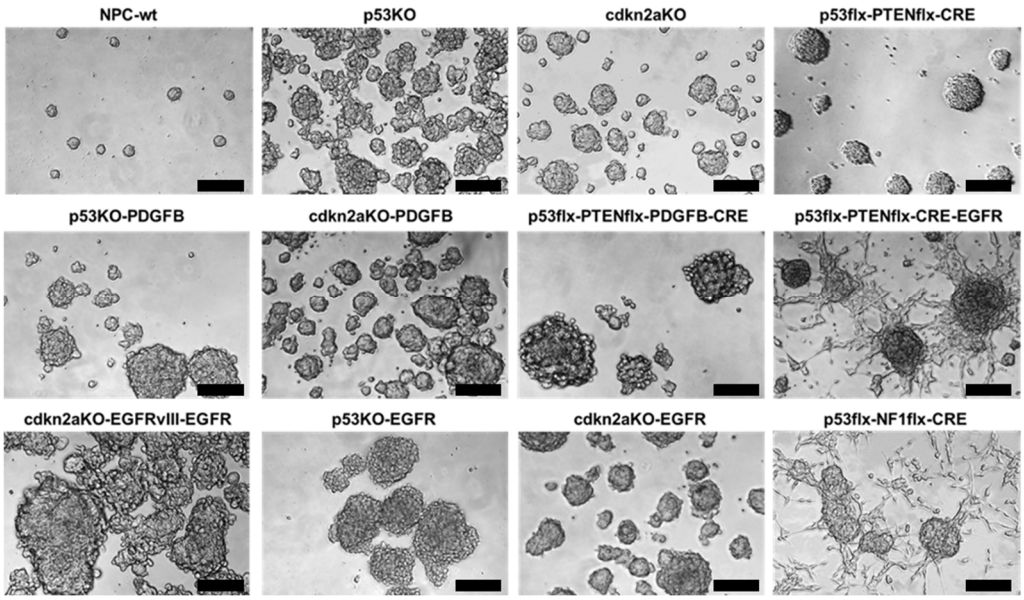

Figure 4.4 Visual inspection of *in vitro* cultures of mouse glioma models. Cells were seeded at a density of 0,2 x 10^6 in 10 ml of culture medium. Pictures were acquired 2 days after seeding using a light microscope at 20x magnification. Scale bars are in black and indicate 100µm.

4.1.3.2. Generated mouse gliomas are distinct in their proliferation capacity

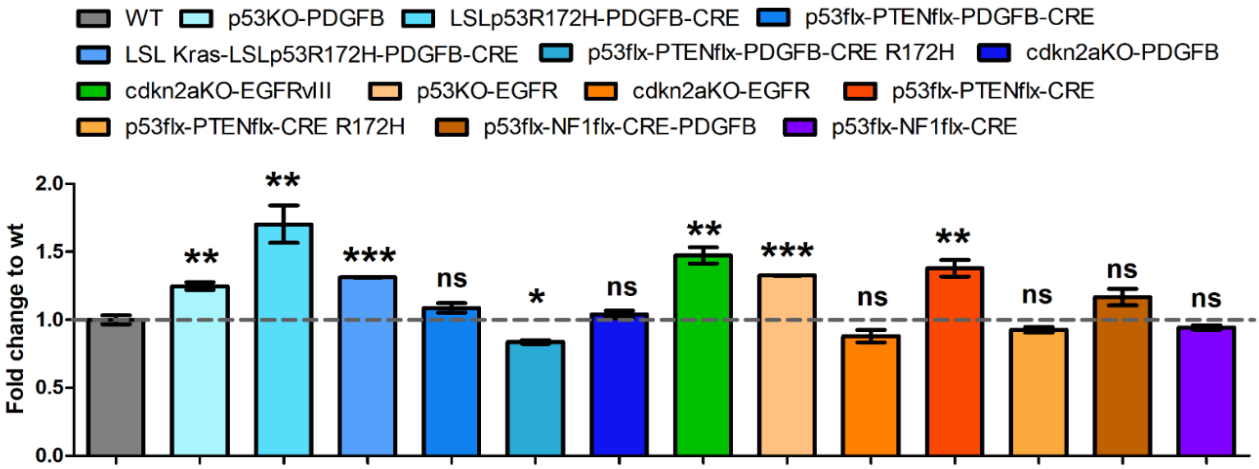

Figure 4.5 End-point (72h) evaluation of *in vitro* proliferation capacity of mouse gliomas. The cells were seeded at a density of 3000 cells/well in 100µl of phenol red-free culture medium. At 72 hours, the MTS assay was carried out. Background was subtracted from all wells. The graph indicates the fold change of the mean +/- SEM of the absorbance of gliomas mimicking different GBM subtypes (colored bars) compared to NPCwt (gray bar).Statistical significance was evaluated using two-tailed paired t test.

To confirm that differences in proliferation capacity/metabolic activity exists between different gliomas and non-malignant NPCs, we performed an MTS assay at 72 h end-point starting with a seeding density of 3000 cells/wells (in quintuplicates) for all gliomas. We found that compared to wt-NPCs, mouse gliomas with genetic alterations characteristics of different human GBM subtypes, had different metabolic activities [Figure 4.5].

4.1.3.3. *In vivo* tumorigenicity of mouse glioma models depends on their genetic background

To verify the capacity of engineered mouse gliomas to generate tumors *in vivo*, immunocompetent mice were inoculated with cultured mouse glioma cells in the right hemisphere. At humane end-point, the mice were processed and the tumorigenicity of the inoculated cells evaluated after H&E staining. We found that tumorigenicity and humane-end was achieved rapidly with two mouse glioma models: p53KO-PDGFB (proneural) needed about 57 days and cdkn2aKO-EGFRvIII (classical) about 15 days [Figure 4.6].

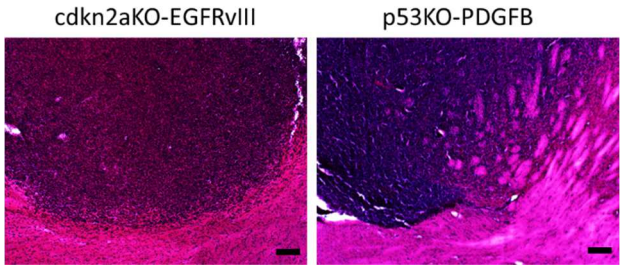

Figure 4.6 H&E staining of mouse glioma models. Immunocompetent mice were inoculated intracranially with 10 000 cells of engineered mouse gliomas representative of two GBM subtypes: cdkn2aKO-EGFRvIII-GFP at 15 days post inoculation (left) or p53KO-PDGFB-GFP at 57 days post inoculation (right). 40µm brain slices were stained with Hematoxylin-Eosin and tumors were visualized in a light microscope at 5x magnification. The scale bars indicate 20µm.

The brain slices of the two mouse models were also imaged for the fluorescence of inoculated mouse glioma cells. As the viral vectors used in engineering the glioma cells also expressed a GFP marker, the brain slices were only counterstained with Hoechst 33342 (blue) and the tissue directly imaged in a fluorescence microscope.

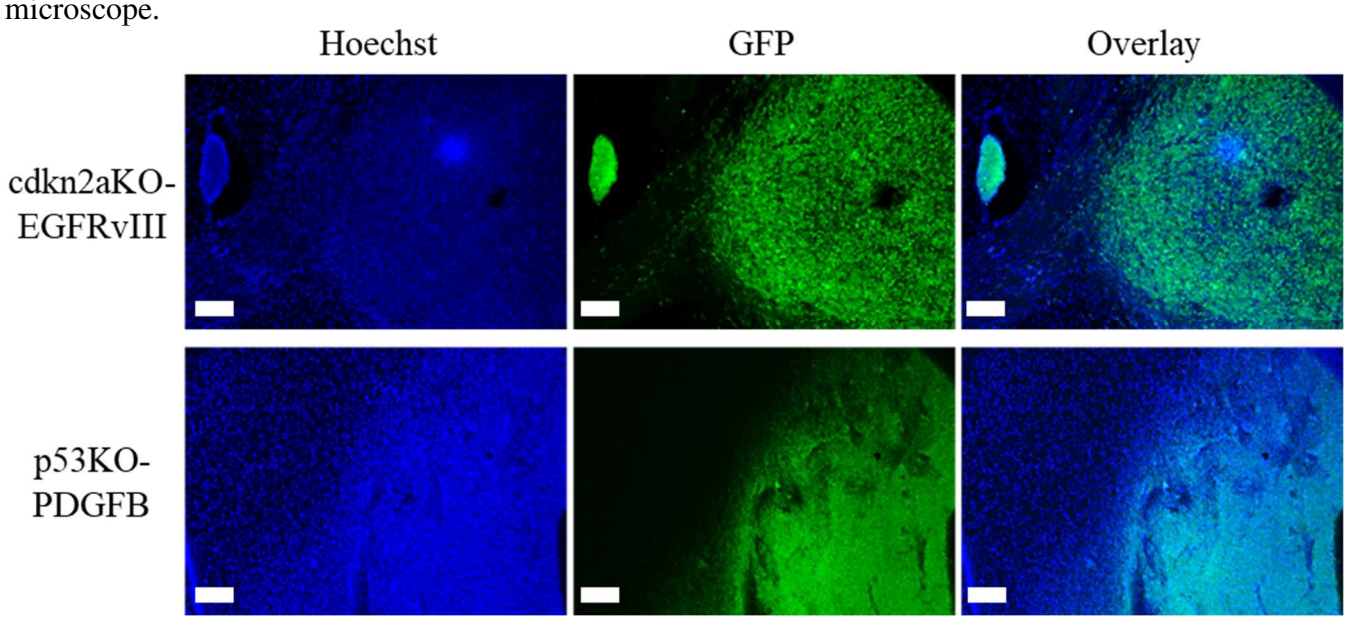

Figure 4.7 Fluorescence imaging of mouse brains inoculated with genetically engineered glioma cells. Immunocompetent mice were inoculated with 10 000 mouse glioma cells in the right hemisphere. 40µm brain slices were counterstained with Hoechst 33342 and mounted for fluorescence imaging. Mouse glioma models cdkn2aKO-EGFRvIII-GFP (top) and p53KO-PDGFB-GFP (bottom) showing from left to right: Hoechst staining for nuclei showing accumulation in the right hemisphere; GFP-positive tumor cells; overlay of GFP-glioma cells and nuclear Hoechst staining. Images were acquired at 10x magnification, scale bar = 100µm.

We found that the GFP signal allowed a good localization of the tumors in situ. The Hoechst counterstaining indicates a massive accumulation of cell nuclei in the same territory of the GFP-positive tumors [Figure 4.7].

4.2. Endovanilloid-rich NPC*wt* conditioned medium induces cytotoxicity in subsets of mouse GBMs

It was previously published that in the young mouse brain, NPC*wt* could migrate to and encircle gliomas. There, they were shown to secrete different lipids called endovanilloids. These endovanilloids by activation of TRPV1 receptors activated ER stress and induced cell death in the gliomas [Stock k. et al. (2012)]. We then investigated the anti-tumorigenic role of NPC-wt conditioned medium on generated mouse gliomas. Mouse glioma cultures representative of glioblastoma subtypes (classical, proneural, mesenchymal) have been tested. In this screen, NPC*wt* conditioned medium shown to be toxic to a selection of mouse gliomas [Figure 4.8].

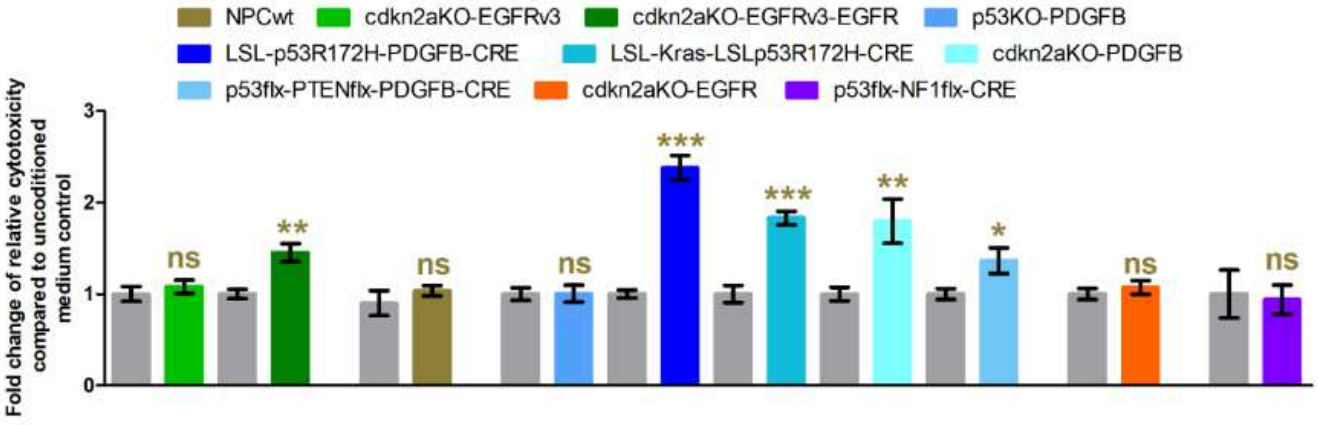

Figure 4.8 NPCwt conditioned medium (CM) induces cytotoxicity in subsets of mouse gliomas. Mouse glioma cells were incubated with unconditioned medium or NPCwt CM for 24 hours and *in vitro* cytotoxicity detected. The graph illustrates the mean +/- SEM of the fold change of cytotoxicity. Two-tailed paired t test statistical analysis was used to compare unconditioned medium (grey bar) to cells cultured in conditioned medium (colored bar).

These results confirm that endovanilloids secreted by NPCwt is not toxic to healthy NPCs while they are capable to kill some gliomas. We also show that some mouse gliomas can resist the cytotoxicity effect of endovanilloids.

4.3. Plant derived vanilloid cannabidiol induces cytotoxicity in mouse and human GBMs with different genetic signatures

To verify if the endovanilloids effect could be obtained with clinical-grade vanilloids, we evaluated the effect of plant-derived vanilloid Cannabidiol (CBD) on engineered mouse gliomas and patient derived GBMs.

4.3.1. *In vitro*, CBD is toxic to a selection of mouse of human GBMs

To evaluate the cytotoxicity of CBD *in vitro*, mouse gliomas were subjected to the cytotoxicity assay as performed for the effect of NPCwt CM. We set a threshold of cytotoxicity to 2-fold of the effect of the vehicle treated cells to exclude inter-experiment variability.

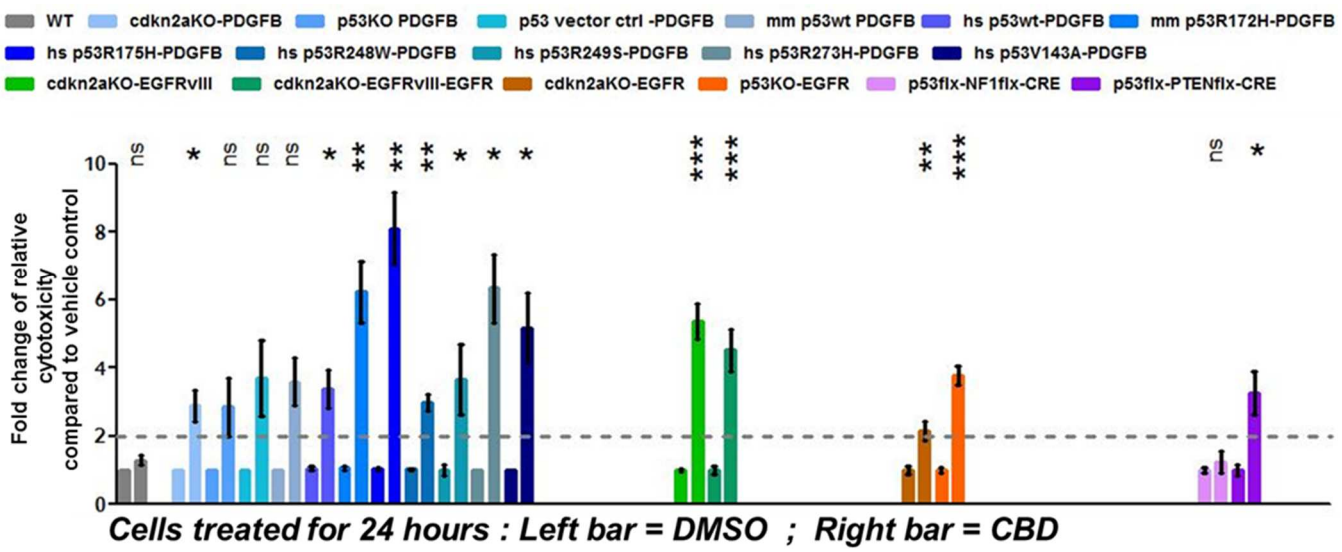

Figure 4.9 CBD is toxic to subsets of mouse GBM models. Mouse cells were treated with 0,01% DMSO (vehicle control) or 10µM CBD (drug). The cytotoxicity detection was carried out as previously. The graph shows the fold change of CBD cytotoxicity compared to vehicle control for each mouse glioma. The experiments were repeated at least 3 times. Statistical analysis: two-tailed paired t test; mean & SEM.

We found that CBD does not induce significant cytotoxicity in NPCwt as well as some mouse gliomas e.g. the mesenchymal mouse glioma p53flx-NF1flx-CRE. However, we show that CBD induces significant cytotoxicity in most mouse gliomas and is more than 5-fold more toxic compared to vehicle control in some proneural gliomas with mutant p53 (R172h, R175H, R273H, V143A) [Figure 4.9].

4.3.1.1. CBD is toxic to mouse gliomas but not NPCwt

In parallel with the cytotoxicity assay, we also corroborated our findings by microscopic evaluation of the treated cultures [Figure 4.10].

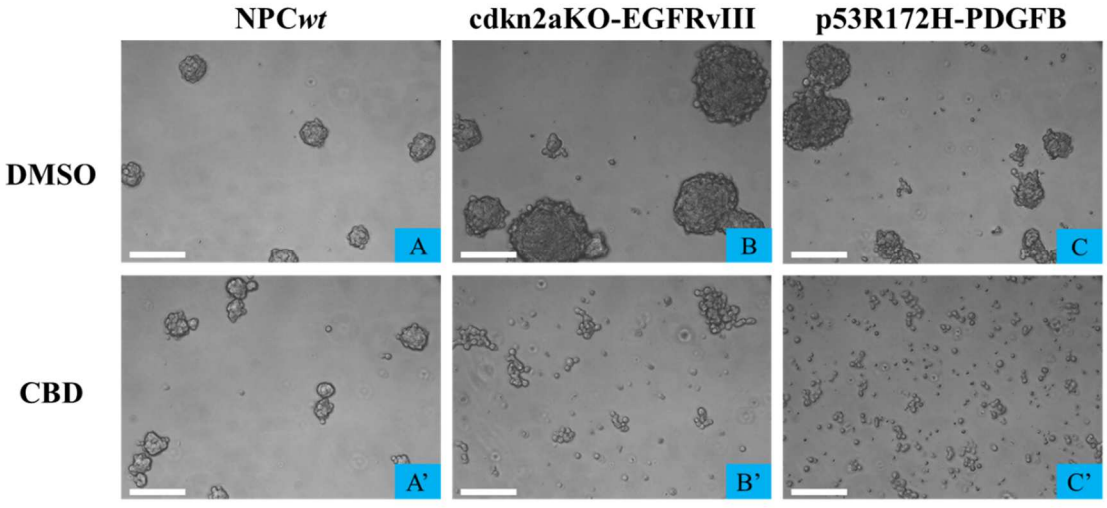

Figure 4.10 Visual inspection of mouse gliomas upon CBD treatment. Mouse NPCwt and glioma cells used for the CBD cytotoxicity assay. NPCwt cells were treated with DMSO (A) or CBD (A'); and mouse gliomas cdkn2aKO-EGFRvIII DMSO (B), CBD (B'); p53R172H-PDGFB DMSO (C), CBD (C'). Microscopic images captured at 20x magnification just before the cytotoxicity detection using a light microscope. Scale bars = 200µm.

Wild-type NPCs that were not affected by CBD in the cytotoxicity assay also did not seem to be affected when the cultures were observed under a microscope. The same is true for the gliomas that showed to be sensitive to CBD in the cytotoxicity assay such as cdkn2aKO-EGFRvIII and p53R172H-PDGFB [Figure 4.10].

4.3.1.2. CBD decreases spheroid size of mouse models of human GBMs

The effect of CBD on glioma spheroids was also evaluated in parallel to the cytotoxicity assay, and we quantified changes in spheroid size 48- and 72-hours post treatment.

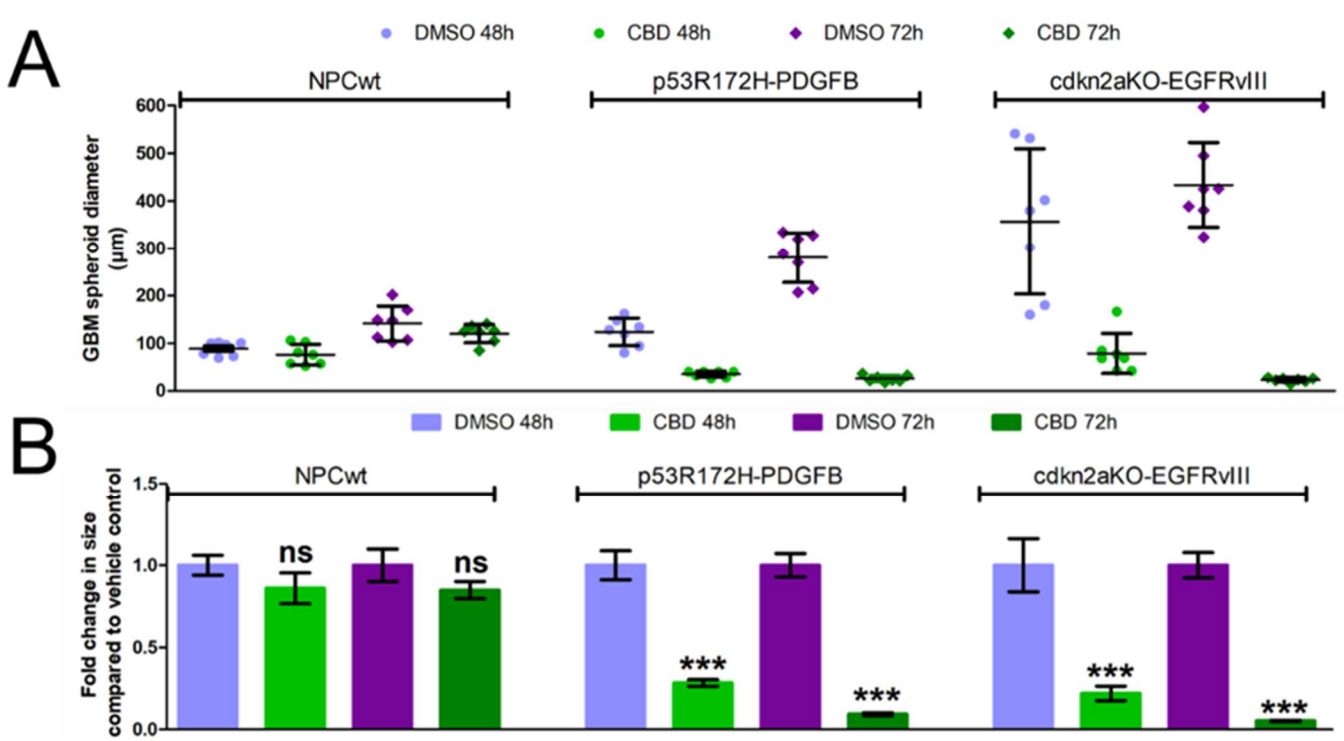

Figure 4.11 CBD treatment decreases mouse glioma spheroid size. Mouse NPCwt and 2 mouse gliomas shown to be very sensitive to CBD, p53R172H-PDGFB (proneural) and cdkn2aKO-EGFRvIII (classical), were treated with 0,01% DMSO or 10µM CBD. At 48- and 72- hours post treatment the wells were microscopically inspected, and pictures of spheroids acquired. The diameter of spheroids was measured using FiJi (A), and the fold change of CBD treated spheroid size compared to vehicle treated spheroids was calculated (B). Graphs with mean & SEM were generated and statistical significance evaluated with two-tailed paired t test comparing DMSO to CBD treated at 48- and 72 hours for each group.

Validating our cytotoxicity assay results, we found that CBD does not affect the size of NPCwt, while significant changes are observed for the proneural p53R172H-PDGFB and the classical glioma cdkn2aKO-EGFRvIII. For the mouse gliomas, the DMSO treated spheroids grew in diameter over time, but the CBD treated spheroids were disaggregated [Figure 4.11].

4.3.2. CBD induces cytotoxicity in human GBMs to different extent

The cytotoxicity effect of CBD on patient-derived GBMs was evaluated in the CytoToxFluor cytotoxicity assay, as performed for the mouse gliomas [Figure 4.9].

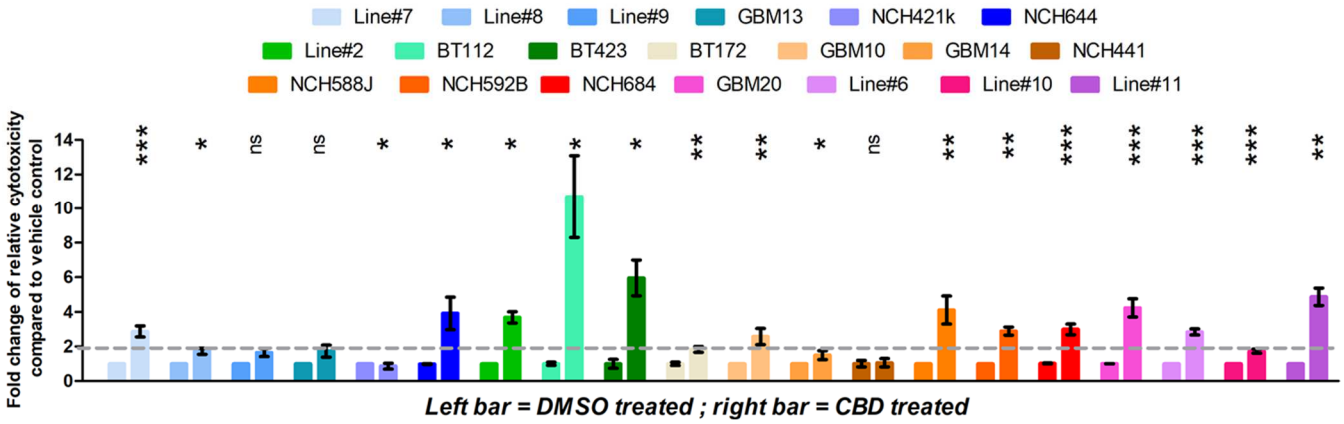

Figure 4.12 *In vitro,* CBD induces cytotoxicity in human GBMs to different extent. Human GBMs were investigated in the cytotoxicity assay using the same settings for the mouse gliomas [Figure 4.9]. The generated graph indicates the fold change of cytotoxicity in GBM cells treated with 0,01% DMSO (left bar) or 10µM CBD (right bar) compared to the vehicle control (DMSO). The different human GBMs were grouped on the graph by genetic subtype using a color-code: proneural GBMs in shades of blue, classical GBMs in shades of green, mesenchymal GBMs in shades of pink, and unclassified GBMs in shades of orange. Mean +/- SEM; two-tailed paired t-test (n = 3 - 10)

As obtained for the mouse gliomas, we found that CBD exerts cytotoxicity effects on human GBMs to different extent [Figure 4.12]. We categorized human GBMs based on CBD response spectrum from the cytotoxicity screening as good responders when the cytotoxicity induced is more than 2-fold compared to vehicle treated, and as low-CBD responders when it is below 2-fold.

As for the mouse glioma cytotoxicity, we visually inspected the treated cells used in the assay to verify if the quantified cytotoxicity was related to some changes in the cultures.

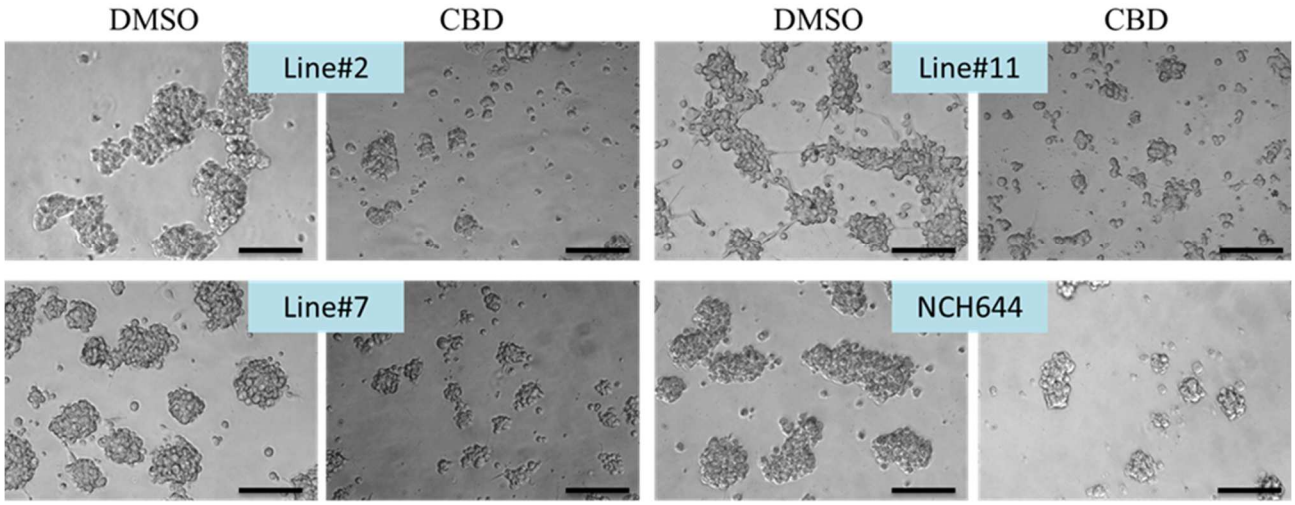

Figure 4.13 Visual inspection of cells used in the *in vitro* cytotoxicity assay of CBD in human GBM spheroids. Human GBM cells were plated for the cytotoxicity assay as previously described for the mouse cytotoxicity screening [Figure 4.9]. Before starting the detection of cytotoxicity, the treated wells were inspected with a light microscope

and pictures acquired at 20x magnification. DMSO treated cells for each GBM are shown left and the CBD treated are on the right. Scale bars = 100µm.

We again observed that CBD treated wells show spheroids which seem smaller with a more disaggregated appearance. In cases where the GBMs grow as adherent, treating with CBD caused loss of adherence e.g. Line#11 [Figure 4.13].

4.3.3. Long-term follow-up post CBD treatment indicates that induced cytotoxicity is durable

To verify the durability of CBD effect, the cells treated and used in the cytotoxicity assay were kept in culture for 11 days. At day 4 and 11 the cells were imaged, and viable cells counted using trypan blue exclusion.

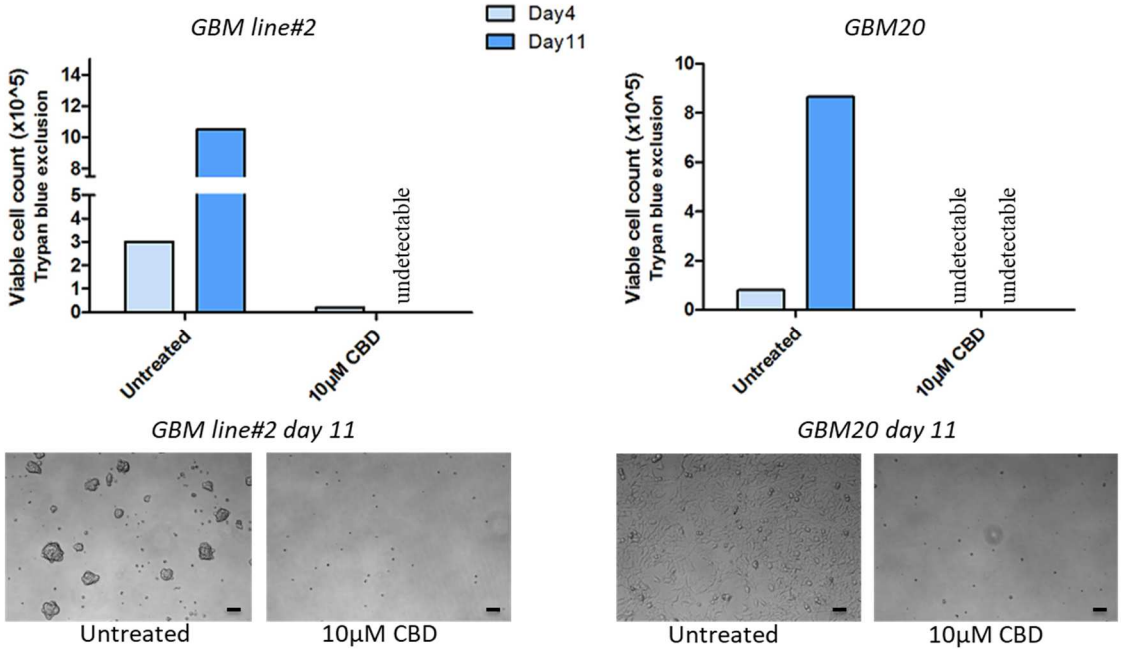

Figure 4.14 CBD induced cytotoxicity is durable. Two good-CBD responders were used for this assay: GBM Line#2 and GBM29. Cells were plated as previously described for cytotoxicity screening [Figure 4.9]. At day 4 and 11, plated cells were visually inspected using light microscopy. The 5 wells were pooled and the viable cell count of untreated and CBD treated wells was evaluated using trypan blue exclusion. Graph show the viable cell count obtained for untreated wells (left bars) and CBD treated wells (right bars). Counts at day 4 post treatment are indicated in light blue and at 11 days are in darker blue. Microscopic inspections at day 11 post treatment are indicated under the graphs and show for both lines untreated samples (left) and CBD treated samples (right) at 10x magnification. The scale bar indicates 100µm.

We found that while cells in untreated wells continued to grow from day 4 to 11, cells in CBD treated wells kept dying until viable cells were undetectable at day 11 [Figure 4.14].

4.3.4. Six-hour-pulse CBD treatment corroborate the findings of the CBD cytotoxicity on human GBMs

In clinical trials involving healthy volunteers *per-os*, CBD was shown to have peak activity from 55 minutes to 3 hours after administration [Blessing E. M. et al (2015)]. To study the effect of CBD within the range of its pharmacokinetics and bioavailability in the brain in our *in vitro* setting, we performed a 6h-pulse CBD

treatment. We pulse treated our collection of human GBMs for 6 hours, removed the drug-containing medium and replaced it with regular culture medium. Then the GBM cells viability was evaluated by counting viable cells using trypan blue exclusion at 24-, 48-, 72 hours post pulse treatment.

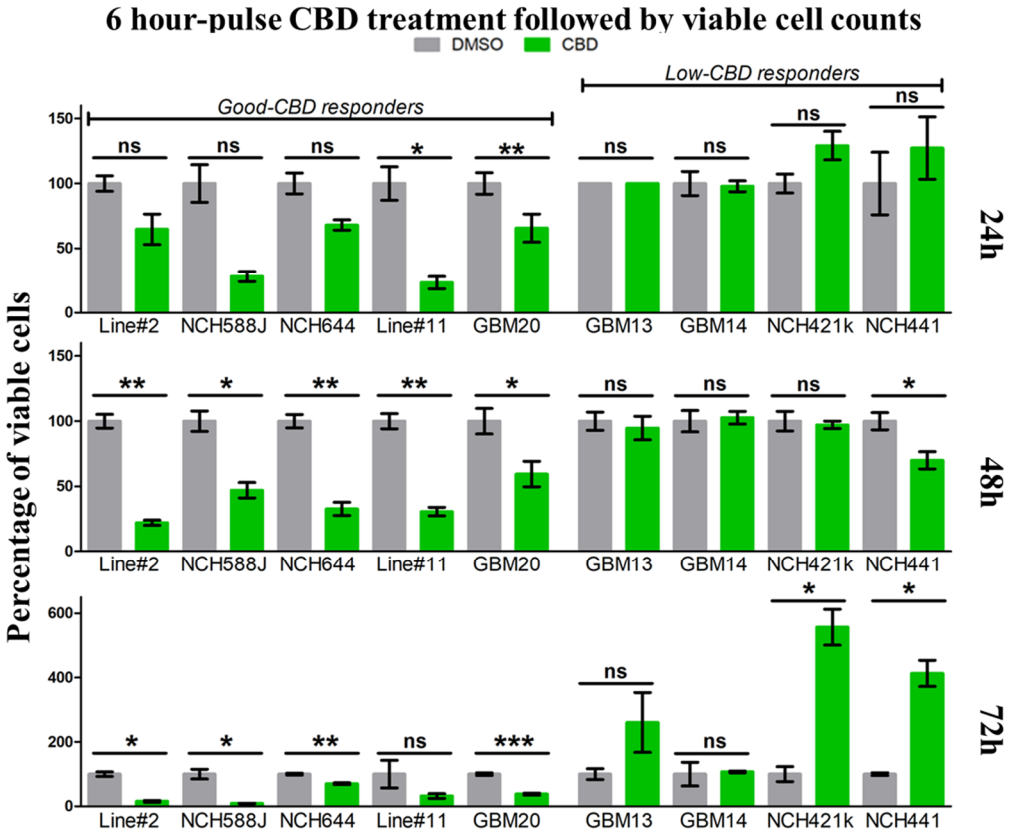

Figure 4.15 Evaluation of viable GBM cells after 6-hour-pulse CBD treatment. GBM cells were plated in 6 well-dishes at a density of 10^6 cells/well in NPC culture medium. Wells were treated either with 0,01% DMSO or 10µM CBD. After 6 hours of incubation, the treatments were removed from all wells and the cells plated in drug-free NPC culture medium. Viable cells were counted at 24-, 48-, and 72 hours using the trypan blue exclusion method. The graphs indicate the percentage of viable cells over a 3-day-period.

Doing so, we confirmed the cytotoxicity assay findings where the GBMs identified as good-CBD responders were the only ones dying after 24 and 48 hours. Interestingly, at 72 hours massive death is observed for the known CBD responders whereas in low-responders viable cell counts were either unchanged or higher in CBD treated when compared to the vehicle controls [Figure 4.15].

4.4. The p53 status of human GBMs determines the cell death mode induced by CBD

4.4.1. CBD induces caspase dependent death in p53wt GBMs

To clarify the mode of cell death induced by CBD, we screened the effect of the pan-caspase inhibitor Q-VD-OPh (quinolyl-valyl-O-methylaspartyl-[2,6-difluorophenoxy]-methyl ketone), on human GBMs in combination with CBD. Q-VD-OPh is a broad-spectrum caspase inhibitor that is effective at low doses (5 µM) and which has been shown to inhibit apoptotic pathways where caspase 8/10, caspase 9/3, and caspase 12 are implicated [Caserta T. M. et al. (2003)].

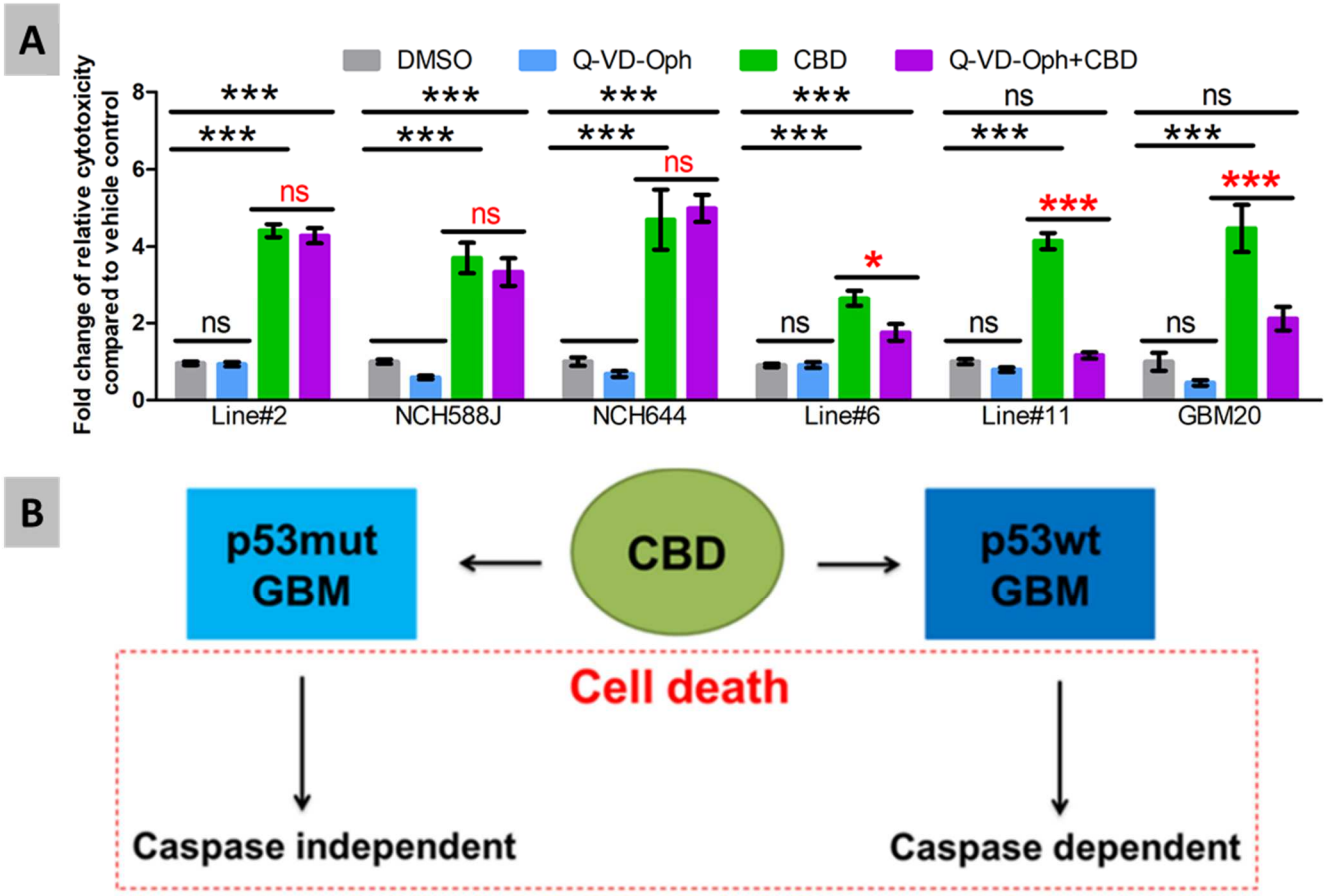

Figure 4.16 The p53 status of human GBMs determines the cell death mode induced by CBD. To determine if CBD kills human GBMs via apoptosis, the effect of pan-caspase inhibitor Q-VD-Oph on CBD induced cytotoxicity in selected GBMs was evaluated: p53mu GBMs (Line#2, NCH588J, NCH644), p53wt GBMs (Line#6, Line#11, GBM20). Four conditions were used in a set of cytotoxicity assays: 0,01% DMSO (20 hours), 10µM CBD (20 hours), 10µM Q-VD-Oph (3 hours), 10µM Q-VD-Oph (3 hours) and 10µM CBD (20 hours). The cytotoxicity assay was conducted as previously described [Figure 4.9] and repeated in 3 to 5 independent experiments. Panel A indicates the mean +/- SEM of the fold change of cytotoxicity compared to vehicle control for all treatment conditions. One-way ANOVA with Bonferroni multiple comparison test was used to statistically compare the cytotoxicity of Q-VD-Oph or CBD alone to the dual effect of Q-VD-Oph and CBD. Panel B is a schematic summary of the cytotoxicity findings, showing that if a p53wt GBM is treated with CBD it dies in a caspase dependent manner, whereas a mutant p53-GBM dies in a caspase independent manner.

Also, it was shown to be a more potent inhibitor than z-VAD-fmk (benzyloxycarbonyl-Val-Ala-Asp(OMe)-fluoromethylketone) and Boc-D-fmk (Boc-aspartyl(OMe)-fluoromethylketone), which only inhibit some classes of apoptotic caspases [Yee S. B. et al (2006)]. Moreover, Q-VD-OPh does not show toxicity *in vitro* or *in vivo* even at prolonged treatment or high doses respectively up to 50µM and daily administration of 10mg/kg for up to 4 months [Keoni C. L. et al. (2014)].

To know if CBD kills GBM via apoptosis, patient-derived GBM cultures, known to be sensitive to CBD in the cytotoxicity screen, were pre-treated with Q-VD-OPh for 3 hours and then received either the vehicle control (DMSO), Q-VD-OPh, CBD, or a combination of Q-VD-OPh and CBD. After 20 hours of further incubation, the cytotoxicity assay revealed that Q-VD-OPh could only decrease CBD induced death in p53wt GBMs that are otherwise sensitive to CBD. This suggests that GBM cells that express a wild-type version of p53 would die in a caspase dependent manner when treated with CBD [Figure 4.16].

Scientific findings have shown that tumor cells die in multiple modes of regulated cell death [Maltese W. A. et al (2014)]. As we could determine the death mode induced by CBD only for some of the investigated GBMs, we developed a cell death flow cytometry panel that includes a phenotypic live/dead labeling and markers for three major regulated cell death modes: apoptosis (increase in cleaved PARP1) [Soldani C. et al. (2002)], necroptosis (increase in MLKL/P-MLKL) [Yoon S. et al. (2017)] and autophagy (p62 degradation) [Bjørkøy G. et al (2009)]. The flow cytometry approach allowed us to quantify at a single cell level, GBM cells that could be dying via multiple pathways.

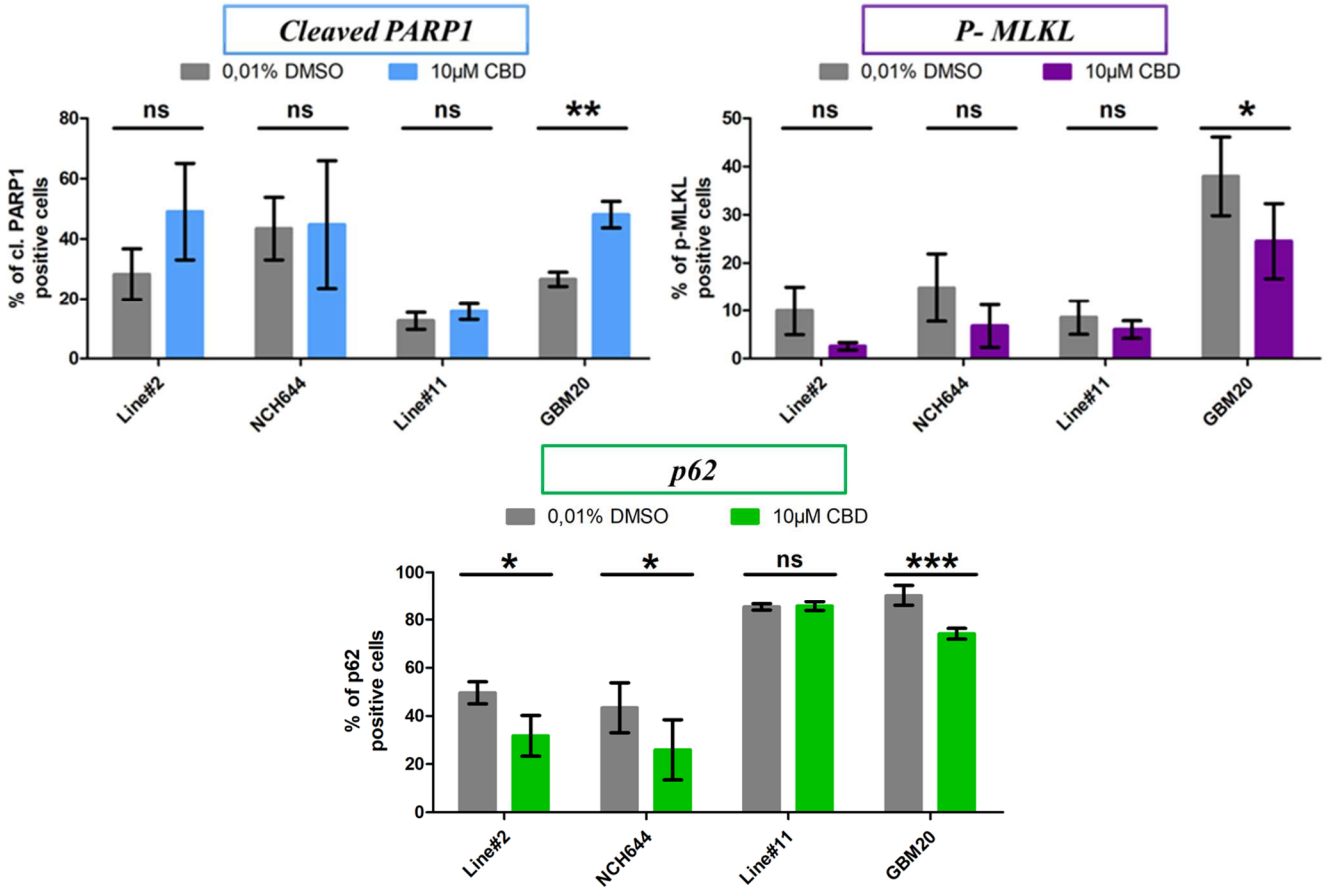

Figure 4.17 CBD induces apoptosis or autophagy in human glioblastoma. Human GBMs treated with DMSO or CBD were stained for makers of apoptosis (cleaved PARP1 increase), necroptosis (p-MLKL increase), and autophagy (p62 decrease) and fluorescence signal acquired by flow cytometry. Graphs indicate the mean +/- SEM of the percentage of marker positive cells for all 3 markers of apoptosis (Cleaved PARP1), necroptosis (p-MLKL), and autophagy (p62). The measurements were repeated in 3 to 6 independent experiments and the statistical significance of the findings was evaluated with two-tailed paired t-test comparing CBD treated to DMSO treated conditions.

We found that, for the GBM tested, CBD does not induce death via necroptosis. But for the p53-mutant GBMs that were not dying in a caspase dependent manner in the previous assay [Figure 4.16], we found that CBD induced a significant decrease in p62, which suggests an autophagic cell death. A mixture of apoptosis and autophagy was found in a p53wt-GBM (GBM20) [Figure 4.17].

4.5.CBD alters the metabolic profile of human and mouse GBMs

Now that we uncovered the major cell death modes that are induced in GBMs upon CBD treatment, we investigated further the metabolic pathways that are mobilized in GBMs that are responsive to CBD. We made use of NMR to profile CBD induced metabolite alterations in polar fractions of mouse and human GBMs. First, a clear separation between DMSO and CBD treated cells could be observed showing a real "CBD effect" in human and mouse GBMs [Figure 4.18 A & B]. Then, the metabolites that are altered upon treatment were identified, along with the variations induced by CBD (increase or decrease compared to control) [Figure 4.18 A' & B'].

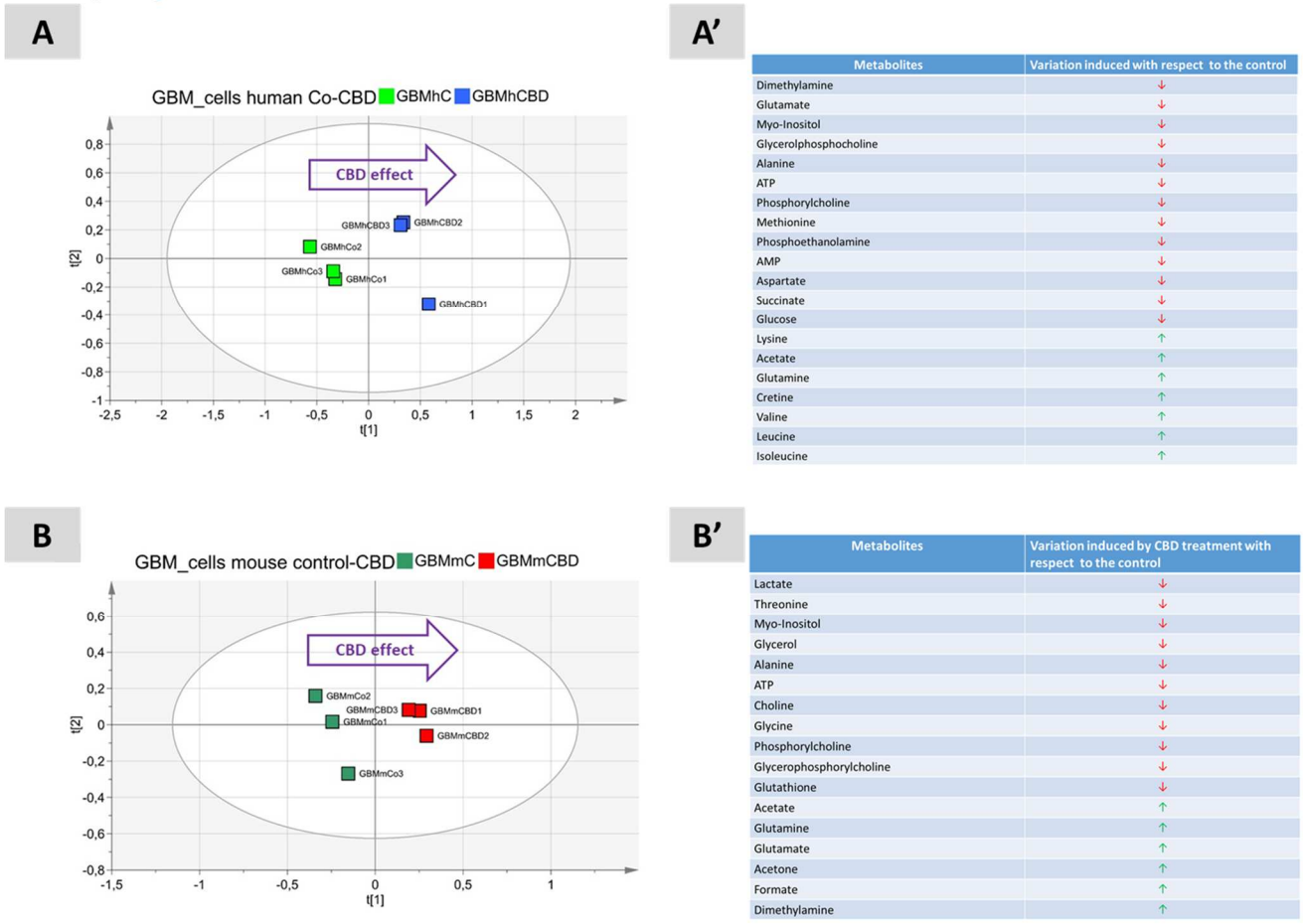

Metabolites	Variation induced with respect to the control
Dimethylamine	↓
Glutamate	↓
Myo-Inositol	↓
Glycerolphosphocholine	↓
Alanine	↓
ATP	↓
Phosphorylcholine	↓
Methionine	↓
Phosphoethanolamine	↓
AMP	↓
Aspartate	↓
Succinate	↓
Glucose	↓
Lysine	↑
Acetate	↑
Glutamine	↑
Cretine	↑
Valine	↑
Leucine	↑
Isoleucine	↑

Metabolites	Variation induced by CBD treatment with respect to the control
Lactate	↓
Threonine	↓
Myo-Inositol	↓
Glycerol	↓
Alanine	↓
ATP	↓
Choline	↓
Glycine	↓
Phosphorylcholine	↓
Glycerophosphorylcholine	↓
Glutathione	↓
Acetate	↑
Glutamine	↑
Glutamate	↑
Acetone	↑
Formate	↑
Dimethylamine	↑

Figure 4.18 NMR profiling reveals metabolic alterations induced by CBD in human and mouse GBM. One human GBM NCH644 (A/A') and one mouse GBM cdkn2aKO-EGFRvIII (B/B'), known to be very sensitive to CBD were selected for the assay. To evaluate differences between DMSO and CBD treated samples, a multivariate statistical data analysis using PCA and PLS-DA projection methods was carried out (A/B) and the metabolites altered upon CBD treatment in human NCH644 and mouse cdkn2aKO-EGFRvIII GBMs are shown in A' and B' respectively.

Similar trends in the metabolic alterations have been found between human and mouse GBMs [Figure 4.18 A', B'] and include increase in acetate and glutamine, and decrease in alanine, ATP, myo-inositol, and phosphorylcholine.

4.6.In GBMs, CBD does not induce ferroptosis or lipid peroxidation

It has been shown that glioblastoma death could be induced by inhibiting cholesterol uptake with the inhibitor LXR-623 [Villa G. R. et al. (2016)]. Lipids and lipid modifications seem then to play a crucial role in tuning glioblastoma survival and their manipulation might be used as a strategy to eradicate this disease. Indeed, lipid peroxidation derived ROS (lipid ROS) has been shown to be closely linked to iron metabolism in the newly described cell death mode ferroptosis [Dixon S. J. et al. (2012)] and [Toyokuni S. et al. (2017)]. To check the impact of lipid peroxidation in CBD induced glioma cell death, we used the lipid peroxidation inhibitory molecule Ferrostatin-1(Fer-1) [Dixon S. J. et al. (2012)] alone or in combination with CBD in the CytoTox-Fluor™ cytotoxicity assay.

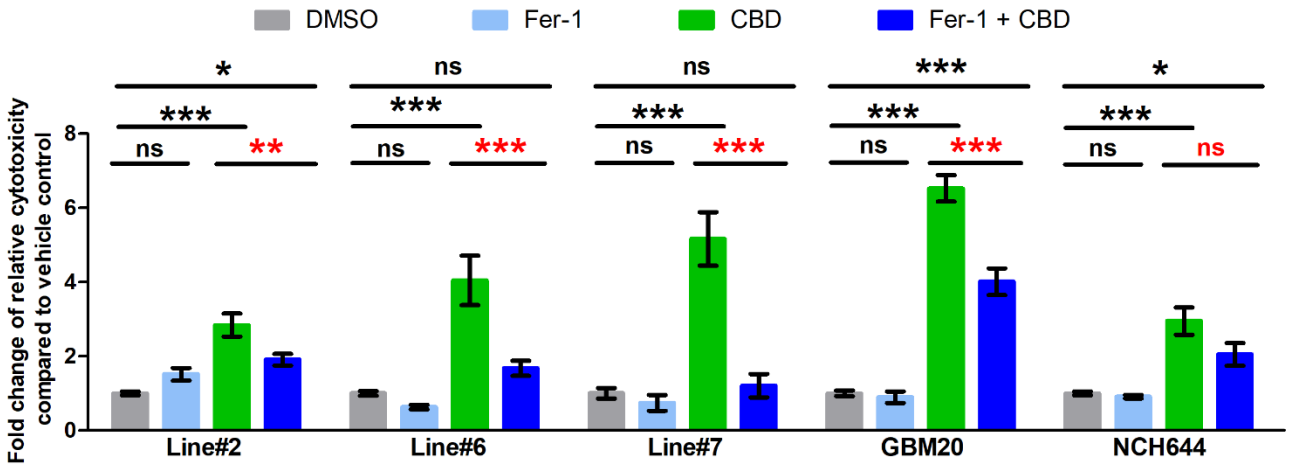

Figure 4.19 CBD and lipid peroxidation. GBM cells were screened in a cytotoxicity assay as previously described, testing for the effect of lipid peroxidation inhibitor Ferrostatin 1 on CBD induced GBM cytotoxicity**.** 4 conditions were used in a set of cytotoxicity assays: DMSO (20 hours), CBD (20 hours), Ferrostatin 1 (3 hours), Ferrostatin 1 (3 hours) and CBD (20 hours). The cytotoxicity assay was conducted as previously described [Figure 4.12] and repeated in 2 to 5 independent experiments. The graph indicates the mean +/- SEM of the fold change of cytotoxicity compared to vehicle control for all treatment conditions. One-way ANOVA with Bonferroni multiple comparison test was used to statistically compare the cytotoxicity of CBD alone to the dual effect of Ferrostatin 1 and CBD. Statistical results for significance comparing to vehicle are in black, and to CBD are in red.

Interestingly, CBD induced cytotoxicity could be significantly reduced by ferroptosis and lipid peroxidation inhibitor Fer-1 in most GBMs regardless of their subtype [Figure 4.19]. Apart from one proneural GBM, inhibiting ferroptosis with Fer-1 significantly reduced CBD cytotoxicity; with the most significant decrease observed in p53wt/ caspase dependent dying GBMs. These first results triggered our interest in a potential role of ferroptosis in CBD induced GBM death. Therefore, we investigated this pathway further. Ferroptosis, death by lipid peroxidation, is characterized by the down-regulation of system xC (SLC7A11), high iron levels and accumulation of lipid ROS [Dixon S. J. et al. (2012)]. As glioblastoma produce high levels of reactive oxygen species (ROS) [Moloney J. N. et al. (2017)], we also explored the importance of ROS in GBM cell death.

Endoplasmic reticulum (ER), mitochondria and peroxisomes are the 3 main cellular organelles producing ROS. As these ROS can be further categorized in 2 types, lipid ROS (lipid hydroperoxides) and the non-lipid ROS or water-soluble ROS e. g. hydrogen peroxide (H_2O_2) superoxide anion ($O_2^{-\cdot}$), hydroxyl radical (•OH) [Birben E. et al. (2012)], we subsequently screened a selection of human GBMs by flow cytometry for these 2 ROS categories. It was recently published that glioblastoma cells heavily rely on cholesterol for

survival, and by blocking cholesterol uptake with the small molecule LXR-623, glioblastoma cell death could be induced both *in vitro* and *in vivo* and was associated with tumor shrinkage and prolonged survival in orthotopically implanted mice [Villa G. R. et al. (2016)]. Potential lipid peroxidation in patient derived GBMs was assessed using the ImageIt lipid peroxidation kit by flow cytometry.

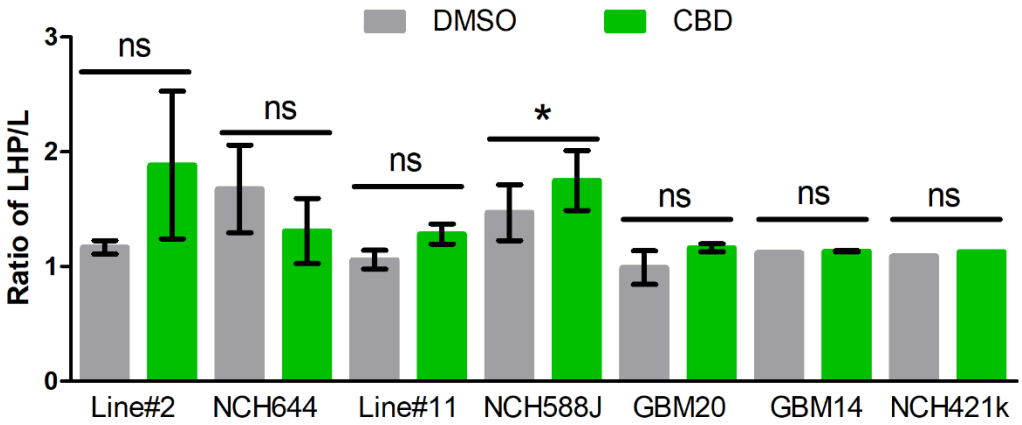

Figure 4.20 CBD does not induce lipid peroxidation in GBMs. GBM cells were treated either with DMSO or CBD for 72 hours, then stained with the ImageIt Lipid peroxidation kit for lipids (red fluorescence) and lipid hydroperoxides (green fluorescence). The graph represents the mean +/- SEM of the ratio of lipid hydroperoxides (LHP) and lipids (L). DMSO treated samples (gray bar) were compared to CBD treated cells (green bar) using two-tailed paired t test.

At 24 hours post-treatment, no changes were detected in neither low- nor good-CBD responders. At 48- and 72 hours we could not detect any change in the ratio of lipids/lipid hydro-peroxides in low/non-CBD responders. However, alterations in lipid hydroperoxides/lipids ratios (increase or decrease) were observed in good CBD responders [Figure 4.20].

4.7.Evaluation of CBD induced ER stress in human GBMs

One pathway previously associated with vanilloid induced glioma death is the ER stress pathway [Stock K. et al. (2012)]. To verify the capacity of CBD to induce ER stress in human GBMs, we performed an activated ER stress transcription factor array. This assay shows ER related transcription factors that are activated. When activated, the transcription factors can bind complementary DNA consensus sequences. In this assay, we compared responses in nuclear extracts of a low-CBD responder (NCH421k) to a good-CBD responder (Line#2).

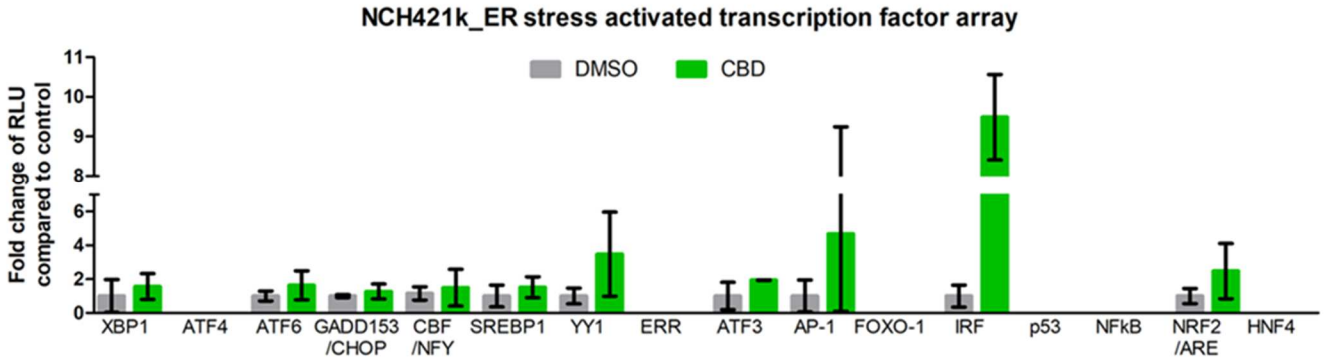

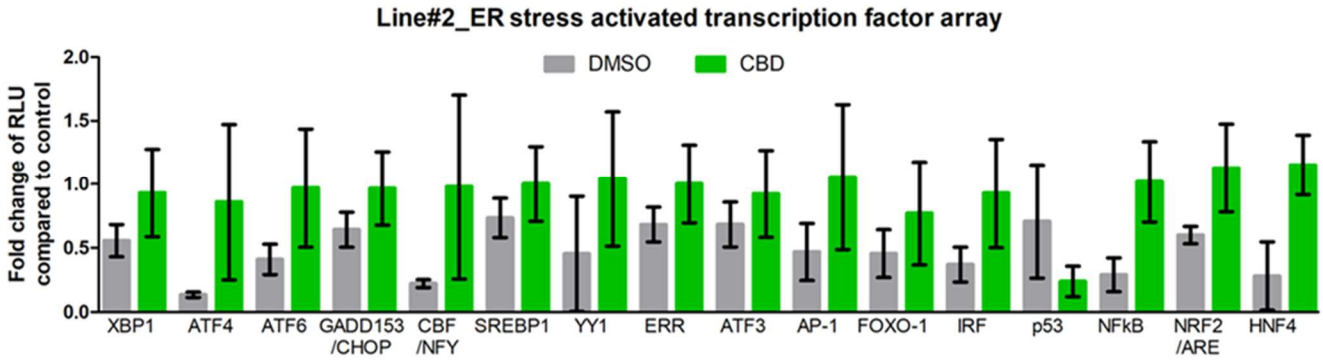

Figure 4.21 CBD induces alterations in the activation of ER stress transcription factors. GBM cells were cultured in NPC culture medium supplemented with 0,01% DMSO or 10µM CBD for 20 hours. 10µg of nuclear proteins were used in the ER stress activated profiling plate array to detect simultaneously 16 ER related transcription factors: XBP-1, ATF4, ATF6, GADD153/CHOP, CBF/NFY, SREBP1, YY1, ERR, ATF3, AP-1, FOXO1, IRF, p53, NFkB, NRF2/ARE, HNF4. Graphs indicate fold change of relative luminescence unit (RLU) of CBD treated samples (green bars) compared to DMSO control (gray bars) for NCH421k and Line#2. Based on the p53 null status of NCH421k, a threshold of relative luminescence unit (RLU) was set by removing all values detected as less than the RLU of p53 in NCH421k. Paired t test was used to evaluate differences between DMSO and CBD treatments but was not significant.

In these two GBMs, we revealed differentially regulated transcription factors implicated in inflammatory response (IRF, NFkB), lipid metabolism (SREBP1, ERR, FOXO1), antioxidant response (NRF2/ARE) [Figure 4.21]. Although the results were not statistically significant, they will serve as a basis for further investigations clarifying the effects of CBD using other assays (fluorescence immunocytochemistry, flow cytometry and other reporter assays).

4.8. CBD decreases the proportion of GBM membrane lipids

Although no significant changes in lipid hydroperoxides were obtained upon CBD treatment we explored alterations in GBM lipids upon CBD. By fluorescence microscopy, we observed that CBD changed lipid distribution and staining [Figure 4.22 panel A].

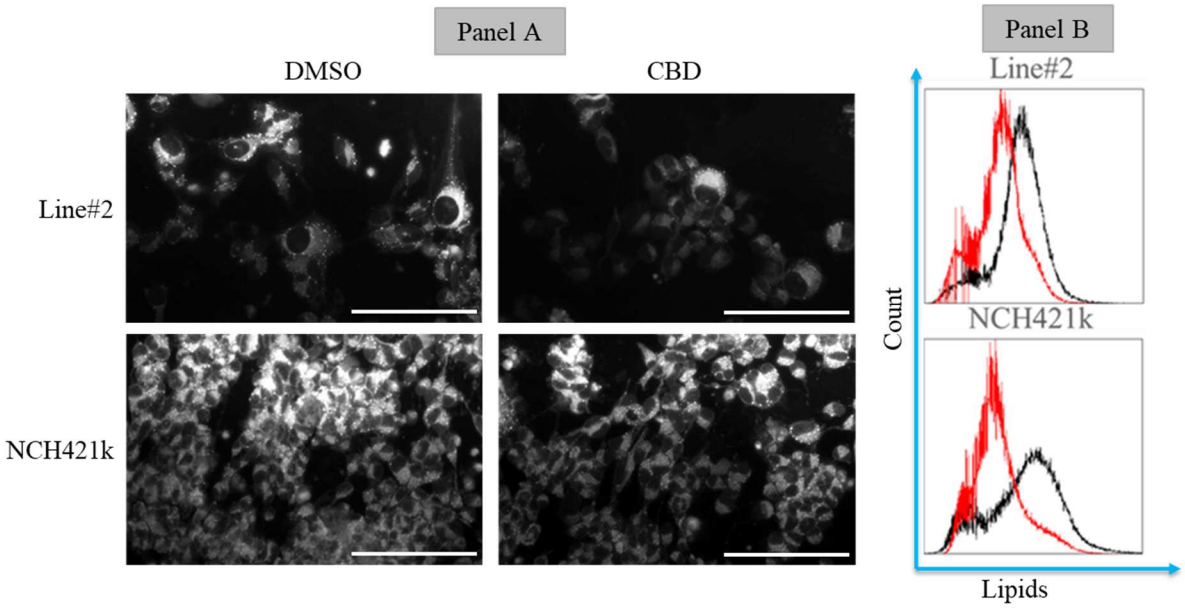

Figure 4.22 CBD decreases GBM membrane lipids. GBM cells (Line#2, NCH421k) were treated either with 0, 01% DMSO or 10µM CBD for 20 hours, after which, the treatment was removed and replaced with 1x PBS containing the ImageIt lipid peroxidation dye. Live cultures were imaged using a fluorescence microscope for DsRed signals. Pictures were acquired at 40x magnification and scale bars indicate 100µm (Panel A). Flow cytometry analysis was conducted at the same time point for GBMs Line#2, NCH421k (Panel B) and shows overlay histograms of lipids (DsRed signal) at 24 hours for these GBMs. GBM treated with DMSO are represented in the black histogram, and CBD treated are red histograms.

To confirm these findings, we turned to flow cytometry and found that CBD treatment decreased lipids in glioblastoma, as shown in the lipid MFI upon treatment. Interestingly the decrease in lipids was observed as early as 24 hours, time point at which massive CBD induced GBM death could not be quantified by flow cytometry. These changes were induced in both good- and low-CBD responders [Figure 4.22 panel B].

4.9. In mouse and human GBMs CBD acts as an antioxidant by decreasing water soluble ROS

Since consistent lipid ROS increase or decrease were not observed upon CBD treatment, we continued the screening for water soluble general ROS using the dye H2-DCFDA (2',7'-dichlorodihydrofluorescein diacetate) [Keston S. et al (1965)].

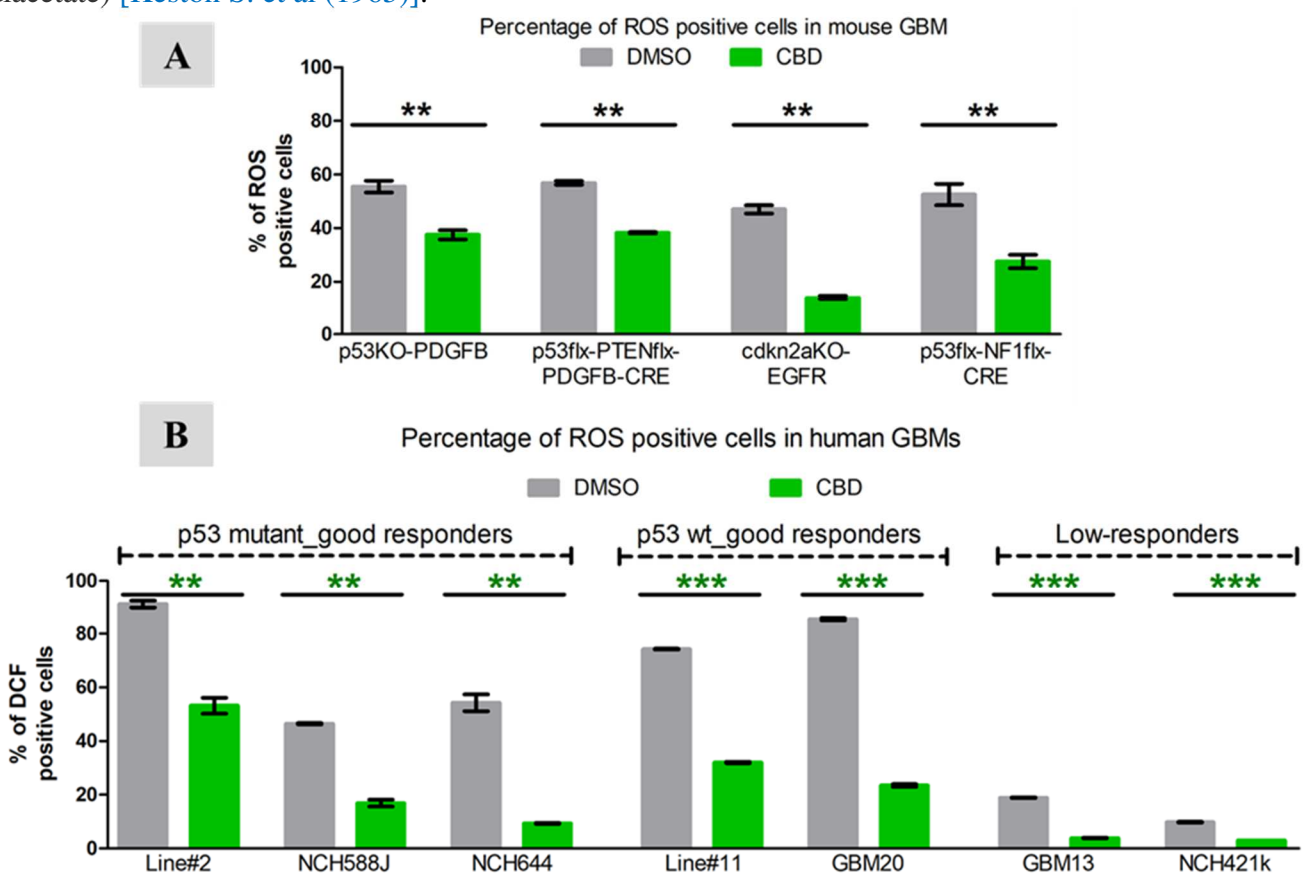

Figure 4.23 In mouse (A) and human (B) GBMs CBD decreases water soluble ROS. Mouse and human GBM cells were treated with 0,01% DMSO or 10µM CBD for 20 hours and stained with H2-DCFDA for flow cytometry. Graphs indicate the mean +/- SEM of the percentage of ROS (DCF) positive cells in mouse (A) and human GBMs

(B) for 3 independent experiments. Two-tailed paired t test was used to evaluate the statistical significance comparing DMSO (gray bar) to CBD (green bar) treated cells for each GBM.

Colorless H2-DCFDA dye diffuses into cell membranes and turns into DCF (2',7'-dichlorodihydrofluorescein) when intracellular ROS oxidizes it, emitting green fluorescence [Berte N. et al. (2016)] proportional to intracellular ROS levels in GBMs. As a general outcome, we found that mouse and human GBMs exhibit different levels of ROS and that CBD significantly decreases ROS levels in all tested GBMs, regardless to their sensitivity to the drug [Figure 4.23].

4.10. CBD induces mitochondrial changes in CBD-sensitive GBMs

4.10.1. CBD increases mitochondrial superoxides in CBD-sensitive GBMs

To complement the study of ROS in CBD induced GBM death we next turned to the mitochondrial compartment which is vital for energy generation in the form of ATP and the main cellular source of ROS in the form of superoxides (SOX). To specifically detect mitochondrial superoxides at a single cell level, we used the MitoSOX-red dye on live human GBMs by flow cytometry [Mukhopadhyay P. et al. (2007)]. Interestingly, we found that CBD treatment significantly increased MitoSOX levels in good-responders while exerting no significant changes in low-responders. [Figure 4.24].

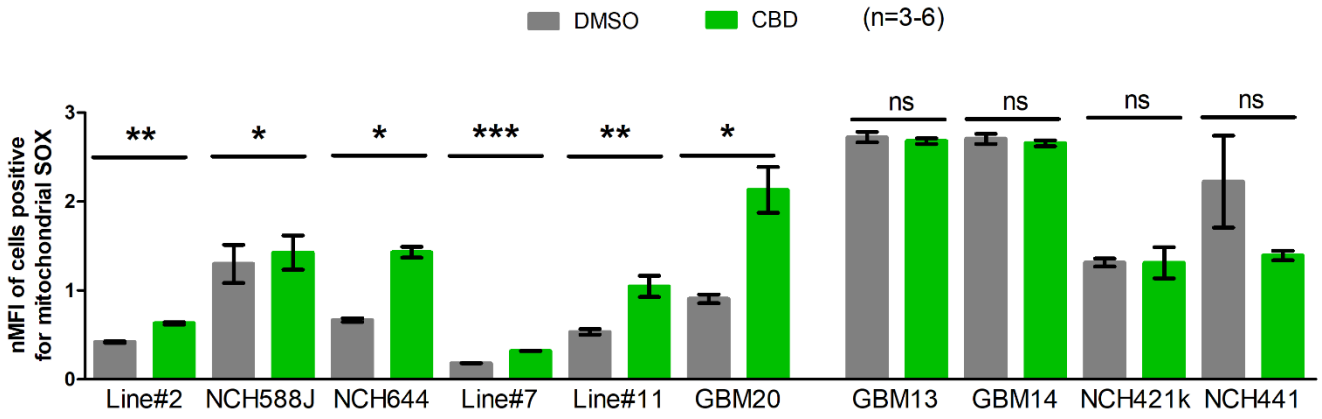

Figure 4.24 CBD increases mitochondrial superoxides only in good-responders. GBM cells were treated with 0,01% DMSO or 10μM CBD for 24 hours. The cell pellets were stained with MitoSOX-red and red fluorescence of the dye was acquired by flow cytometry. All gates were set using unstained controls for each GBM used and the gates were synchronized between unstained, DMSO, and CBD treated GBMs. The median fluorescence intensity (MFI) of positive cells was calculated for each gate and normalized to the number of positive cells (nMFI). The generated graph indicates the mean +/- SEM of the nMFI for DMSO (gray bar) and CBD (green bar) treated conditions. The experiment was repeated 3 to 6 times and the statistical significance of changes in mitochondrial superoxides was estimated with two-tailed paired t test.

4.10.2. CBD tends to increase mitochondrial mass and MMP in human GBMs

As significant changes in mitochondrial superoxides were observed in CBD-sensitive GBMs upon treatment, we investigated possible changes induced in the mitochondria themselves (mitochondrial mass). For this purpose, we used the MitoSpy-green, an equivalent to MitoTracker™ Green FM [Agnello M. et al. (2008)], as a mitochondrial localization probe that labels mitochondria independently of membrane potential. Mitochondrial mass was measured as green fluorescence positive signals by flow cytometry

[Pendergrass W. et al. (2004)]. There, we found a tendency towards an increase in mitochondrial mass upon CBD treatment [Figure 4.25-A].

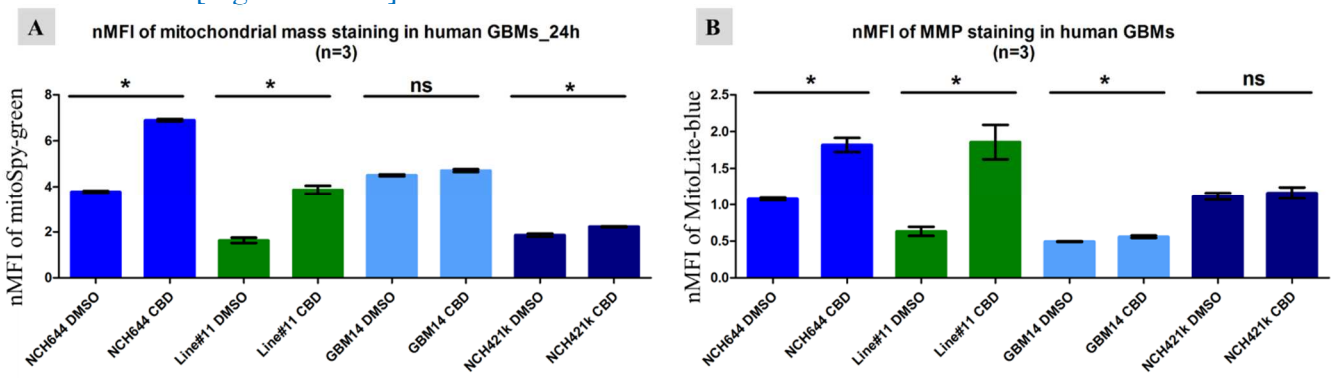

Figure 4.25 CBD induces changes in mitochondrial mass and membrane potential. GBM cells were cultured with 0,01% DMSO or 10µM CBD for 24 hours and stained with MitoSpy-green for mitochondrial mass (A) or MitoLite-Blue for MMP (B). Green and blue fluorescence intensities were detected by flow cytometry and the median fluorescence intensity (MFI) of positively stained cells determined. Graphs are representative of 3 independent experiments and show the MFI normalized to the number of positive events/cells (nMFI). For each GBM culture, the CBD treatment was compared to DMSO using two-tailed paired t test of mean +/- SEM.

As the formation of MitoSOX is dependent on mitochondrial membrane potential (MMP) [Li R. et al. (2011)], we investigated potential changes in MMP after CBD treatment. We used MitoLite™ Blue FX490 (MitoLite-blue), a cationic fluorogenic dye that utilizes the MMP to accumulate in mitochondria of live cells. Doing so, we found that CBD also tended to increase mitochondrial membrane potential in GBMs [Figure 4.25-B].

These data suggest that CBD treatment induces significant changes in GBM cell mitochondria in term of their mass, their membrane potential, and their production of superoxides.

4.11. Antioxidants for GBM therapy: friend or foe?

As we found that CBD could decrease the levels of water-soluble ROS, we tested the use of 7 pro-/anti-oxidants as potential combination therapeutics to potentiate CBD cytotoxic effect. Two substances yielded consistent results: EGCG and NAC. EGCG (Epigallocatechin gallate) is the most abundant polyphenol found in green tea and is described as a potent oxidative stress regulator in cancer cells [Du G-J. et al. (2012)]. However, in certain context (iron Fe^{3+}), EGCG may increase the production of hydrogen peroxides and act as a prooxidant [Kim H-S. et al. (2014)].

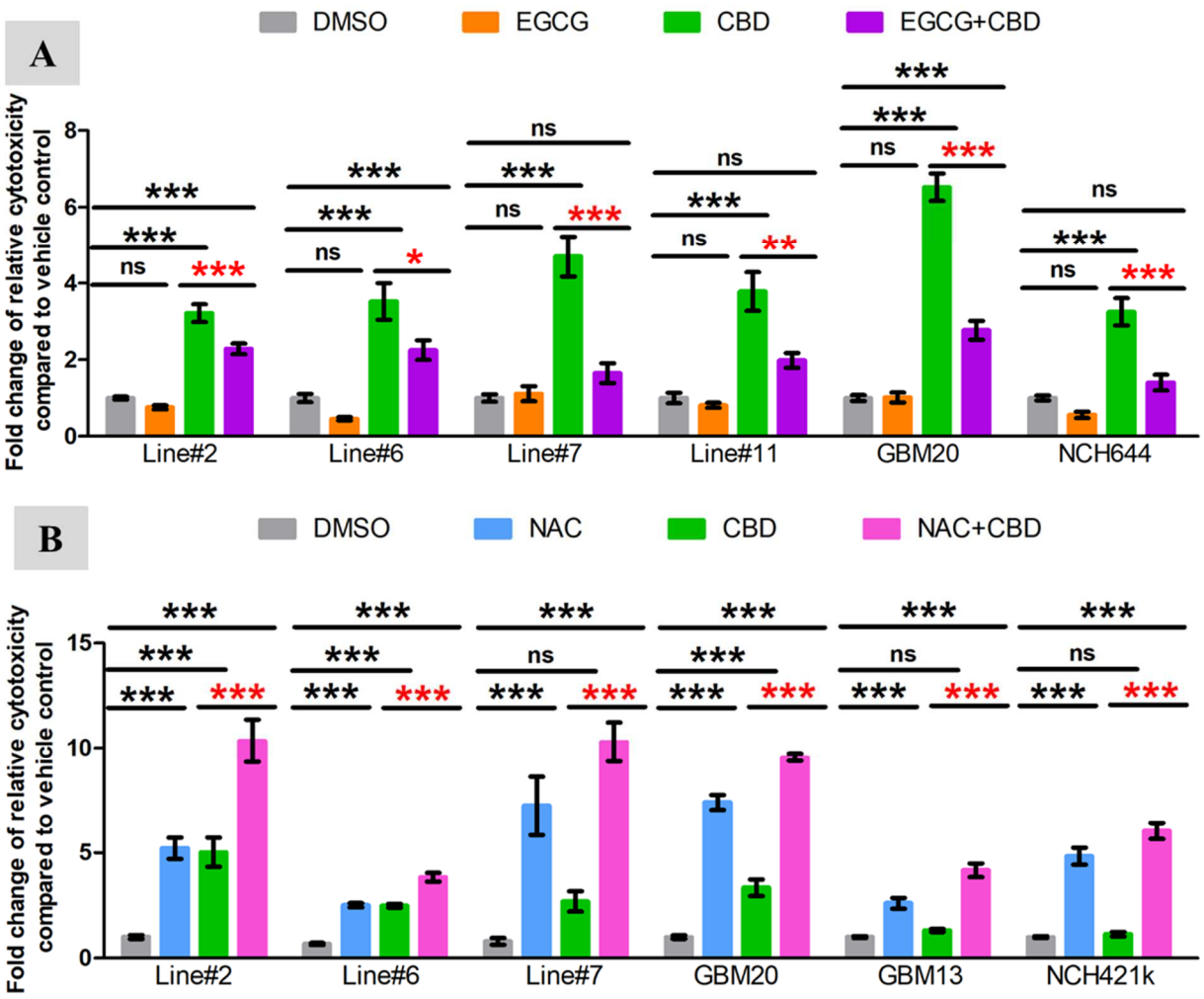

Figure 4.26 Redox regulators EGCG and NAC induce opposite effects on CBD induced GBM cytotoxicity. Human GBM cells were treated with DMSO, CBD and when evaluating the effect of EGCG 50µM EGCG, or 50µM EGCG and 10µM CBD or for NAC 5mM NAC, 5mM NAC+10µM CBD. The CytoToxFluor assay was carried out as previously described [Figure 4.9]. Graphs show the fold change of relative cytotoxicity compared to vehicle control for all conditions for the mean +/- SEM. One-way ANOVA with Bonferroni post-test was used to evaluate changes between different treatments: drug versus vehicle control (in black) or the CBD mono-treatment to the combination treatment of CBD with EGCG or NAC (in red).

We evaluated the effect of this polyvalent redox regulator on human GBMs and found that EGCG systematically reduced CBD cytotoxicity [Figure 4.26-A]. Another antioxidant, used in several assays *in vitro* and *in vivo* as ROS quencher, N-acetyl-L-cysteine (NAC) [Mokhtari V. et al. (2017)] was also used as a potential candidate for CBD potentiation *in vitro*. At 5mM, NAC showed to be a good candidate to potentiate the cytotoxicity effect of CBD on human GBMs. Interestingly, NAC exerted a significant cytotoxicity effect when used alone; and systematically increased CBD cytotoxicity even in low-CBD responders (GBM13, NCH421k) [Figure 4.26-B].

4.12. The level of intrinsic antioxidant response of human GBMs determines their sensitivity to CBD

4.12.1. CBD activates intracellular antioxidant systems

Data from the basal flow cytometry screen for ROS levels upon CBD treatment and the cytotoxicity effects of the antioxidant NAC alone and in combination with CBD, suggest that ROS are important for the survival of GBM cells. Indeed, we showed that CBD acted as an antioxidant by decreasing the ROS levels in the GBMs, and that the antioxidant NAC exerted cytotoxicity in GBM cells and potentiated CBD effect [Figure 4.26-B].

To evaluate the intrinsic antioxidant response of GBMs, cells were co-transfected with luminescent reporter plasmids encoding an antioxidant response element promoter (ARE-firefly) + internal control 4.74 HSV-tk (renilla luminescence) or a minimal promoter control (4.27 firefly + 4.74 renilla luminescence). At basal levels, we evaluated the extent of ARE activity in a good- and low-CBD responder. There, we found that the low-responder (GBM14) showed a significantly higher ARE activity compared to the good-responder NCH644 [Figure 4.27-A].

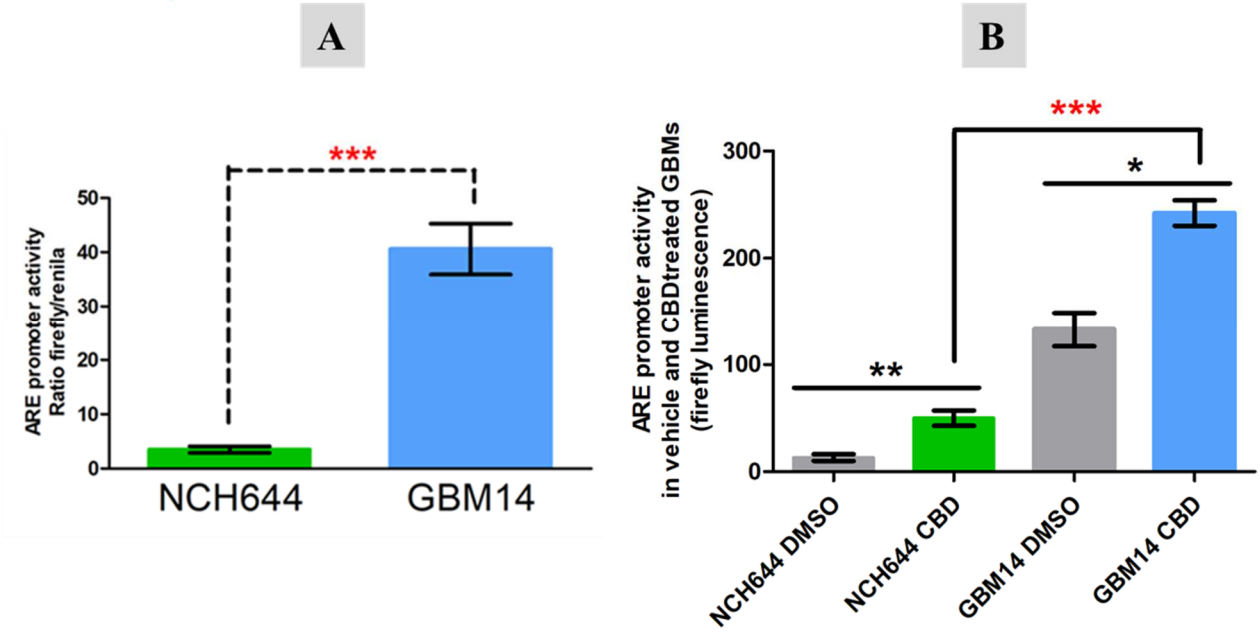

Figure 4.27 CBD increases antioxidant responses in human GBMs. GBM cells were co-transfected with 4.74-hRluc (expression control) and either 4.27-luc2P (minimal promoter) or 4.37-luc2P (ARE). Five cultures of two stably transfected human GBMs (NCH644 and GBM14) were treated with 0,01% DMSO or 10µM CBD for 24 hours. ARE promoter activity was calculated as the ratio of firefly/renilla luminescence at basal level (A). Two-tailed paired t test was used to evaluate the statistical significance of the changes comparing DMSO to CBD conditions (B) for a same GBM (in black) and changes in antioxidant responses between CBD treated good-responder NCH644 to low-responder GBM14 (in red) were evaluated using one-way ANOVA with Bonferroni post-test.

After treatment, we found that CBD could increase the levels of ARE activity in both low- and good-CBD responders; however, the extent of increase was more important in the good- responder NCH644 than in NCH421k [Figure 4.27-B]. Here again our data suggest that although GBM cells an intrinsic basal level of antioxidant responses, they are still under oxidative stress. Also, we showed that levels of water-soluble ROS were decreased upon CBD treatment [Figure 4.23] which could be linked to CBD inducing the mobilization of cellular antioxidant systems [Figure 4.27-B].

4.13. NFkB signaling pathway is crucial to CBD induced GBM death

4.13.1. Clues from mouse model of NFkB-p65 loss

The transcription factor array revealed CBD increasing NFkB nuclear binding in the good responder line#2, as opposed to the low-responder NCH421k [Figure 4.21]. This prompted us to explore the NFkB pathway further. To study the importance of NFkB signaling in CBD induced GBM death, we examined the changes in CBD effect in the presence or absence of NFkB. We have previously shown that p53 mutant status of some mouse proneural GBMs influenced their sensitivity to CBD induced cytotoxicity, e. g. p53R1272H mutation combined with PDGFB [Figure 4.9]. To generate a proneural glioma mouse model of inducible p53R172H expression with concomitant p65 loss, we used a mouse model of Li-Fraumeni syndrome with inducible p53R172H mutation [Olive K. P. et al. (2004)] in combination with conditional p65 loss. In this model, p53R172H mutated codons are preceded by LoxP sites flanking a STOP codon (Lox-STOP-Lox), assuring that the mutant p53 is not expressed without CRE mediated recombination [Tuveson D. A. et al. (2004)]. Concomitantly, the rel-a (p65) gene on chromosome 19 is also preceded by another set of LoxP sites flanking a STOP codon (Lox-STOP-Lox).

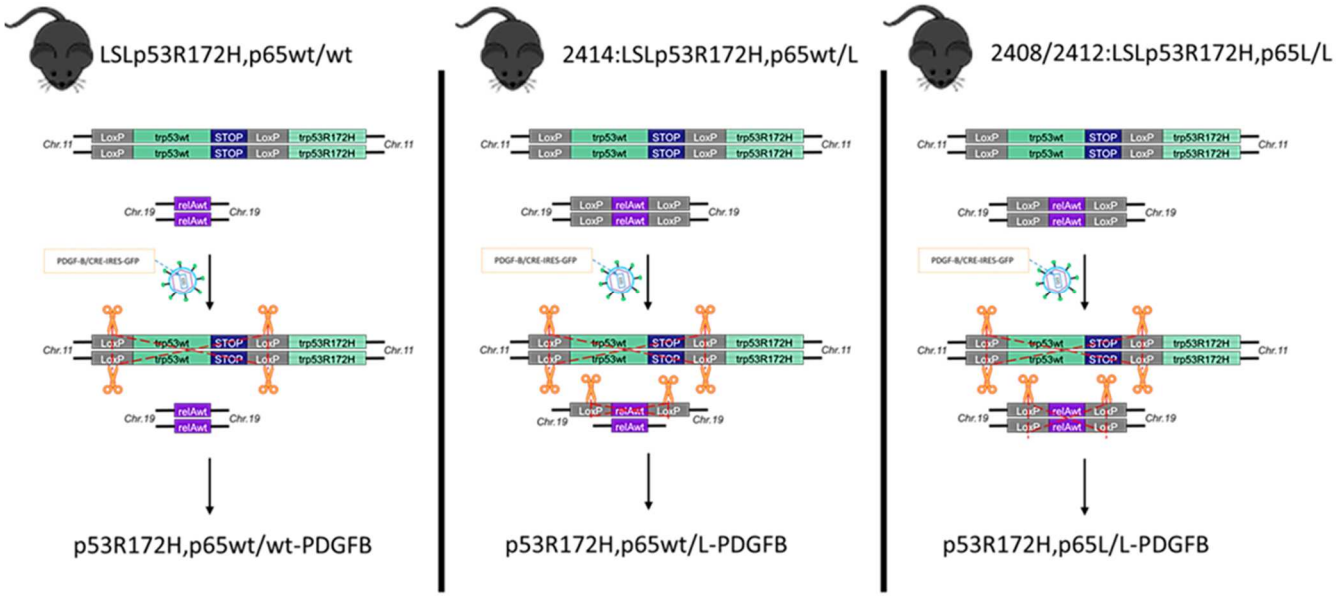

Figure 4.28 Generation of proneural mouse model with mutant p53 status and NFkB-p65 loss. Mice were engineered for p53R172H (chromosome 11) and p65 (chromosome 19) preceded by Lox-STOP-Lox sites. NPC cultured were generated from SVZ of engineered mice, expanded, and transduced with recombinant viral vectors encoding CRE recombinase and PDGFB under biosafety level 2 conditions. The genetic recombinations to obtain the different models are indicated: p53R172H,p65 wt/wt-PDGFB (after viral transduction the cells express p53R172H, express wild type p65 from both alleles, and overexpress PDGFB), p53R172H,p65wt/L-PDGFB (after viral transduction the cells express p53R172H, have one functional allele of p65, and overexpress PDGFB), p53R172H,p65L/L-PDGFB (after viral transduction the cells express p53R172H, lose their p65 on both alleles, and overexpress PDGFB).

We generated SVZ-NPC cultures from the genetically engineered mice and transduced the cells with viruses encoding CRE recombinase and PDGFB. This model was controlled using two other models of p53R172H-PDGFB proneural glioma with two intact alleles of p65wt or only one functional allele [Figure 4.28].
The genotypes of the mice used for the models and the recombination have been re-verified by fluorescence microscopy for viral transduction efficiency. Recombination PCR was conducted for trp53 mutant and p65,

and we obtained after CRE recombination a band at the correct size of 330bp for trp53 mutant [Figure 4.29-A1] and 1,7 kb for p65 deletion [Figure 4.29-A2].

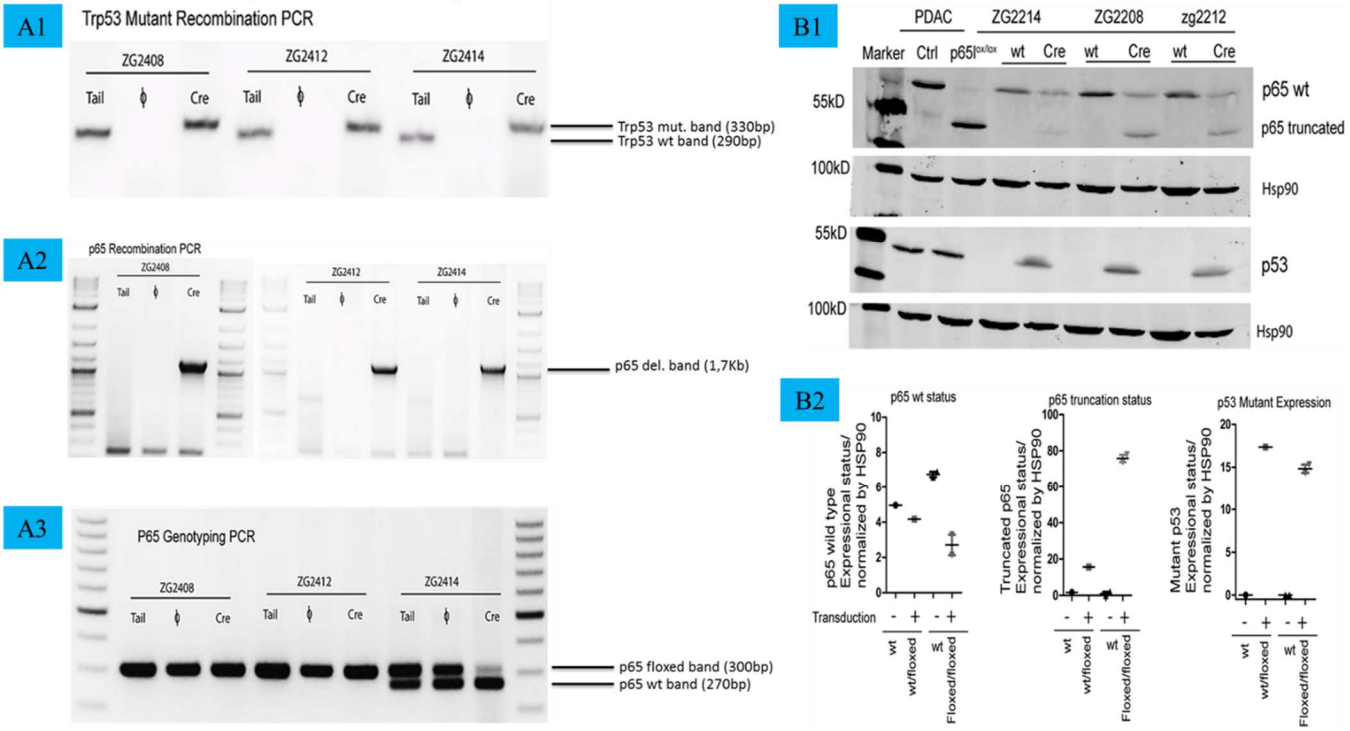

Figure 4.29 Characterization of generated mouse proneural glioma models with NFkB-p65 loss. SVZ-NPC cultures were generated from the genetically engineered mice and the cells were virally transduced to express CRE recombinase and PDGFB. To verify the virally induced genetic recombination, 10^6 cells from each model were pelleted and DNA extracted. PCR was carried out to verify the recombination at p53 (A1) and p65 (A2) loci followed by agarose gel electrophoresis. For p53 recombination, samples from the mouse tail and un-transduced NPCs (no recombination = no mutant band at 330bp) versus samples after CRE show a mutant band at 330bp (A1). Recombination PCR for p65 deleted band (1,7Kb) also comparing mouse tail, un-transduced NPC and CRE transduced NPCs (A2). A p65 genotyping PCR was conducted to detect p65flx band (300bp) or p65-wt band (270bp) in the 3 models (A3). Western blot was carried out to verify the modifications at the protein level for p53 and p65. Pancreatic ductal adenocarcinoma cells (PDAC) with known genetic background were used as control for blot detection of mouse cells with p65 wild-type allele, p65 truncated allele, and mutant p53. Hsp90 housekeeping protein was used as loading control (B1). Blots were quantified in ImageJ for expression of p65-wt, p65-truncated, and mutant-p53 for samples 2414 and 2408 by comparing the intensity of protein bands before and after CRE recombination and the value was normalized to that of the loading control HSP90 (B2).

Genotyping PCR was conducted for p65 using DNA from all 3 mouse models before and after CRE recombination. For models with homozygous loxP sites around p65 loci (2408 and 2412), no wild-type band was detected, while wild-type (270bp) and floxed (300bp) bands were detected for 2414 with heterozygous p65 deletion [Figure 4.29-A3]. Western blot was performed to detect the changes at the protein level and show truncated band of p65 after CRE recombination along with mutant p53 bands in the samples [Figure 4.29-B1]. The quantification of the blots clearly shows decreased p65wt expression, increased truncated p65, and increased p53-mutant expression after recombination. [Figure 4.29-B2].
After the background genotype and the induced recombinations have been verified, the cytotoxicity effect of CBD was re-evaluated on the transgenic glioma models.

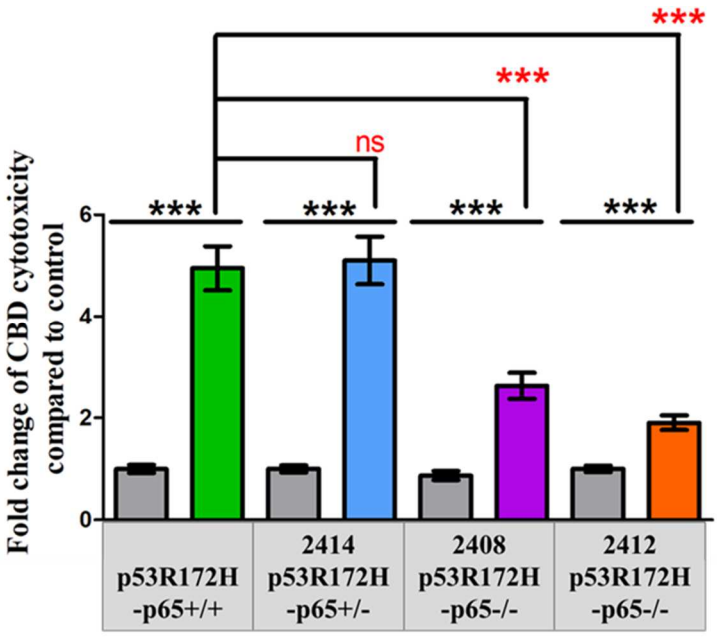

Figure 4.30 Importance of NFkB-p65 for CBD induced cytotoxicity / mouse models. Mouse glioma cells with alterations in NFkB-p65 were obtained after genetic recombination [Figure 4.30 &4.31] and used in quintuplicates in the CytoTox Fluor cytotoxicity assay for at least 3 independent experiments. The graph indicates the fold change of cytotoxicity compared to DMSO control with DMSO treated samples as gray bars, CBD treated samples as colored bars. Data are represented as mean +/- SEM and two tailed paired t test was used to compare CBD to DMSO treated cells for a same model (black stars) and one-way ANOVA with Bonferroni multiple comparison test (in red) was used when comparing the cytotoxicity of CBD in model with homozygous wild-type p65 (p65+/+) and the models with deleted alleles of p65 (p65+/- and p65-/-).

We found that the propensity of CBD induced cytotoxicity for the model with one allele of p65wt is comparable to the model with a full p65wt condition. However, when both alleles of p65 are deleted, the CBD induced cytotoxicity is significantly reduced. Therefore, intact p65 seems to play a critical role in CBD induced GBM death [Figure 4.30].

4.13.2. CBD induces NFkB-p65 nuclear translocation in drug sensitive GBMs.

To confirm the importance of NFkB-p65 in CBD induced GBM death, we started by comparing Line#2 (good-responder) to NCH421k (non-responder) for NFkB-p65 nuclear translocation upon treatment. Indeed, active NFkB complex is a nuclear complex composed most commonly of a heterodimer between the p65 and p50 subunits. The subunits both have DNA binding sequences and p65 contains the transactivation domain of the complex which is used by IkB to retain the subunit in the cytoplasm. Upon activation, NFkB-p65 is freed from its interaction with IkB and its nuclear localization signal is made available to direct its translocation to the nucleus [Ganchi P. A. et al. (1999)].

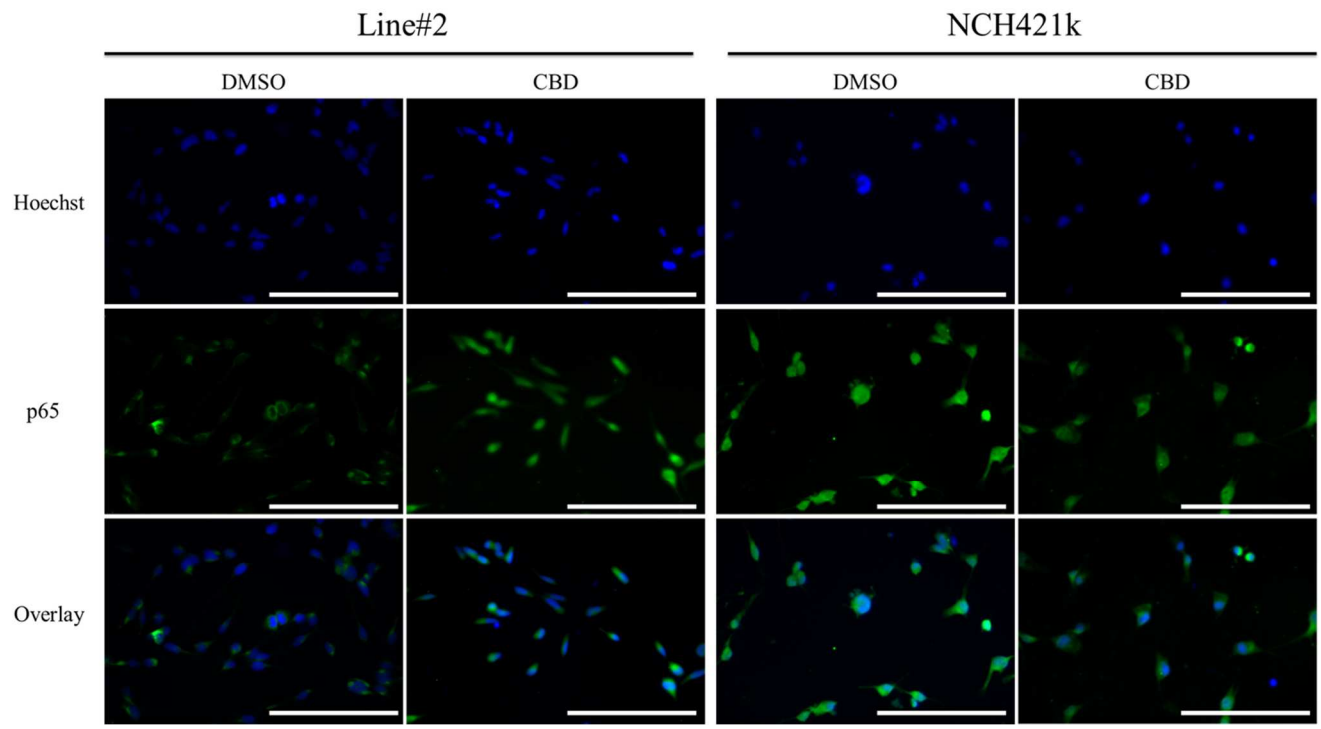

Figure 4.31 Immunofluorescence staining for NFkB-p65 nuclear translocation (group1). Human GBM cells good-CBD responder (Line#2) and a low-responder (NCH421k) were treated with DMSO or CBD for 20 hours. All wells were stained with rabbit anti-p65 primary antibody and nuclei counter stained with Hoechst 33342. Fluorescent pictures were acquired at 40x magnification and show from top to bottom the Hoechst staining (blue), the p65 (green) and the overlay of Hoechst and p65. Scale Bars = 150µm.

Consistent with the transcription factor array, we found that CBD induced nuclear translocation of NFkB-p65 only in Line#2. In the low-CBD responder, the levels of NFkB-p65 were already high at basal levels and tended to decrease upon treatment [Figure 4.31].

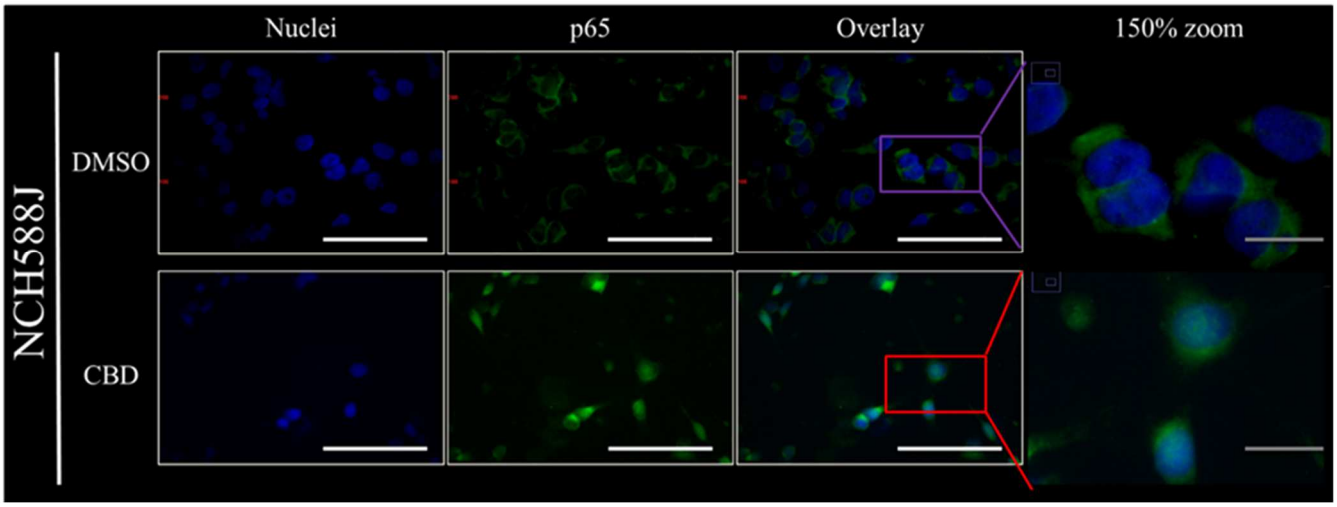

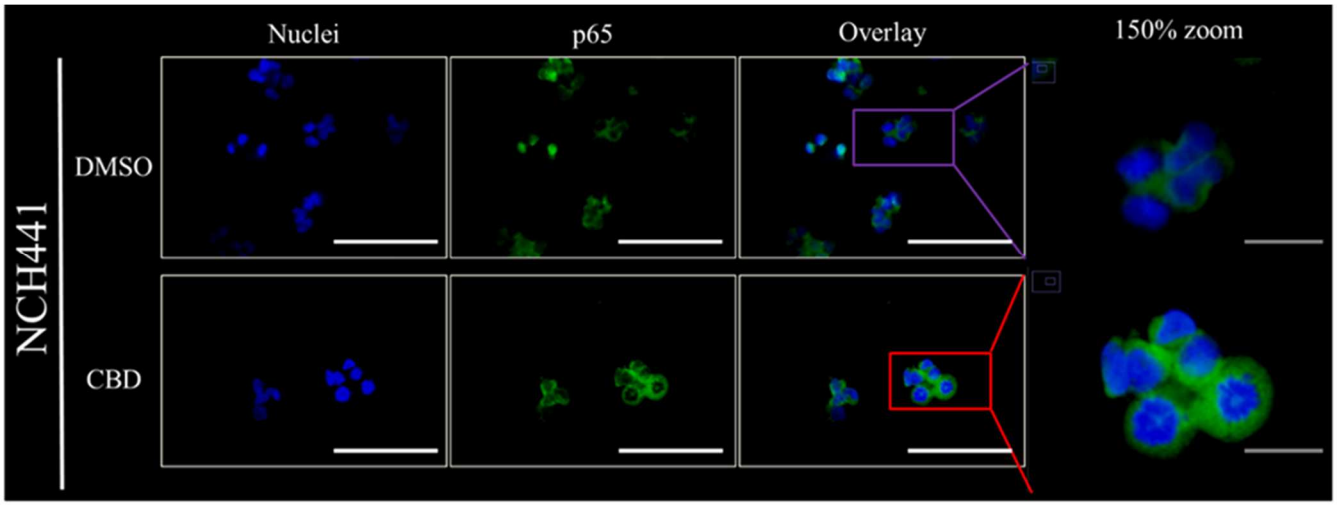

Figure 4.32 Immunofluorescence staining for NFkB-p65 nuclear translocation (group2). Cells plated in 8 well glass dishes coated with poly-ornithine and laminin were treated for 20 hours with 0,01% DMSO or 10µM CBD. Staining was conducted as previously [Figure 4.31]. The staining of a good-responder (NCH588J) and a low-responder (NCH441) are shown; the figure shows from left to right the nuclei counterstained with Hoechst 33342 (blue), p65 staining (green), and the overlay of nuclei and p65 staining with a 150% enlargement showing a closer image of the nuclei. For each GBM, the DMSO treated cells are on top and the CBD treated on the bottom. White scale bars indicate 100µm, and gray scale bars for the zoom indicate 25µm.

We enlarged the screening panel to obtain 3 responders versus 3 low-responders. Again, the finding was confirmed. We concluded that CBD induced GBM death does not occur if NFkB-p65 is not functional to be translocated to the GBM nuclei [Figure 4.32].

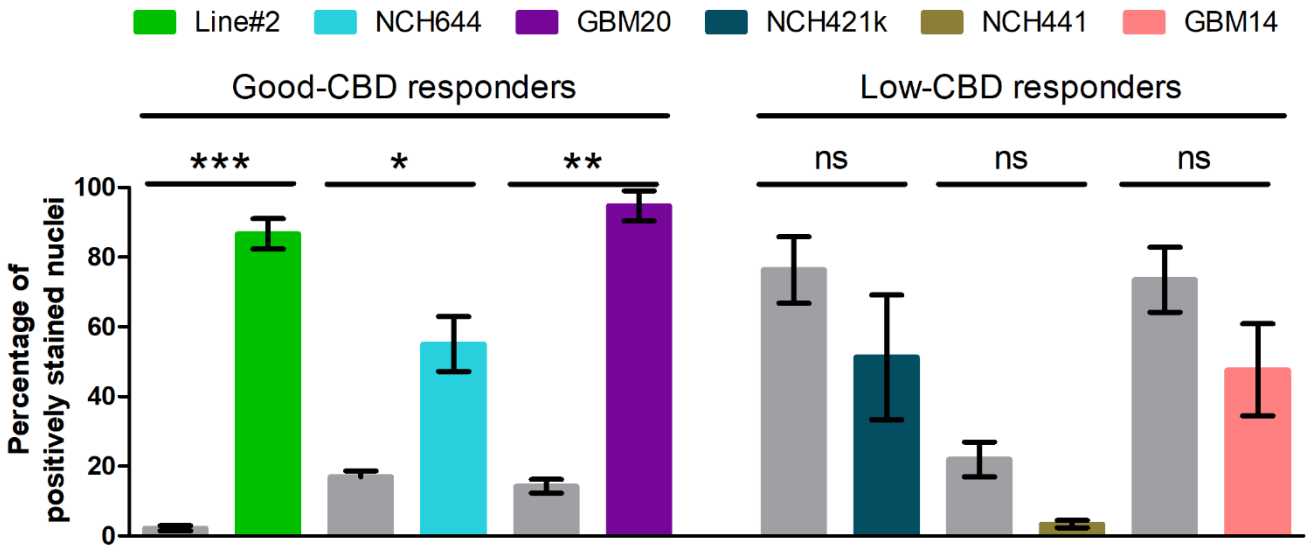

Figure 4.33 CBD treatment increases the nuclear accumulation of NFkB-p65 only in good-CBD responders. p65 immunofluorescence antibody staining and pictures acquisition were conducted as described previously [Figure 4.34]. The graph indicates the percentage of positively stained nuclei in DMSO (gray bar) and CBD (colored bar) treated GBMs. Three good-responders (Line#2, NCH644, GBM20) and 3 low-responders (NCH421k, NCH441, GBM14) were used. Two-paired t test statistical analysis was conducted comparing the mean +/- SEM of CBD (colored bars) to DMSO (gray bars) treated cells.

We quantified the staining for at least 3 independent experiments and found that CBD significantly increased nuclear translocation of p65 only in good-CBD responders (Line#2, NCH644, GBM20), while no significant changes were seen in low-responders (NCH421k, NCH441, GBM14) [Figure 4.33].

4.13.3. CBD decreases TNFα induced NFkB promoter activity

4.13.3.1. TNFα can induce NFkB promoter activity only in good-CBD responders

As nuclear translocation was observed in responders, we checked the capacity of CBD to induce NFkB promoter activation in a promoter activation reporter assay. The reporter plasmid contains a destabilization domain (DD) which in the absence of the small molecule Shield1 will target the reporter fluorescence for proteasomal degradation [Banaszynski L. A. et al (2006)]. When Shield1 was applied with DMSO, we could monitor the basal NFkB promoter activity in the GBMs and compare it to the CBD treated cells. TNFα was used as positive inducer of NFkB promoter activity [Poligone B. et al (2001)].

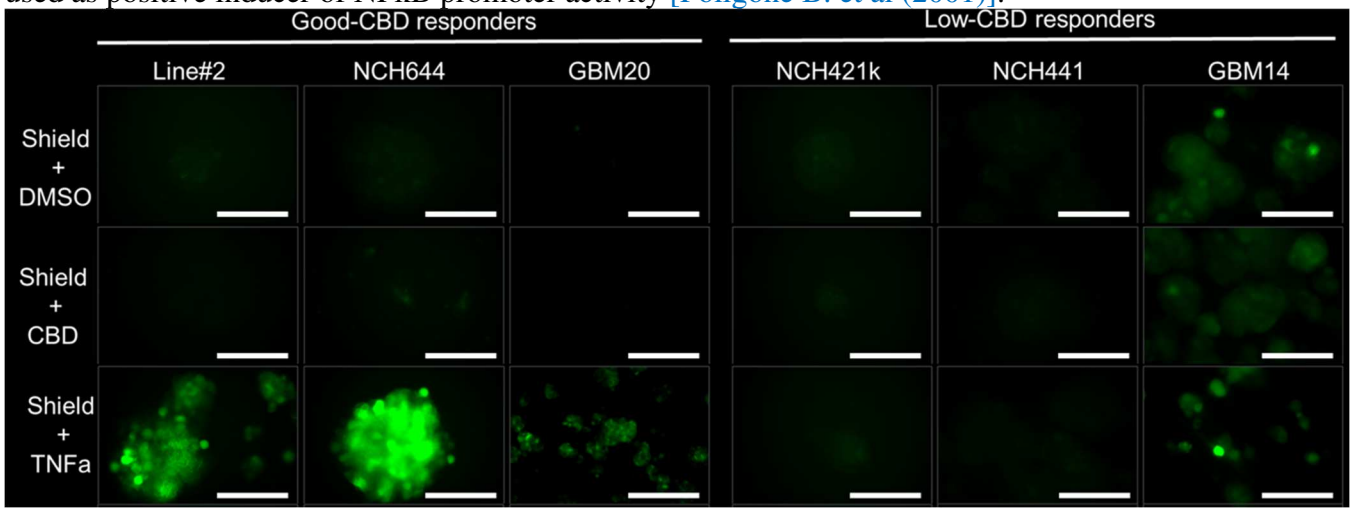

Figure 4.34 Evaluating the effect of CBD on GBM NFkB promoter activity. Human GBM cells stably transfected with the pNFkB-DD-ZsGreen1-neo reporter plasmid were exposed to 3 treatment conditions after addition of stabilizing molecule Shiled-1: 0,01% DMSO, 10μM CBD, or 10ng/ml of TNFα. A panel of 3 good-(Line#2, NCH644, GBM20) and Low-(NCH421k, NCH441, GBM14) CBD responders was used. After 20 hours of incubation, wells were inspected for green fluorescence as a reporter for NFkB promoter activation. Images were acquired in a fluorescence microscope at 40x magnification. Scale bars = 100μm.

We found that CBD did not induce an increase in NFkB promoter activity in the responders. In the non-responders NH421k and NCH441 no changes where observed as well and not even when using TNFα. The non-responder GBM14 already had a high basal level of NFkB promoter activity that did not change upon CBD or TNFα treatment. Unexpectedly, only in good-CBD responders could TNFα induce promoter activation [Figure 4.34].

4.13.3.2. CBD decreases TNFα induced NFkB promoter activity

We turned to flow cytometry to quantify the changes in NFkB promoter activity at the single cell level, starting with the good-CBD responder Line#2.

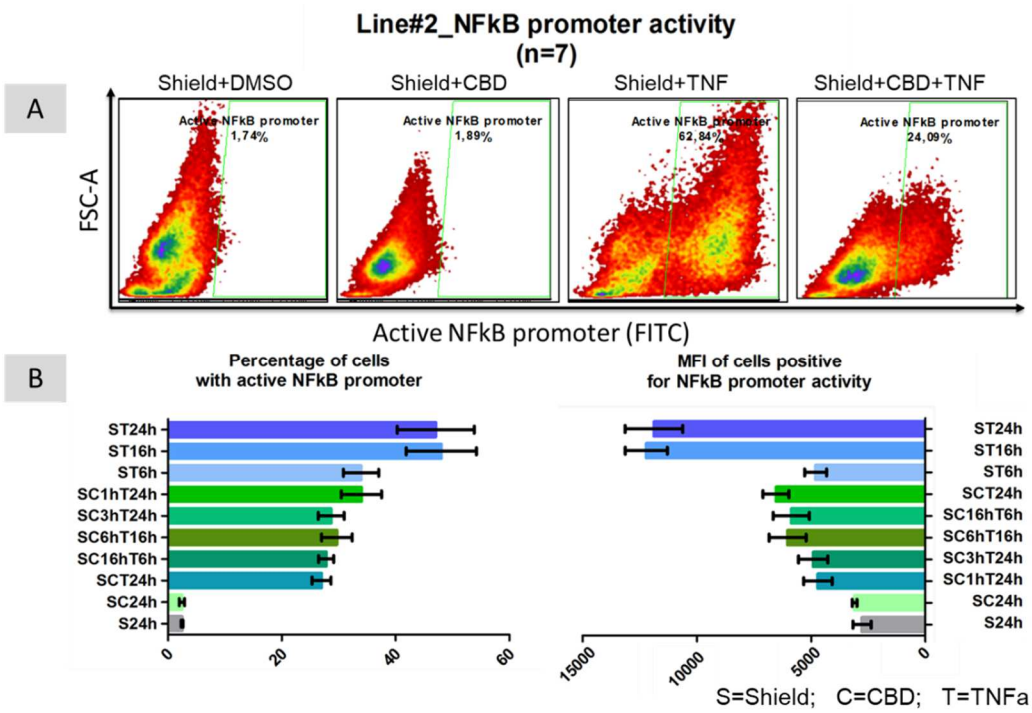

Figure 4.35 CBD decreases TNFα induced NFkB promoter activation. Line#2 stably transfected with pNFkB-DD-Zsgreen1-neo reporter plasmid was treated with TNFα at 0-, 1-, 2-,4-,8-,10-,20-,30-,40-, and 50 ng/ml. After 24 hours, green fluorescence reporter of NFkB promoter activity was acquired by flow cytometry. The graph shows the mean +/- SEM of the percentage of cells positive for NFkB promoter activity for 3 independent experiments (Panel I). The effect of CBD treatment on TNFα induced NFkB promoter activation was evaluated in Line#2. Flow cytometric density plots of Line#2 treated with a combination of shield and DMSO, CBD, TNFα, TNFα+CBD are represented in Panel II. The effect of CBD pre-treatment (1-, 3-, 6-, 16 hours) on promoter activation was measured by flow cytometry. The percentage and median fluorescence intensity (MFI) of cells with active NFkB promoter are indicated in Panel B.

Density FACS plots show no induction of promoter activity when Line#2 is treated with Shield+DMSO or Shield+CBD. Upon TNFα treatment cells accumulate in the positive gate and we observe a decrease in this accumulation when cells receive CBD and TNFα [Figure 4.35-A]. To evaluate the inhibitory role of CBD on NFkB promoter activation, we pre-treated a good CBD responder Line#2 with CBD for 1-, 3-, 6-, or 16 hours before applying TNFα. At all considered time points, pre-treating Line#2 with CBD before adding TNFα for 24 hours reduced the promoter activity [Figure 4.35-B].

We enlarged the screening to other good- (NCH588J, NCH644, Line#11, GBM20) and low- (NCH421k, NCH441, GBM13) CBD responders, and came to the same conclusion. Although CBD induces NFkB-p65 nuclear translocation in good-CBD responders [Figure 4.33], it does not induce NFkB promoter activity, but decreases promoter activation induced by TNFα [Figure 4.36].

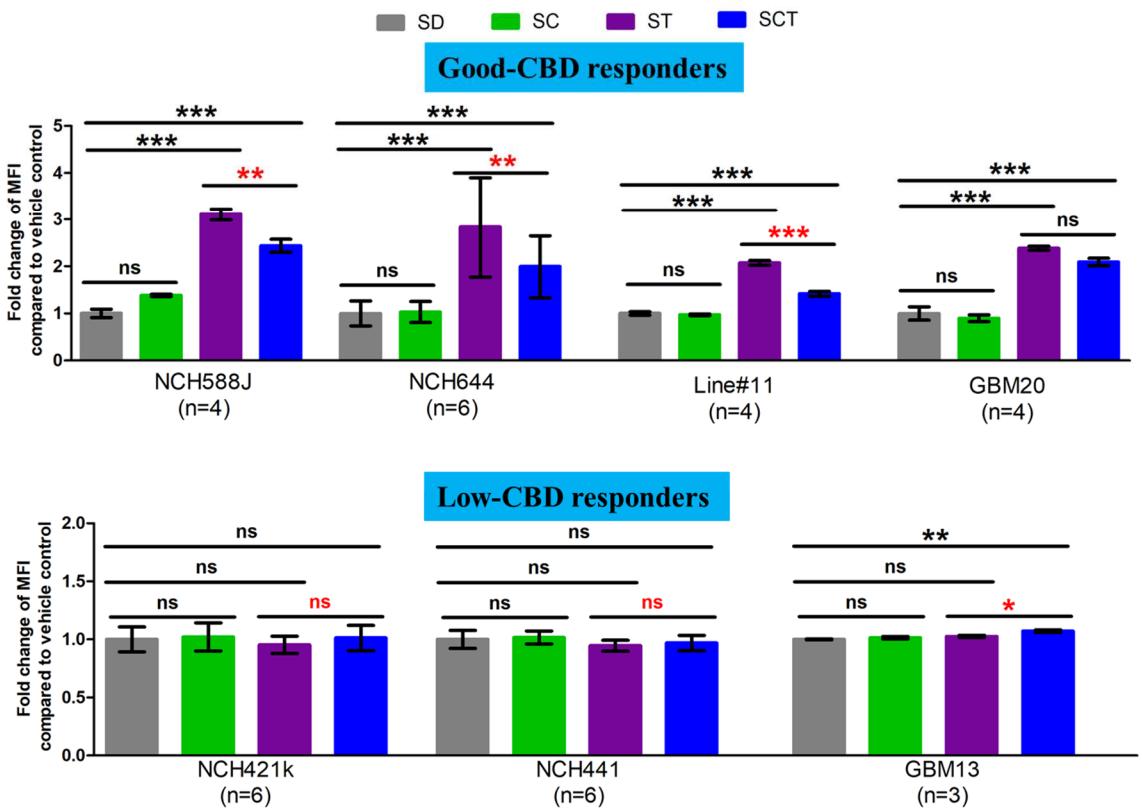

Figure 4.36 Only in good-CBD responders does CBD decrease TNFα induced NFkB promoter activation. GBM cells, good- (NCH588J, NCH644, Line#11, GBM20) and low- (NCH421k, NCH441, GBM13) CBD responders, were subjected to 4 treatment conditions: 500nM Shield + 0,01% DMSO (SD), 500nM Shield + 10μM CBD (SC), 500nM Shield + 1ng/ml TNFα (ST), or pre-treated with 10μM CBD for 6 hours then incubated with 10μM CBD for 20 hours (SCT). Green fluorescence of the pNFkB-DD-ZsGreen1 plasmid in cells with active NFkB promoter was measured by flow cytometry. Graphs show the mean +/- SEM of percentage of cells with active promoter activity. Two-tailed paired t test was used to evaluate the changes between ST treatment condition and SCT condition.

In low-CBD responders, both TNFα and CBD failed to induce NFkB promoter activity. In one low-responder, GBM13, we found a significant increase in promoter activity when TNFα and CBD are used in combination, but it is probably due to the low variability observed in this sample.

4.13.4. The NRF2 activator DMF potentiates CBD induced cytotoxicity

We have shown that although functional NFkB-p65 is needed for CBD induced GBM death [Figure 4.33], CBD treatment does not induce NFkB transcriptional activity, but rather decreases TNFα induced NFkB promoter activation [Figure 4.36]. Also, we showed that antioxidant response elements (ARE) are active at basal level in GBMs and that CBD treatment, while decreasing water-soluble ROS [Figure 4.23], significantly increases ARE activity in good- and low-CD responders [Figure 4.27]. Therefore, increasing antioxidative response in GBMs seems to be detrimental to GBM survival. Dimethyl fumarate (DMF) is a clinically approved antioxidant, that activates NRF2 pathway. It is used for the treatment of multiple sclerosis and psoriasis [Wang Q. et al. (2015)] and was shown to decrease the expression of stem cell marker CD133 and NFkB in glioblastoma and to inhibit the transcription of inflammatory cytokines such as IL6 and TNFα [Ghods A. L. et al. (2013)]. We tested the effect of DMF on a CBD sensitive GBM Line#2 in MTT and cytotoxicity assays.

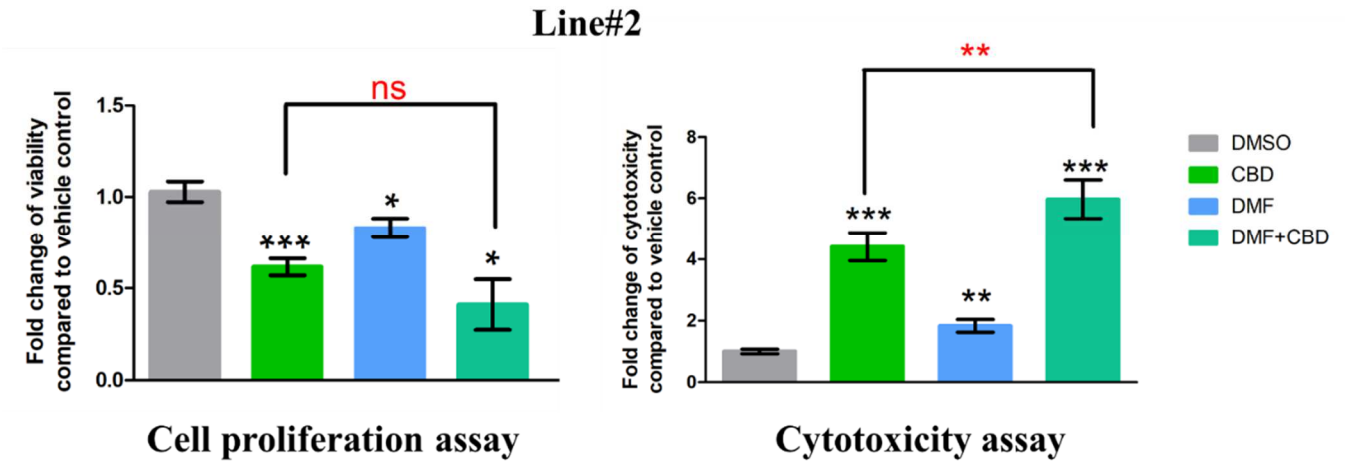

Figure 4.37 DMF potentiates CBD cytotoxicity in a combination therapy of GBM-Line#2. Line#2 (good-CBD responder) was used to test the effect of Dimethyl fumarate (DMF) used a mono-treatment or in combination with CBD in a MTT assay and cytotoxicity assay. Cells were treated for 72 hours for the MTT assay and for 20 hours for the cytotoxicity assay. Treatment conditions were either 0,01% DMSO, 10µM CBD, 10µM DMF, or co-treated with 10µM CBD + 10µM DMF. The absorbance was recorded for the MTT assay whereas the fluorescence intensity was measured for cytotoxicity assay. Graphs were generated for both assays and indicate the fold change in viability/proliferation (left) and cytotoxicity (right) induced by CBD and/or DMF compared to vehicle control. The experiments were repeated 3 times and two-tailed paired t test of mean +/- SEM was used to compare the different treatments to DMSO control (black stars) and One-way ANOVA with Bonferroni post-test comparing CBD to CBD+DMF (red).

In good-CBD responder Line#2, DMF alone already decreased the viability of the cells and increased their death. Combining DMF and CBD, significantly increased CBD cytotoxicity in this GBM [Figure 4.37]. Therefore, DMF might be a good candidate to potentiate antioxidative cytotoxicity effect of CBD in GBMs.

4.14. Evaluation of a patient stratification scheme for beneficial CBD therapy

4.14.1. Sets of genetic alterations qualifying for successful CBD therapy

To evaluate if GBM genetic alterations could be used to predict their response to CBD treatment, we started by comparing the outcome of the cytotoxicity assay for the genetically engineered mouse models [Figure 4.9]. These glioma models bear either loss or mutation of tumor suppressors (p53, cdkn2a, PTEN, NF1), and overexpress oncogenes (PDGFB, EGFR/EGFRvIII) [Figure 3.1].

The cytotoxicity assay allowed us to categorize the mouse gliomas into low- and good-CBD responders, and we used their genetic make-up to evaluate a stratification scheme predicting CBD response. We found that classical mouse gliomas were always sensitive to CBD (4 to 10-fold cytotoxicity), depending on genetic alterations, some proneural mouse gliomas were very sensitive (e.g. p53R172H-PDGFB) whereas other are less sensitive (e. g. cdkn2aKO-PDGFB) [Figure 4.9]. Therefore, a stratification based only on the genetic subtype would not be accurate. Therefore, we ought to find a more reliable stratification strategy.

4.14.2. Metabolic markers to predict the outcome of CBD mediated GBM therapy

4.14.2.1. *In vitro*, basal ROS levels inversely correlate with the extent of CBD induced GBM death

We showed that CBD treatment decreased ROS in mouse and human GBMs regardless of CBD sensitivity, we wanted to discover if we could differentiate between prospective CBD sensitive and insensitive GBM subsets before any treatment. GBMs were taken at basal levels without any treatment and stained for water soluble ROS using the cell permeant-H2DCFDA dye. Quantitative flow cytometry was performed to obtain the molecules of equivalent fluorescein (MEFL) of DCF positive GBMs.

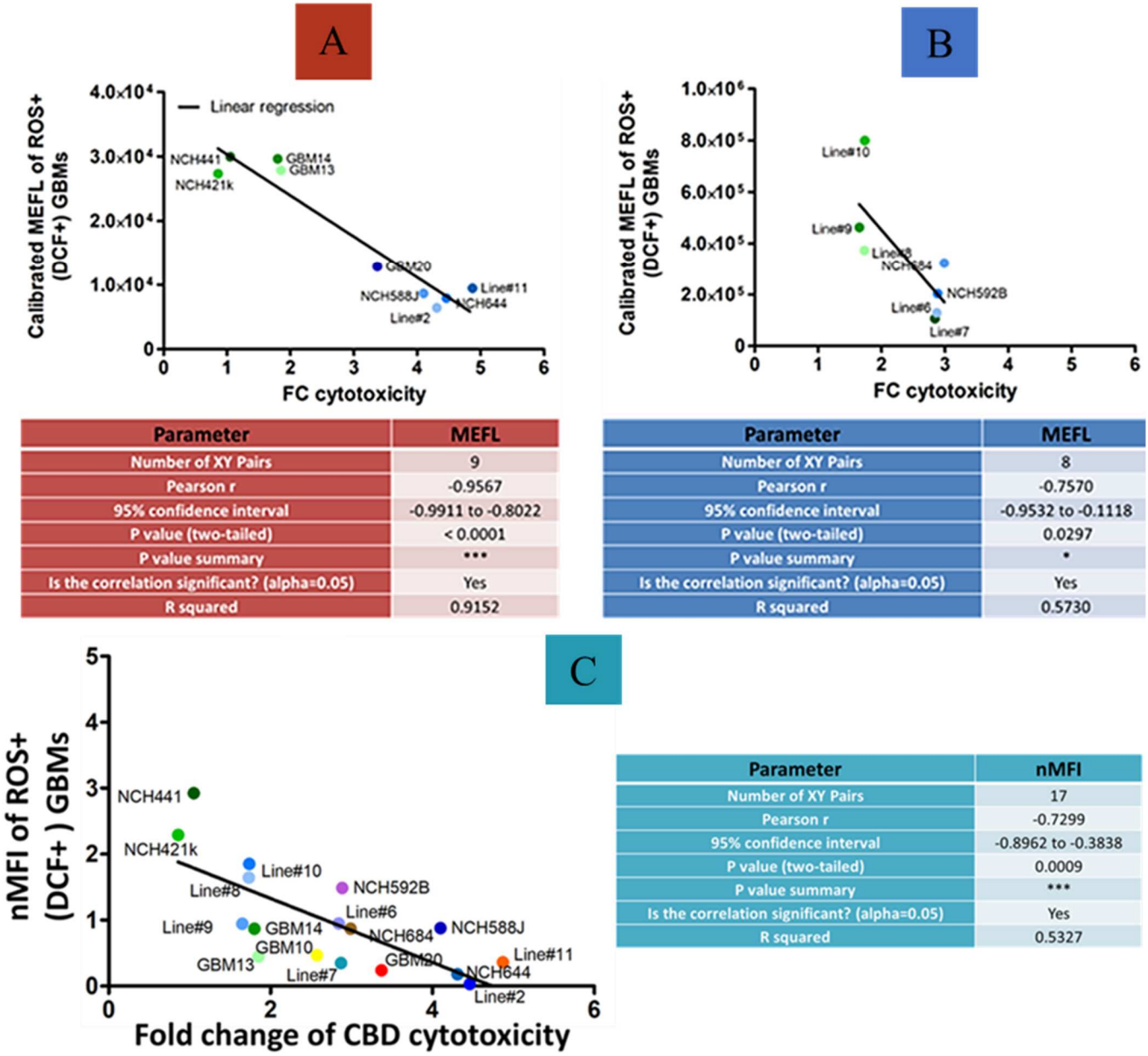

Parameter	MEFL
Number of XY Pairs	9
Pearson r	-0.9567
95% confidence interval	-0.9911 to -0.8022
P value (two-tailed)	< 0.0001
P value summary	***
Is the correlation significant? (alpha=0.05)	Yes
R squared	0.9152

Parameter	MEFL
Number of XY Pairs	8
Pearson r	-0.7570
95% confidence interval	-0.9532 to -0.1118
P value (two-tailed)	0.0297
P value summary	*
Is the correlation significant? (alpha=0.05)	Yes
R squared	0.5730

Parameter	nMFI
Number of XY Pairs	17
Pearson r	-0.7299
95% confidence interval	-0.8962 to -0.3838
P value (two-tailed)	0.0009
P value summary	***
Is the correlation significant? (alpha=0.05)	Yes
R squared	0.5327

Figure 4.38 CBD cytotoxicity inversely correlates with basal GBM ROS levels. Human GBMs were stained with H2-DCFDA, washed and immediately acquired by flow cytometry. Rainbow calibration particles (RCP) of known concentration of molecules of equivalent fluorescein (MEFL) were acquired using the same laser settings. The median

fluorescence intensities (MFI) of DCF positive GBMs and RCP were determined in positive gates. The MFI of DCF positive GBMs was used to calculate their molecules of equivalent fluorescein (MEFL) based on the MFI of the RCPs with known MEFL. The generated graphs show the linear regression comparing the MFL of DCF positive GBMs to their fold change (FC) of CBD induced cytotoxicity (A and B). The MFI normalized to number of positive cells (nMFI) was also compared to the fold change of CBD induced cytotoxicity (C). Correlation analysis was conducted for all comparisons and summarizes in a table the 95% confidence interval, the p value and the R squared.

Linear regression analyses showed that levels of ROS inversely correlate with the fold change of cytotoxicity induced by CBD [Figure 4.38 A, B]. Because of two different instruments settings and more than one-year elapsed time between the two rounds of measurements, two different correlation graphs were generated. Therefore, we also normalized MFI of ROS in all GBMs (nMFI) were plotted in a single graph and again compared to CBD induced cytotoxicity, and we again found a significant inverse correlation between basal ROS level and putative CBD sensitivity [Figure 4.38 C].

4.14.2.2. Basal ROS levels can serve as predictive biomarker for CBD response in *ex vivo* GBM biopsies

We engaged in translating our *in vitro* findings to a setting that could be applied in the clinics, by performing *ex vivo* measurements of ROS in patient derived GBM xenografts from mouse brains in bulk tumor tissue or in xenograft single cell suspension.

4.14.2.2.1. Measurement of *ex vivo* ROS in bulk tumor tissue

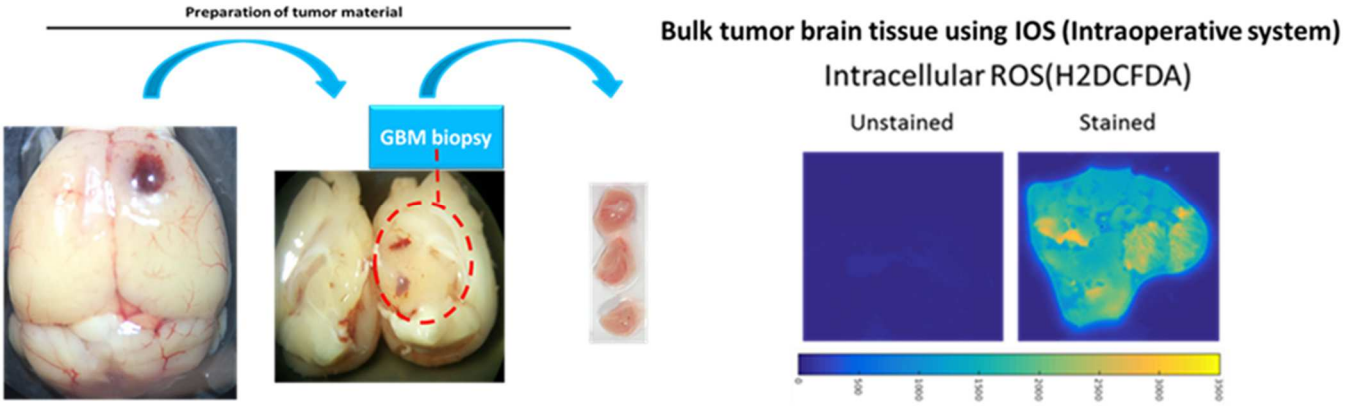

Figure 4.39 GBM ROS can be detected *ex vivo* in bulk tumor tissue. Staining of bulk biopsy and detection of intracellular ROS. The tumor was localized on the right hemisphere and dissected from nude mice brain. The tumor mass was chopped into 2mg pieces, and tumor tissue inoculated with H2DCFDA ROS dye. The bulk tumor tissue was surrounded by 2 glass coverslips and the ROS fluorescence imaged in the intraoperative system (IOS) and compared to the unstained tissue. The color scale indicates the extent of ROS detection from dark blue (no fluorescence detected) to bright yellow (the most intense fluorescence detected).

To evaluate the suitability of the intraoperative system (IOS) for our detection purpose, we first tested bulk tumor biopsies comparing unstained to H2DCFDA (intracellular) ROS dye. There, we showed that intracellular ROS could be detected in bulk GBM tissue, but proper quantification would be difficult because of uneven dye distribution in the tumor tissue [Figure 4.39]. Therefore, we tested the use of cells and/or mashed biopsy suspension in the IOS.

4.14.2.2.2. Basal GBM ROS measurement is reliable across different platforms

The *ex vivo* measurement of basal ROS levels was conducted in different platforms and different combination of low- and good-CBD responders in the IOS using tubes or glass capillaries, in fluorescence spectroscopy using another water-soluble ROS dye (MAK-142) and in flow cytometry (H2-DCFA).

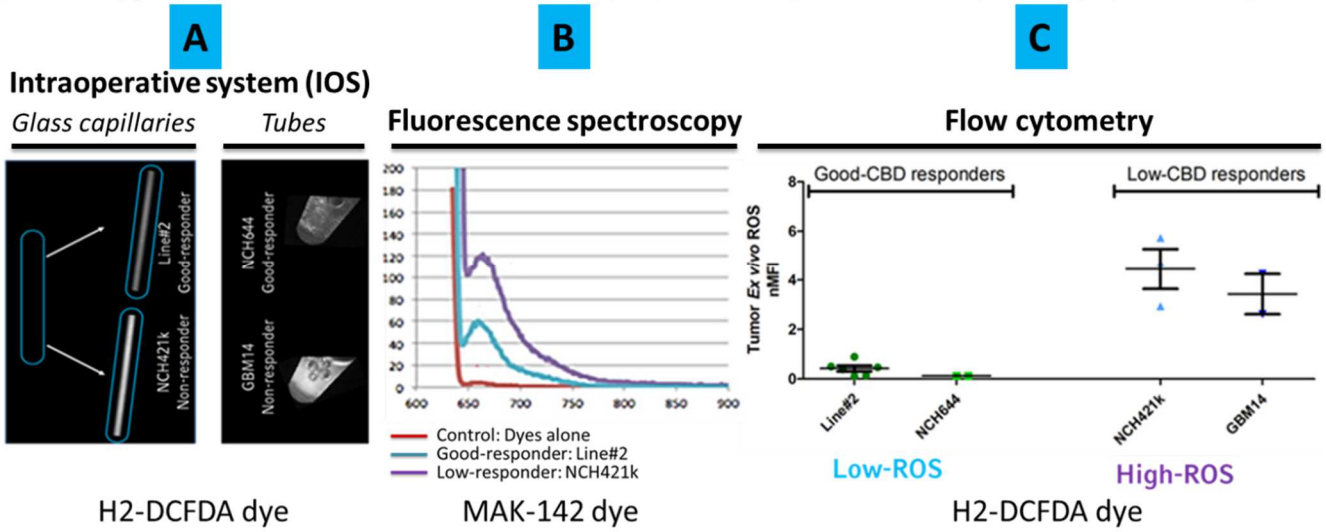

Figure 4.40 *Ex vivo,* low basal ROS levels are associated with good prospective CBD response. Basal ROS measurements comparing low- (NCH421k / GBM14) versus good- (Line#2 / NCH644) CBD responders - from left to right - in the IOS (panel A), fluorescence spectroscopy (panel B) and flow cytometry (panel C). In the IOS, *ex vivo* GBM biopsies of Line#2 and NCH421k were stained with H2-DCFDA, loaded in glass capillaries, and their fluorescence compared to unstained samples. GBM14 and NCH644 cultured cells were stained with H2-DCFDA, loaded in 1,5ml tubes and measured in the IOS. Another water-soluble ROS dye (MAK-142) was used in fluorescence spectroscopy for *ex vivo* mashed human GBM biopsies comparing the dye alone (red wave), Line#2 (blue wave), and NCH421k (purple wave). In flow cytometry, *ex vivo* mashed GBM biopsies of good CBD responders (Line#2, NCH644) and low CBD responders (NCH421k, GBM14) were measured for their DCF fluorescence. The median fluorescence intensity of positive event was determined and normalized to the number of cells (nMFI). Each point on the graph represents an individual tumor from one mouse and the mean +/-SEM of the ROS nMFI for the independent experiments is shown.

In all cases, we found good-CBD responders having lower levels of ROS fluorescence compared to good-CBD responders [Figure 4.40]. This is consistent with our *in vitro* data for H2-DCFDA staining where we showed an inverse correlation between the water-soluble ROS levels and the prospective CBD response [Figure 4.38]. The measurement of *ex vivo* GBM biopsies for their ROS levels could easily be translated to the clinics to predict a tumor sensitivity to CBD treatment.

4.15. *In vivo*, CBD prolongs the survival of mice bearing CBD sensitive patient derived GBMs

To verify our *in vitro* data, postulating the differential impact of CBD on GBMs, we implanted mice with low- and good-CBD responding GBMs of human (NCH421k, Line#2) and mouse origin (Cdkn2aKO-PDGFB, p53R172H-PDGFB). We found that in mice bearing good-responders, CBD had a positive impact on survival compared to the vehicle treatment.

The statistical significance of *in vivo* CBD therapy was evaluated for mouse and human GBMs.

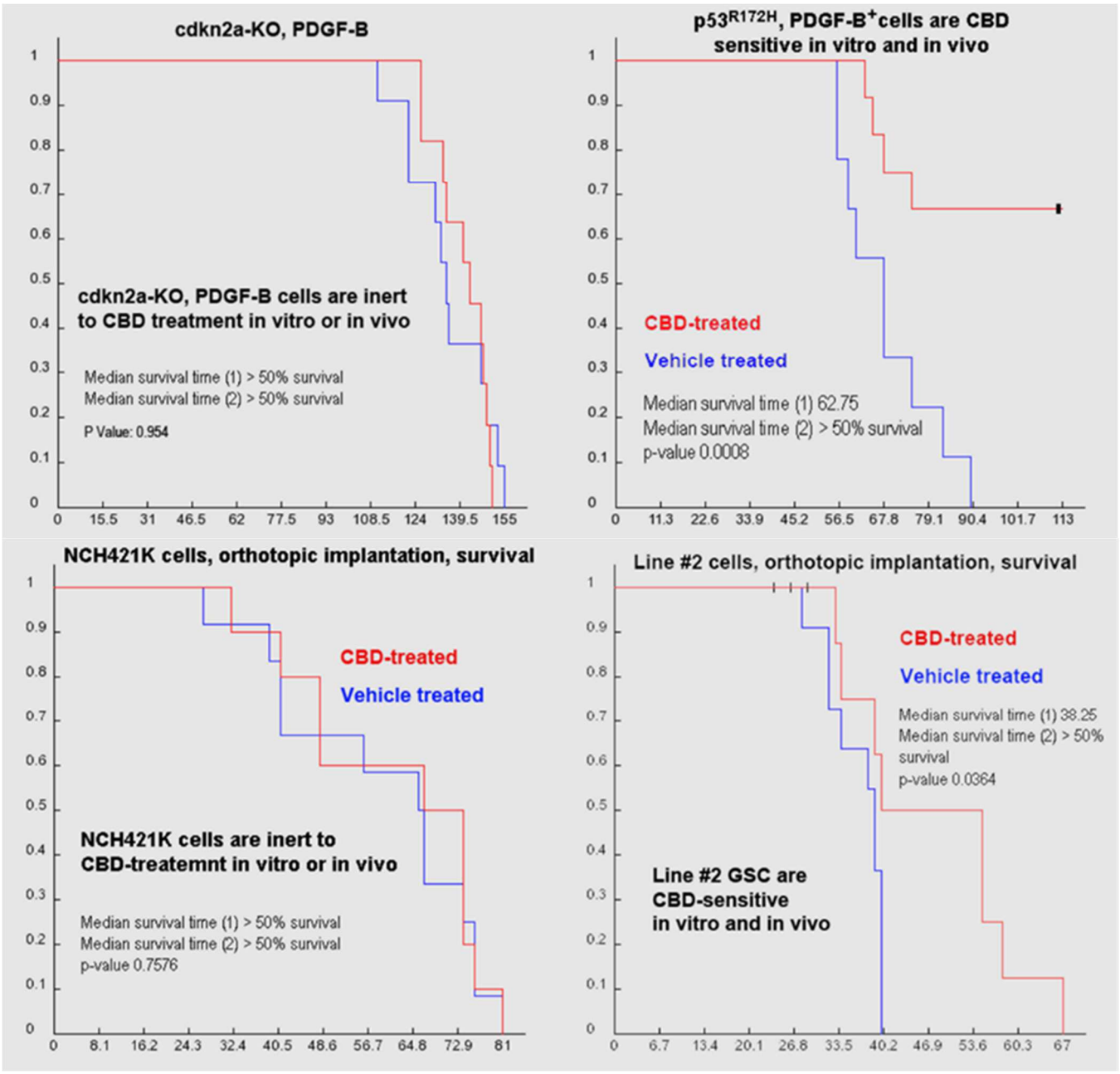

Figure 4.41 Analysis of overall survival of CBD treated mice. Mice with human (Line#2, NCH421k) or mouse gliomas (p53R172H-PDGFB, cdkn2aKO-PDGFB) were treated daily intraperitoneally with 1µl/g of freshly mixed vehicle (0) or CBD (15mg/kg) in tween80-NaCl. The overall survival was evaluated using Kaplan-Meier estimation with median survival for each treatment group and the p-value. Survival of vehicle treated mice is indicated in blue and those of CBD treated mice is indicated in red. Mice bearing mouse gliomas are in the top panel and mice with human GBM are in the bottom panel. Low-CBD responders cdkn2aKO-PDGFB (mouse) and NCH421k (human) are on the left side of the figure and show no benefit to the treatment, whereas good-CBD responders p53R172H-PDGFB (mouse) and Line#2 (human) are on the right side of the figure and treated groups showed prolonged survival.

Trials of human (Line#2 and NCH421k) and mouse cohorts (Cdkn2aKO-PDGFB and p53R172H-PDGFB) confirmed beneficial CBD effect for mice bearing good-CBD responders [Figure 4.41-right], whereas cohorts of low-CBD responders did not benefit from the treatment [Figure 4.41-left].

5. Discussion

It has previously been shown that vanilloids secreted by NPCwt have the capacity to kill gliomas [Stock K. et al. (2012)]. Here, we confirmed the ability of endovanilloids from NPCwt to induce cytotoxicity in a selection of genetically engineered mouse glioma models while sparing NPCwt, which is encouraging for clinical use of vanilloids.

One potential candidate to the clinical application of vanilloids is the plant derived vanilloid CBD, which is advanced to phase IIb of clinical trials for the treatment of glioblastoma. In human GBMs and in genetically engineered mouse gliomas mimicking genetic alterations described in human GBMs, we showed that CBD induced cytotoxicity to different extent. We categorized our panel of GBMs into low- and good-CBD responders. Depending on the genetic background of the gliomas (human or mouse) we were able to pinpoint sets of genetic alterations that are associated with CBD sensitivity. These include classical GBM subtype with EGFRVIII overexpression or proneural GBM subtype with cdkn2a loss and PDGFB overexpression. Interestingly and in accordance with current literature, we showed that CBD selectively killed glioma cells without affecting the viability of NPCwt [Shrivastava et al. (2011)]. Therefore, CBD would not be toxic to healthy NPC when used *in vivo*.

We determined the cell death mode induced by CBD and found that GBMs with wt-p53 die in a caspase dependent manner as their cell death is blocked by the pan-caspase inhibitor Q-VD-Oph. GBMs with a mutant p53 were not affected by the inhibitor. Using a newly established flow cytometry panel we revealed that mutant-p53 GBMs mainly die via autophagy. Some p53wt GBMs also showed sensitivity to autophagic cell death, highlighting that CBD could induce more than one death pathway in glioblastoma. Numerous studies showed that cannabinoids and CBD in particular could induce apoptosis or autophagy induced apoptosis in glioma cells [Fisher T. et al. (2016)]. However, we were able to screen the effect of CBD on a large panel of patient derived glioblastoma and to link the p53 status to the predominant cell death mode induced by CBD.

CBD was previously shown to shift cancer cell metabolism [Kalenderoglou N. et al. (2017)] but there is a scarcity of reports regarding metabolic profiling of its effect on patient derived GBMs. In our study we characterized the metabolic impact of CBD on human and mouse GBMs using NMR and showed that there was a clear separation between DMSO and CBD treated gliomas. Also, we detected similar trends in metabolic alterations between mouse and human such as decrease in energy levels in the form of ATP, aminoacids. Which suggest that CBD could metabolically slow down the GBM cell metabolism as less ATP is available upon treatment.

CBD is a lipophilic compound and needs to be solubilized in hydrophobic carriers [(Zgair A. et al. (2016)]. Independently from its solubility and bioavailability, Olar and collaborators showed CBD exerting a sebostatic effect via activation of TRPV4. This resulted in an inhibition of the ERK/MAPK pathway. Therefore, CBD is considered a good candidate in the treatment of acne vulgaris [Olar A. et al. (2014)]. In the transcription factor array we showed that CBD could alter factors implicated in *de novo* lipid synthesis in GBMs. We corroborated this finding in a microscopy study of a panel of good- and low-CBD responders and found that in both cases CBD altered the distribution of lipids at the plasma membrane of human GBMs. Our finding is in accordance with the study of Villa et al. showing GBM being highly dependent on cholesterol for survival. By inhibiting cholesterol uptake, they could successfully decrease GBM size *in vivo* and prolong the survival of the mice [Villa G. R. et al. (2016)]. However, as CBD decreased lipids in both low- and good- responders, this cannot be used as a stratification strategy.

While screening for the cell death mode induced by CBD, we found that combining CBD treatment with the lipid peroxidation inhibitor Ferrostatin-1 could significantly reduce CBD induced GBM death,

suggesting the importance of lipid peroxidation in CBD induced GBM death. However, this finding could not be confirmed when we specifically looked at lipids and their peroxidation (ratio of lipid hydroperoxides/lipids). Besides lipid related reactive oxygen species, we evaluated water soluble ROS and found that CBD had the capacity to reduce water soluble ROS in mouse and human GBMs, regardless of their sensitivity to CBD treatment. This prompted us to consider CBD having antioxidant properties in GBMs to the contrary of what some previous studies have shown. Indeed, Singer et al. described CBD exerting its cytotoxicity effect on a selection of GSCs by increasing the levels of ROS which later induced CBD resistance in these tumor cells [Singer E. et al. (2015)]. In 2015, Scott al. also showed CBD increasing ROS and concomitantly HSPs at the gene and protein levels in GBMs. Although our data disagree with these findings, a more recent study did show CBD as an antioxidant drug with ROS scavenging properties and neuroprotective effects against oxidative stress insults in a hippocampal neuron injury model [Sun S. et al. (2017)].

Although our data on CBD decreasing water soluble ROS seems in opposition with some published studies, we also found that CBD could indeed induce ROS increase in GBMs when considering a specific type of ROS namely mitochondrial superoxides (MitoSOX). We showed that only in good- CBD responders, exposure of these GBM to CBD for 24 hours significantly increased MitoSOX levels while also inducing changes in mitochondrial mass and membrane potential. This is in opposition with previous studies showing CBD decreasing mitochondrial SOX and membrane potential. CBD-induced apoptosis was linked to its ability to target voltage dependent anion channel 1 (VDAC1) at the mitochondrial outer membrane in microglial cell line BV2 [Rimmerman N. et al (2013)]; and in breast cancer cells, CBD was shown to decrease mitochondrial membrane potential while inducing autophagy and apoptosis [Shrivastava et al. (2011)] and [Massi P. et al. (2013)]. Altogether, these studies highlighted an impact of CBD on mitochondria in the protection of healthy and the dismissal of deleterious cells.

The antioxidant effect of CBD on mouse and human GBMs prompted us to broaden our screen to potential therapeutics that could be used to potentiate CBD effect. The high metabolic rate of GBMs and their high levels of ROS drove us to screen the effect of other pro- and anti-oxidants especially N-acetyl-L-cystein (NAC) and epigallacto-catechine-gallate (EGCG). NAC was also shown to inhibit TNFa induced NFkB activation by suppressing IkappaB and NFkB-inducing kinases [Oka S. et al. (2000)]. EGCG was shown to inhibit NFkB pathway by promoting NRF2 dissociation from Keap1. Nuclear translocated NRF2 induces ARE genes that inhibit NFkB activation [Jiang J. et al. (2012)]. However, in our experiments we obtained opposing results with these two antioxidants. EGCG consistently decreased CBD induced death in GBMs whereas NAC, a well-established ROS quencher, consistently increased CBD induced death while already showing cytotoxicity effect on its own. Our data on NAC effect on GBMs is corroborated by the study of Monticone et al. demonstrating the efficacy of NAC and other antioxidants in decreasing GBM viability and impairing cell cycle progression [Monticone M. et al. (2014)]. However, more explorations will be needed to shed light on the mechanism of action of these two antioxidants and discover why they have such distinct effects on CBD induced GBM death.

Vanilloids were previously shown to kill gliomas via the induction of ER stress induced apoptosis [Stock K. et al. (2012)]. We confirmed ER stress induction in patient derived GBMs using the ER stress activation profiling plate array and pinpointed differentially ER related transcription factors between low-CBD responder NCH421k and good-CBD responder line#2. Trends of alterations in these differentially regulated transcription factors were also corroborated by other assays for example when showing CBD decreasing lipid metabolism which was also corroborated by other published studies [Villa G. R. et al. (2016)]. We also showed some interesting alterations in transcription factors implicated in redox homeostasis and inflammation such as NRF2 and NFkB. The increase in NRF2 observed was in line with our finding that CBD acts as an antioxidant by decreasing water soluble ROS levels in GBMs.

One interesting transcription factor differentially regulated between low- and good-CBD responders in the TF array was NFkB. In good-CBD responder Line#2, we showed that CBD increased the nuclear binding of NFkB-p65 to TNIP1 consensus sequence used in the array. We confirmed this CBD-induced nuclear shuttling by immunofluorescence staining for the NFkB-p65 and observed that its nuclear translocation was increased by CBD only in good-CBD responders. As NFkB is routinely described as a promoter of tumor cell survival and proliferation [Masilamani A. P et al. (2017)] and [Soubannier V. et al. (2017)], we found our data in opposition with the literature. Activated NFkB signaling was even proposed to play a role in the establishment of glioma by promoting the differentiation of cancer stem cells with constitutive NFkB activation [Widera D. et al. (2008)]. Indeed, it is described in the case of glioblastoma that inactivation of NFkB and other pathways such as ERK/MAPK is important for glioblastoma apoptosis [Liu P. C. et al. (2017)]. Results from our mouse model of NFkB-p65 loss showed the importance of p65 in CBD induced GBM death as mouse proneural gliomas with homozygous loss of p65 lose their sensitivity to CBD induced cytotoxicity. This important role of NFkB-p65 in CBD mediated death prompted our interest to uncover which action was p65 carrying out in GBM nuclei upon CBD induced translocation. In our NFkB promoter activation reporter assay, we showed that although CBD selectively induces p65 translocation in good-responders, it does not induce NFkB promoter activity. In fact, we showed that in good-CBD responders, CBD treatment could significantly decrease TNFα induced NFkB promoter activation. Therefore, CBD induced translocation would promote a blockage of NFkB transcriptional activity instead of a detrimental activation. A recent study of Hackler et al. supports in many ways our findings in that the antioxidant curcumin (C-150) which also shows anti-inflammatory properties, induced profound cytotoxicity in glioma cells by inhibiting the transcriptional activity of NFkB [Hackler L. Jr. et al. (2016)]. Further investigations will be needed to discover the exact molecular pathways induced in the nuclei of dying GBMs upon CBD treatment; may it be p65 translocation-binding and blocking the access of NFkB promoter for activation or the re-distribution of p65 to other nuclear territories such as the nucleolus, where p65 has been shown to induce cell death after inducing nuclear export of nucleophosmin (NPM) and mitochondrial mobilization for cell death induction [Khandelwal N. et al. (2011)]. Moreover, the nucleolus is now specifically being considered in novel cancer therapeutic strategies as it was shown to be dysregulated in many cancers and playing a crucial role in NFkB regulation of tumor death [Chen J. et al. (2017)].

The main transcription factor balancing NFkB effect is NRF2, which signaling pathway is the main system controlling redox homeostasis in all cells. They both exert reciprocal feed-back loops to balance their effects and balanced activation of NFkB and NRF2 is mandatory to assure proper control of inflammation and oxidative damage [Wardyn J. D. et al. (2015)]. In a selection of patient derived glioblastoma, one low-responder versus one good-responder, we showed that at basal level, GBM cells have active NRF2/ARE pathway activity, with the low-responder showing higher levels of oxidative stress compared to the good-responder. Upon CBD treatment we obtained in both cases an increase in antioxidant responses, further supporting our data on CBD antioxidant properties. However, the shift in antioxidant response in the low-CBD responder was lower compared to the good-CBD responder. As we showed that CBD rather induced an inhibitory effect on NFkB transcriptional activity we realized that these two master regulators are again brought to collaboration by CBD. Although NFkB has been described in numerous studies to promote the production of ROS, other studies demonstrated an anti-oxidative role of NFkB by promoting the transcription of certain antioxidant proteins. The most famous target of NFkB antioxidant activity is manganese superoxide dismutase (MnSOD), a mitochondrial antioxidant which induces the conversion of MitoSOX ($O_2^{\cdot -}$) into water soluble ROS hydrogen peroxide (H_2O_2) [Morgan M. J. et al. (2011)]. Although we did observe reduction in water soluble ROS upon CBD treatment, we cannot adhere to the concept that NFkB would be involved in promoting antioxidant activity in GBMs because we could not show any induction of promoter transcriptional activity. Therefore, we assumed that CBD effect on water soluble ROS

levels and NFkB-p65 could be two distinct effects of CBD ultimately leading to GBM death. When we consider CBD reducing ROS in both good- and low-CBD responders, we would be inclined to think that the cytotoxicity effect of CBD is not linked to its impact on ROS levels. But when we add the selective effect of CBD on increasing MitoSOX levels we are driven back to the importance of ROS in CBD induced GBM death. It might be that the cellular antioxidant machinery was mobilized for a first round of ROS decrease but a second increase in MitoSOX, selectively in good-CBD responders, would generate more water-soluble ROS, that would overwhelm cellular antioxidant systems. This situation leading to accumulation of new ROS could oxidize translocated p50-p65 complexes thus leading to destabilization of DNA binding and changes in specific phosphorylation of p50 serines and chromatin remodeling processes required for adequate transcriptional activity [Zhang J. et al. (2016)] and [Morgan M. J. et al. (2011)]. CBD is a pleiotropic drug that affects multiple interconnected signaling pathways. The challenge of future studies will be to clarify a step further the variations of NFkB nuclear modifications in the form of phosphorylation, binding capabilities and intranuclear territory localization that could directly play a role in CBD mediated GBM therapy.

As NFkB and NRF2 pathways are mutually regulated, and we found that NFkB was not transcriptionally active, but important in CBD induced GBM death, we ought to look at the NRF2 pathway deeper. NRF2 inducer dimethyl fumarate (DMF) [Gopal S. et al. (2017)] and [Galloway D. A. et al. (2017)] significantly increased CBD induced GBM death in one CBD responder. Therefore, DMF could be considered a good candidate to GBM CBD combination therapy. Indeed, DMF has been shown to sensitize lymphoma cells to apoptosis via NFkB targeting [Nicolay J. P. et al. (2016)], to induce breast cancer cell death by covalent binding of NFkB-p65 and inhibiting transcriptional activity [Kastrati I. et al. (2016) and Kastrati I. et al. (2017)]. Also, there is already a phase I GBM clinical trial involving DMF, radiotherapy and temozolomide, where DMF is used to sensitize GBM cells to radiotherapy [Shafer D. A. et al. (2017)]. In any case, further investigations should be conducted on CBD combination therapy not only using DMF but also promising antioxidants such as NAC and other phytovanilloids.

To support ongoing CBD clinical trials and their successful outcome, showing induction of cytotoxicity in multiple GBM cells is not sufficient. Indeed, such a simple screen, does not help in trial enrolment selection and future therapeutic decisions where patient stratification for prospective drug response is crucial. Therefore, we extensively screened our palette of human and mouse GBMs and described 2 options for patient stratification for beneficial CBD therapy. The first one considers sets of genetic alterations that we found associated with CBD sensitivity such as proneural GBMs with p53 hot-spot mutations in the DNA binding domain or GBMs of the classical subtype with EGFR/EGFRvIII overexpression. We also highlighted genetic signatures associated with poor CBD sensitivity such as dual loss of p53 and NF1. The second stratification scheme we propose is based on GBM ROS levels as metabolic marker of CBD sensitivity. In our *in vitro* screen of all human GBMs, we showed that the lower the ROS levels of GBMs without any drug treatment, the higher the prospective response to CBD. To move our experiments a step closer to possible clinical applications, we performed basal ROS measurements on *ex vivo* human tumor biopsies from athymic nude mice. Aiming to find a straightforward method to predict CBD sensitivity for clinical patient biopsies, we corroborated our *in vitro* results with the *ex vivo* experiments across 3 measurement platforms (glass capillaries in the IOS, fluorescence spectroscopy, and flow cytometry) to obtain qualitative and quantitative results. To validate the application of this simple method to predict CBD sensitivity in human GBMs, we would need to enlarge our screening pool and, in the future, collaborate with neurosurgical departments either agreeing to deliver fresh biopsies as they perform biopsies or surgical resections, or sharing with them the protocols to detect the basal ROS levels onsite.

Our *in vitro* cytotoxicity screening data were verified in *in vivo* experiments where we compared CBD effect in mice bearing a low- versus good-CBD responders. Indeed, no beneficial effect was seen in the low-CBD

responders whereas good-CBD responders showed significantly increased survival compared to vehicle treated mice. The good-CBD responder Line#2 showed to be very aggressive when we visually inspected the tumor brains at humane end-point in the vehicle treated mice. The last mouse of the vehicle died about 25 days earlier than the last mouse of the CBD treated group. It would be interesting to enlarge the cohorts of mice bearing human GBMs with known CBD sensitivity *in vitro* and validate the CBD effect *in vivo*. Also, a trial of immunocompetent mice bearing genetically engineered mouse gliomas of known CBD sensitivity corroborated the message of our *in vitro* screens showing CBD differentially inducing cytotoxicity in GBMs depending on their genetic backgrounds. Another interesting approach of *in vivo* studies would be to consider treating GBM bearing mice at different stages of tumorigenesis and evaluate a time point of best drug efficacy. Equally, *in vivo* evaluation of other therapeutics such as other vanilloids or antioxidants that could be used to potentiate CBD effect would also be interesting.

Clinical trials of CBD for several diseases are already ongoing. Epidiolex® is a pure CBD oral solution in Phase III clinical trials for the treatment of epileptic seizures in Lennox-Gastaut syndrome (one trial) and Dravet syndrome (two trials). They so far have proven safe [Iffland K. et al. (2017)] and showed beneficial effect in reducing convulsive seizures for Dravet syndrome in children. The double-blind study included 120 children randomly assigned into placebo or CBD cohorts. It showed that 43% of patients taking Epidiolex® experienced a 50% decrease in convulsive seizures against 24% for placebo patients [Devinsky O. et al. (2017)]. The drug Sativex®(Nabiximols), a 1:1 formulation of CBD and THC applied as oromucosal spray, has been trialed for symptomatic relief of multiple sclerosis spasticity and chronic cancer pain [Fallon M. T. et al. (2017)]. The latest study published early 2018 was a Phase III, placebo controlled, double blinded study, randomly allocating patients to self-titrated CBD/Nabiximols (n=199) or placebo (n=198) [Lichtman A. H. et al. (2018)]. The recruited patients were diagnosed with advanced cancers and experienced chronic pain that optimized opioid therapy failed to relieve. Considering the primary efficacy endpoint, CBD failed to show superior effect to placebo. However, CBD showed a significant advantage to placebo in US patients who received lower opioid doses. Pain associated TRP receptors have been extensively studied as modulable targets for anti-nociceptive therapy [McEntire D. M. et al. (2016)] and [Pecze L. et al. (2017)], and TRPV1, TRPV3, TRPA1 antagonists have entered clinical trials as analgesics candidates [Kaneko Y. et al. (2017)]. Studies of vanilloids effect on TRP channels have been documented not only as analgesics [Lindvall O. et al. (2009)] but also as multitarget agents affecting pathways of inflammation, metabolism, and death. Anti-tumorigenic potential of vanilloids is of particular interest and CBD is currently one of the most studied vanilloids for peripheral and CNS disorders [Scuderi C. et al. (2009)], [Hill A. J. et al. (2012)], [Morales P. et al. (2017)], and [Morales P. and Reggio P. H. et al. (2017)]. For glioma, CBD was described as an agonist to TRPV2 channels and sensitized tumor cells to *in vitro* cytotoxic effect of TMZ, BCNU or doxorubicin [Nabissi M. et al. (2013)]. Combination therapy of THC and CBD have also been investigated and showed these two vanilloids acting via distinct signaling pathways yet inducing synergistic reduction in glioma viability [Marcu J. P. et al. (2011)] and [Torres S. et al. (2011)]. These promising *in vitro* and pre-clinical *in vivo* data fueled the initiation of Phase II clinical trials of Sativex® in combination with first line therapeutic agent TMZ (Temodar) for the treatment of recurrent GBMs. The study showed positive results for patients receiving Sativex® (83% one-year survival rate) against 53% for placebo treated patients [GW Pharmaceuticals communications Feb 07, 2017]. To ensure success throughout other phases of the trials, it will be necessary to apply robust stratification strategies during trial enrollment. A good example of trial success is the current first line therapeutics TMZ where good segregation of drug sensitive and inert tumors was clearly established, with TMZ sensitivity associated with active mismatch repair (MMR) and resistance associated with overexpression of MGMT and/or insufficient DNA repair [Lee S. Y. (2016)]. In our study, we engineered mouse models of glioma based on established genetic alterations of different human GBM subtypes [Brennan C. W. et al. (2013)] and [Plaisier

C. L. et al. (2016)]. Genetic alterations have previously been proposed for survival prognostics. Indeed, Purkait et al. recently proposed a classification of IDHwt GBMs into three prognostic subtypes based on their teleomerase reverse transcriptase (TERT) and O (6)-methyl guanine methyltransferase (MGMT) promoter methylation status and that regardless of other genetic alterations [Purkait S. et al. (2016)]. Using our *in vitro* cytotoxicity screening data, we proposed a stratification strategy based on sets of genetic alterations that indicate prospective good-CBD responders. We also uncovered basal ROS levels as potential biomarker of CBD sensitivity. The method we developed is fast and easy to carry out and needs small GBM tumor biopsies. Therefore, prospective CBD responders could be identified within hours the same day and therapeutic decision taken accordingly.

6. Summary

To mimic the genetic diversity of human GBMs, we genetically engineered mouse glioma models to express sets of tumor suppressor deficiencies and overactive proto-oncogenes that have been associated with different human GBM subtypes. There, we created a simple tool to study the effect of few key genes on glioma genesis, evolution, and their role in sensitizing to potential therapeutics. The effect of NPCwt conditioned medium was evaluated on a selection of our mouse glioma models and we showed endovanilloids exerting cytotoxicity in gliomas of different genetic backgrounds. We then tested the effect of plant-derived vanilloid CBD not only on the generated mouse gliomas, but also on a collection of 21 patient-derived GBMs and found CBD inducing GBM death to different extent. We classified GBMs into prospective good- and low-CBD responders. We validated our *in vitro* cytotoxicity screen by *in vivo* therapy studies comparing the effect of CBD in prospective low- and good-CBD responders. There, only the prospective good-CBD responders benefited from CBD therapy in the form of prolonged survival. We characterized the cell death mode induced by CBD in human GBMs as being apoptosis in p53wt GBMs or autophagy in p53 mutant GBMs. Upon treatment, levels of water-soluble ROS systematically decreased in mouse and human GBMs regardless of their sensitivity to CBD while mitochondria-specific ROS (MitoSOX) were increased only in good-CBD responders. Although CBD can be considered having an antioxidant effect on GBMs, we revealed that not all antioxidants are beneficial in CBD therapy. Screening for combination therapeutics to potentiate CBD effect, we found NAC increasing CBD effect while EGCG decreased induced cytotoxicity. We revealed NFkB-p65 as indispensable in CBD induced GBM death in an established proneural mouse glioma model of p65 loss. We showed that CBD increases NFkB-p65 nuclear translocation in good-CBD responders while it tended to decrease sometimes already high nuclear accumulations of p65 in low-CBD responders. Further investigations to uncover the functional importance of nuclear p65 revealed that although CBD induces nuclear translocation of p65, it does not activate NFkB transcriptional activity and would decrease TNFα induced activation, only in good-CBD responders. In low-CBD responders, we were however unable to induce promoter activity even with TNFα. As NFkB and NRF2 pathways are two co-regulated arms in oxidative stress, we evaluated the status of NRF2/ARE activity comparing a low- to a good-CBD responder at basal levels. To the contrary of the good-responder, the low-responder displayed high NRF2/ARE pathway activation. After CBD treatment, levels of NRF2 pathway activation increased in both GBMs with the most increase observed in the good-responder. Our study is well-suited in the personalized medicine era as we proposed two approaches to help in predicting CBD therapy outcome in GBM patients. In the first one we highlighted sets of genetic alterations that sensitized GBMs to CBD in our cytotoxicity screens (e.g. loss or mutation in cdkn2a and EGFRvIII overexpression, hot spot p53mutant and PDGFB overexpression). The second method proposed to use a metabolic approach to predict CBD response. Indeed, *in vitro*, we showed that water soluble ROS levels inversely correlate with the propensity of GBMs to respond to CBD. In a pre-clinical setting, we showed that GBM biopsies of

prospective low- and good-CBD responders could be identified based on their ROS levels without any drug treatment: the lower the ROS levels, the higher the sensitivity to CBD. Further investigation of this straightforward method using larger panels of GBMs will be needed to apply this prognostic tool in clinical practice.

7. References

Achyut B. R., Angara K., Jain M., Borin T. F., Rashid M. H., Iskander A. S. M., Ara R., Kolhe R., Howard S., Venugopal N., Rodriguez P. C., Bradford J. W., Arbab A. S. (2017). Canonical NFκB signaling in myeloid cells is required for the glioblastoma growth. *Sci Rep.* 2017 Oct 23;7(1):13754.

Agnello M., Morici G., and Rinaldi A. M. (2008). A method for measuring mitochondrial mass and activity. *Cytotechnology.* 2008 Mar; 56(3): 145–149.

Agnihotri S., Zadeh G. (2016). Metabolic reprogramming in glioblastoma: the influence of cancer metabolism on epigenetics and unanswered questions, *Neuro-Oncology*, Vol. 18, Issue 2, 2016 Feb 1; Pages 160–172.

Aktan M., Koc M., Kanyilmaz G. (2015). Survival following reirradiation using intensity-modulated radiation therapy with temozolomide in selected patients with recurrent high grade gliomas. *Ann Transl Med.* 2015 Nov; 3(20): 304.

Andor N., Graham T. A., Jansen M., Xia L. C., Aktipis C. A., Petritsch C., Ji H. P., Maley C. C. (2016). Pan-cancer analysis of the extent and consequences of intratumor heterogeneity. *Nat Med.* 2016 Jan;22(1):105-13.

Anjum K., Shagufta B. I., Abbas S. Q., Patel S., Khan I., Shah S. A. A., Akhter N., Hassan S. S. U. (2017). Current status and future therapeutic perspectives of glioblastoma multiforme (GBM) therapy: A review. Biomed Pharmacother. 2017 Aug; 92:681-689.

Arcuri C., Fioretti B., Bianchi R., Mecca C., Tubaro C., Beccari T., Franciolini F., Giambanco I., Donato R. (2017). Microglia-glioma cross-talk: a two-way approach to new strategies against glioma. *Front Biosci (Landmark Ed).* 2017 Jan 1; 22:268-309.

Audia A., Conroy S., Glass R., Bhat K. P. L. (2017). The Impact of the Tumor Microenvironment on the Properties of Glioma Stem-Like Cells. *Front Oncol.* 2017; 7: 143.

Banaszynski L. A., Chen L-C., Maynard-Smith L. A., Ooi A. G. L., and Wandless T. J. (2006). A Rapid, Reversible, and Tunable Method to Regulate Protein Function in Living Cells Using Synthetic Small Molecules. *Cell.* 2006 Sep 8; 126(5): 995–1004.

Berte N., Lokan S.,Eich M., Kim E.,and Kaina B. (2016). Artesunate enhances the therapeutic response of glioma cells to temozolomide by inhibition of homologous recombination and senescence. *Oncotarget.* 2016 Oct 11; 7(41): 67235–67250.

Bhat T. A., Chaudhary A. K., Kumar S., O'Malley J., Inigo J. R., Kumar R., Yadav N., Chandra D. Endoplasmic reticulum-mediated unfolded protein response and mitochondrial apoptosis in cancer. (2017). *Biochim Biophys Acta.* 2017 Jan;1867(1):58-66.

Binda E., Visioli A., Giani F., Lamorte G., Copetti M., Pitter K. L., Huse J. T., Cajola L., Zanetti N., DiMeco F., De Filippis L., Mangiola A., Maira G., Anile C., De Bonis P., Reynolds B. A., Pasquale E. B., Vescovi A. L. (2012). The EphA2 receptor drives self-renewal and tumorigenicity in stem-like tumor-propagating cells from human glioblastomas.
Cancer Cell. 2012 Dec 11;22(6):765-80.

Birben E., Sahiner U. M., Sackesen C., Erzurum S., and Omer Kalayci. (2012). Oxidative Stress and Antioxidant Defense. *World Allergy Organ J.* 2012 Jan; 5(1): 9–19.

Bjørkøy G., Lamark T., Pankiv S., Øvervatn A., Brech A., Johansen T. (2009). Monitoring autophagic degradation of p62/SQSTM1. *Methods Enzymol.* 2009; 452:181-97.

Blessing E. M., Steenkamp M. M., Manzanares J., Marmar C. R. (2015). Cannabidiol as a Potential Treatment for Anxiety Disorders. *Neurotherapeutics.* 2015 Oct;12(4):825-36.

Bradshaw A., Wickremsekera A., Tan S. T., Peng L., Davis P. F., Itinteang T. (2016). Cancer Stem Cell Hierarchy in Glioblastoma Multiforme. *Front Surg.* 2016; 3: 21.

Brennan C. W., Verhaak R. G., McKenna A., Campos B., Noushmehr H., Salama S. R., Zheng S., Chakravarty D., Sanborn J. Z., Berman S. H., Beroukhim R., Bernard B., Wu C. J., Genovese G., Shmulevich I., Barnholtz-Sloan J., Zou L., Vegesna R., Shukla S. A., Ciriello G., Yung W. K., Zhang W., Sougnez C., Mikkelsen T., Aldape K., Bigner D. D., Van Meir E. G., Prados M., Sloan A., Black K. L., Eschbacher J., Finocchiaro G., Friedman W., Andrews D. W., Guha A., Iacocca M., O'Neill B. P., Foltz G., Myers J., Weisenberger D. J., Penny R., Kucherlapati R., Perou C.M., Hayes D. N., Gibbs R., Marra M., Mills G. B., Lander E., Spellman P., Wilson R., Sander C., Weinstein J., Meyerson M., Gabriel S., Laird P. W., Haussler D., Getz G., Chin L; TCGA Research Network. (2013). The somatic genomic landscape of glioblastoma. *Cell.* 2013 Oct 10;155(2):462-77.

Brown T. J., Brennan M. C., Li M., Church E. W., Brandmeir N. J., Rakszawski K. L., Patel A. S., Rizk E. B., Suki D., Sawaya R., Glantz M. (2016). Association of the extent of resection with survival in glioblastoma: A Systematic Review and Meta-analysis. *JAMA Oncol.* 2016 Nov 1;2(11):1460-1469.

Cahill K. E., Morshed R. A., Yamini B. (2016). Nuclear factor-κB in glioblastoma: insights into regulators and targeted therapy. *Neuro Oncol.* 2016 Mar;18(3):329-39.

Calvaruso G., Pellerito O., Notaro A., Giuliano M. (2012). Cannabinoid-associated cell death mechanisms in tumor models (review). *Int J Oncol.* 2012 Aug;41(2):407-13.

Calzolari F., Appolloni I., Tutucci E., Caviglia S., Terrile M., Corte G., Malatesta P. (2008). Tumor Progression and Oncogene Addiction in a PDGF-B-Induced Model of Gliomagenesis. *Neoplasia.* 2008 Dec; 10(12): 1373–1382.

Camargo N., Goudriaan A., van Deijk A-l. F., Otte W. M., Brouwers J. F., Lodder H., Gutmann D. H., Nave K-L., Dijkhuizen R. M., Mansvelder H. D., Chrast R., Smit A. B., Mark H. G. Verheijen M. H. G. (2017). Oligodendroglial myelination requires astrocyte-derived lipids. *PLoS Biol.* 2017 May; 15(5): e1002605.

Campos B., Wan F., Farhadi M., Ernst A., Zeppernick F., Tagscherer K. E., Ahmadi R., Lohr J., Dictus C., Gdynia G., Combs S. E., Goidts V., Helmke B. M., Eckstein V., Roth W., Beckhove P., Lichter P., Unterberg A., Radlwimmer B., Herold-Mende C. (2010). Differentiation therapy exerts antitumor effects on stem-like glioma cells. *Clin Cancer Res.* 2010 May 15;16(10):2715-28.

Cabral G. A., Jamerson M. (2014). Marijuana use and brain immune mechanisms. *Int Rev Neurobiol.* 2014; 118:199-230.

Caserta T. M., Smith A. N., Gultice A. D., Reedy M. A., Brown T. L. (2003). Q-VD-OPh, a broad-spectrum caspase inhibitor with potent antiapoptotic properties. *Apoptosis.* 2003 Aug;8(4):345-52.

Chen J., Stark L. A. (2017). Aspirin Prevention of Colorectal Cancer: Focus on NF-κB Signalling and the Nucleolus. *Biomedicines.* 2017 Jul 18;5(3). pii: E43.

Chen W., Xia T.,Wang D.,Huang B., Zhao P., Wang J., Qu X., Li X.. (2016). Human astrocytes secrete IL-6 to promote glioma migration and invasion through upregulation of cytomembrane MMP14. *Oncotarget.* 2016 Sep 20; 7(38): 62425–62438.

Davis M. E. (2016). Glioblastoma: Overview of Disease and Treatment. *Clin J Oncol Nurs.* 2016 October 1; 20(5): S2–S8.
Devinsky O., Cross J. H., Wright S. (2017). Trial of Cannabidiol for Drug-Resistant Seizures in the Dravet Syndrome. *N Engl J Med.* 2017 Aug 17 ;377(7):699-700.

Dossi E., Vasile F., Rouach N. (2017). Human astrocytes in the diseased brain *Brain Res Bull.* 2017 Feb 13. pii: S0361-9230(17)30082-5.

Du G-J., Zhang Z., Wen X-D, Yu C., Calway T., Yuan C-S., and Wang C-Z. (2012). Epigallocatechin Gallate (EGCG) Is the Most Effective Cancer Chemopreventive Polyphenol in Green Tea. *Nutrients.* 2012 Nov; 4(11): 1679–1691.

Dumitru C. A., Sandalcioglu I. E., Karsak M. (2018). Cannabinoids in Glioblastoma Therapy: New Applications for Old Drugs. *Front. Mol. Neurosci.* 2018 ; 11 :159.

Falenski K. W., Carter D. S., Harrison A. J., Martin B. R., Blair R. E., DeLorenzo R. J. (2009). Temporal characterization of changes in hippocampal cannabinoid CB(1) receptor expression following pilocarpine-induced status epilepticus. *Brain Res* 2009; 1262:64–72.

Fallon M. T., Albert Lux E., McQuade R., Rossetti S., Sanchez R., Sun W., Wright S., Lichtman A. H., Kornyeyeva E. (2017). Sativex oromucosal spray as adjunctive therapy in advanced cancer patients with chronic pain unalleviated by optimized opioid therapy: two double-blind, randomized, placebo-controlled phase 3 studies. *Br J Pain.* 2017 Aug;11(3):119-133.

Ferguson S. D., Joanne Xiu J., Shiao-Pei Weathers S-P., Zhou S., Kesari S.,Weiss S. E., R. J.Verhaak R. G., Hohl R. J., Barger G. R., Reddy S. K., Heimberger A. B. (2016). GBM-associated mutations and altered protein expression are more common in young patients. *Oncotarget.* 2016 Oct 25;7(43):69466-69478.

Ferrari D., Binda E., De Filippis L., Vescovi A. L. (2010). Isolation of neural stem cells from neural tissues using the neurosphere technique. *Curr Protoc Stem Cell Biol.* 2010 Nov;Chapter 2:Unit2D.6.

Fisher T., Golan H., Schiby G., PriChen S., Smoum R., Moshe I., Peshes-Yaloz N., Castiel A., Waldman D., Gallily R., Mechoulam R., Toren A. (2016). In vitro and in vivo efficacy of non-psychoactive cannabidiol in neuroblastoma. *Curr Oncol.* 2016 Mar;23(2): S15-22.

Friedmann-Morvinski D., Narasimamurthy R., Xia Y., Myskiw C.,Soda Y.,Verma I. M. (2016). Targeting NF-κB in glioblastoma: A therapeutic approach. *Sci Adv.* 2016 Jan; 2(1): e1501292.

Galli R., Binda E., Orfanelli U., Cipelletti B., Gritti A., De Vitis S., Fiocco R., Foroni C., Dimeco F., Vescovi A. (2004). Isolation and characterization of tumorigenic, stem-like neural precursors from human glioblastoma. *Cancer Res.* 2004 Oct 1; 64(19):7011-21.

Galloway D. A., Williams J. B., Moore C. S. (2017). Effects of fumarates on inflammatory human astrocyte responses and oligodendrocyte differentiation. *Ann Clin Transl Neurol.* 2017 May 4;4(6):381-391.

Ganchi P. A., Sun S. C., Greene W. C., Ballard D. W. (1992). I kappa B/MAD-3 masks the nuclear localization signal of NF-kappa B p65 and requires the transactivation domain to inhibit NF-kappa B p65 DNA binding. *Mol Biol Cell.* 1992 Dec;3(12):1339-52.

Ge W., Zhao K., Wang X., Li H., Yu M., He M., Xue X., Zhu Y., Zhang C., Cheng Y., Jiang S., Hu Y. (2017). iASPP Is an Antioxidative Factor and Drives Cancer Growth and Drug Resistance by Competing with Nrf2 for Keap1 Binding. *Cancer Cell.* 2017 Nov 13;32(5):561-573.e6.

Ghods A. L., Glick R., Braun D., and Feinstein D. 2013. Beneficial actions of the anti-inflammatory dimethyl fumarate in glioblastomas. *Surg Neurol Int.* 2013; 4: 160.

Gieryng A., Pszczolkowska D., Walentynowicz K. A., Rajan W. D., Kaminska B. (2017). Immune microenvironment of gliomas. *Lab Invest.* 2017 May;97(5):498-518.

Glaser S. M., Dohopolski M. J., Balasubramani G. K., Flickinger J. C., Beriwal S. (2017). Glioblastoma multiforme (GBM) in the elderly: initial treatment strategy and overall survival. *J Neurooncol.* 2017 Aug;134(1):107-118.

Glass R., Synowitz M., Kronenberg G., Walzlein J. H., Markovic D. S., Wang L. P., Gast D., Kiwit J., Kempermann G., Kettenmann H. (2005). Glioblastoma-induced attraction of endogenous neural precursor cells is associated with improved survival. *J Neurosci.* 2005 Mar 9;25(10):2637-46.

Gollapalli K., Ghantasala S., Kumar S., Srivastava R., Rapole S., Moiyadi A., Epari S. & Srivastava S. (2017). Subventricular zone involvement in Glioblastoma – A proteomic evaluation and clinicoradiological correlation. *Sci Rep.* 2017 May 3;7(1):1449.

Gopal S., Mikulskis A., Gold R., Fox R. J., Dawson K. T., Amaravadi L. (2017). Evidence of activation of the Nrf2 pathway in multiple sclerosis patients treated with delayed-release dimethyl fumarate in the Phase 3 DEFINE and CONFIRM studies. *Mult Scler.* 2017 Jan 1:1352458517690617.

Gorpas D., Koch M., Anastasopoulou M., Klemm U., Ntziachristos V. (2017). Benchmarking of fluorescence cameras through the use of a composite phantom. *J Biomed Opt.* 2017 Jan 1;22(1):16009.

Gzell C., Back M., Wheeler H., Bailey D., Foote M. (2017). Radiotherapy in Glioblastoma: the Past, the Present and the Future. *Clin Oncol (R Coll Radiol).* 2017 Jan;29(1):15-25.

Hackler L. Jr., Ózsvári B., Gyuris M., Sipos P., Fábián G., Molnár E., Marton A., Faragó N., Mihály J., Nagy L. I., Szénási T., Diron A., Párducz Á., Kanizsai I., Puskás L. G. (2016). The Curcumin Analog C-150, Influencing NF-κB, UPR and Akt/Notch Pathways Has Potent Anticancer Activity In Vitro and In Vivo. *PLoS One.* 2016 Mar 4;11(3): e0149832.

Hanif F., Muzaffar K.., Perveen K, Malhi S. M., Simjee Sh. U. (2017). Glioblastoma Multiforme: A Review of its Epidemiology and Pathogenesis through Clinical Presentation and Treatment. *Asian Pac J Cancer Prev.* 2017 Jan 1;18(1):3-9.

Hanuš L. O., Meyer S. M., Muñoz E., Taglialatela-Scafati O., Appendino G. (2016). Phytocannabinoids: a unified critical inventory. *Nat Prod Rep.* 2016 Nov 23;33(12):1357-1392.

Hempel N., Trebak M. (2017). Crosstalk between calcium and reactive oxygen species signaling in cancer. *Cell Calcium*. 2017 May; 63:70-96.

Hervey-Jumper S. L., Li J., Lau D., Molinaro A. M., Perry D. W., Meng L., Berger M. S. (2015). Awake craniotomy to maximize glioma resection: methods and technical nuances over a 27-year period. *J Neurosurg.* 2015 Aug;123(2):325-39.

Hill A. J., Williams C. M., Whalley B. J., Stephens G. J. (2012). Phytocannabinoids as novel therapeutic agents in CNS disorders. *Pharmacol Ther.* 2012 Jan;133(1):79-97.

Hofmann K., Rodriguez-Rodriguez R., Gaebler A., Casals N., Scheller A., Kuerschne L. (2017). Astrocytes and oligodendrocytes in grey and white matter regions of the brain metabolize fatty acids. *Sci Rep.* 2017; 7: 10779.

Holzerová E., Prokisch H. (2015). Mitochondria: Much ado about nothing? How dangerous is reactive oxygen species production? *Int J Biochem Cell Biol.* 2015 Jun; 63: 16–20.

Iffland K., Grotenhermen F. (2017). An Update on Safety and Side Effects of Cannabidiol: A Review of Clinical Data and Relevant Animal Studies. *Cannabis Cannabinoid Res.* 2017 Jun 1;2(1):139-154.

Iskedjian M., Bereza B., Gordon A., Piwko C., Einarson T. R. (2007). Meta-analysis of cannabis-based treatments for neuropathic and multiple sclerosis-related pain. *Curr. Med. Res. Opin.* 2007, 23, 17–24.

Jiang J., Mo Z. C., Yin K., Zhao G. J., Lv Y. C., Ouyang X. P., Jiang Z. S., Fu Y., Tang C.K. (2012). Epigallocatechin-3-gallate prevents TNF-α-induced NF-κB activation thereby upregulating ABCA1 via the Nrf2/Keap1 pathway in macrophage foam cells. *Int J Mol Med.* 2012 May;29(5):946-56.

Jiang S., Zhang E., Zhang R., Li X. (2016). Altered activity patterns of transcription factors induced by endoplasmic reticulum stress. *BMC Biochem.* 2016; 17: 8.

Jones N.A., Hill A. J., Smith I., Bevan S. A., Williams C. M., Whalley B. J., Stephens G. J. (2010). Cannabidiol displays antiepileptiform and antiseizure properties in vitro and in vivo. *J. Pharmacol. Exp. Ther.* 2010, 332, 569–577.

Kalenderoglou N., Macpherson T., Wright K. L. (2017). Cannabidiol Reduces Leukemic Cell Size – But Is It Important? *Front Pharmacol.* 2017; 8: 144.

Kaneko Y., Szallasi A. (2014). Transient receptor potential (TRP) channels: a clinical perspective. *Br J Pharmacol.* 2014 May;171(10):2474-507.

Kastrati I., Siklos M. I., Calderon-Gierszal E. L., El-Shennawy L., Georgieva G., Thayer E. N., Thatcher G. R., Frasor J. (2016). Dimethyl Fumarate Inhibits the Nuclear Factor κB Pathway in Breast Cancer Cells by Covalent Modification of p65 Protein. *J Biol Chem.* 2016 Feb 12;291(7):3639-47.

Kastrati I., Delgado-Rivera L., Georgieva G., Thatcher G. R., Frasor J. (2017). Synthesis and Characterization of an Aspirin-fumarate Prodrug that Inhibits NFκB Activity and Breast Cancer Stem Cells. J Vis Exp. 2017 Jan 18;(119).

Kenny T. C., Manfredi G., Germain D. (2017). The Mitochondrial Unfolded Protein Response as a Non-Oncogene Addiction to Support Adaptation to Stress during Transformation in Cancer and Beyond. *Front Oncol.* 2017 Jul 26; 7:159.

Keoni C. L., Brown T. L. (2015). Inhibition of Apoptosis and Efficacy of Pan Caspase Inhibitor, Q-VD-OPh, in Models of Human Disease. *J Cell Death.* 2015 Apr 8; 8:1-7.

Keston A. S., Brandt R. (1965). The fluorometric analysis of ultramicro quantities of hydrogen peroxide. *Anal Biochem* 11, 6 (1965).

Khandelwal N., Simpson J., Taylor G., Rafique S., Whitehouse A., Hiscox J., Stark L. A. (2011). Nucleolar NF-*κ*B/RelA mediates apoptosis by causing cytoplasmic relocalization of nucleophosmin. *Cell Death Differ.* 2011 Dec; 18(12): 1889–1903.

Kim H-S., Quon M. J., and Kim J-a. (2014). New insights into the mechanisms of polyphenols beyond antioxidant properties; lessons from the green tea polyphenol, epigallocatechin 3-gallate. *Redox Biol.* 2014; 2: 187–195.

Kim J. H., Jung T. Y., Hwang E. C., Jung S. H., Jung S., Kim I. Y., Jang W. Y., Moon KS, Lee KH, Kim S.K. (2017). Disease progression patterns of bevacizumab responders with recurrent malignant gliomas. *Oncol Lett.* 2017 Sep; 14(3): 3529–3535.

Kıray H., Lindsay S. L., Hosseinzadeh S., Barnett S. C. (2016). The multifaceted role of astrocytes in regulating myelination. *Exp Neurol.* 2016 Sep;283(Pt B):541-549.

Kole A. J., Park H. S., Yeboa D. N., Rutter C. E., Corso C. D., Aneja S., Lester-Coll N. H., Mancini B. R., Knisely J. P., Yu J. B. (2017). Concurrent chemoradiotherapy versus radiotherapy alone for "biopsy-only" glioblastoma multiforme. *Cancer.* 2016 Aug 1;122(15):2364-70.

Lee S. Y. (2016). Temozolomide resistance in glioblastoma multiforme. *Genes & Diseases* (2016) 3, 198-210.

Li R., Jen N., Yu F., and Hsiai T. K. (2011). Assessing Mitochondrial Redox Status by Flow Cytometric Methods: Vascular Response to Fluid Shear Stress. *Curr Protoc Cytom.* 2011 Oct; CHAPTER: Unit9.37.

Li Y. M., Suki D., Hess K., Sawaya R. (2017). The influence of maximum safe resection of glioblastoma on survival in 1229 patients: Can we do better than gross-total resection? *J Neurosurg.* 2016 Apr;124(4):977-88.

Lichtman A. H., Lux E. A., McQuade R., Rossetti S., Sanchez R., Sun W., Wright S., Kornyeyeva E., Fallon M. T. (2018). Results of a Double-Blind, Randomized, Placebo-Controlled Study of Nabiximols Oromucosal Spray as Adjunctive Therapy in Advanced Cancer Patients with Chronic Uncontrolled Pain. *J Pain Symptom Manage.* 2018 Feb;55(2):179-188.e1.

Liebelt B. D., Shingu T., Zhou X., Ren J., Shin S. A., Hu J. (2016). Glioma Stem Cells: Signaling, Microenvironment, and Therapy. *Stem Cells Int.* 2016; 2016: 7849890.

Lindholm D., Korhonen L., Eriksson O., Kõks S. (2017). Recent Insights into the Role of Unfolded Protein Response in ER Stress in Health and Disease. *Front Cell Dev Biol.* 2017; 5: 48.

Lindon J. C., Keun H. C., Ebbels T. M., Pearce J. M., Holmes E., Nicholson J. K. (2005). The Consortium for Metabonomic Toxicology (COMET): aims, activities and achievements. *Pharmacogenomics.* 2005 Oct;6(7):691-9.

Lindvall O., Kokaia Z. (2009). Prospects of stem cell therapy for replacing dopamine neurons in Parkinson's disease. Trends Pharmacol Sci. 2009 May;30(5):260-7.

Linker R. A. and Haghikia A. (2016). Dimethyl fumarate in multiple sclerosis: latest developments, evidence and place in therapy. *Ther Adv Chronic Dis.* 2016 Jul; 7(4): 198–207.

Liu P. C., Lu G.,Deng Y., Wang D. C., Su X. W., Zhou J. Y., Chan T. M., Hu X.,Poon W. S. (2017). Inhibition of NF-κB Pathway and Modulation of MAPK Signaling Pathways in Glioblastoma and Implications for Lovastatin and Tumor Necrosis Factor-Related Apoptosis Inducing Ligand (TRAIL) Combination Therapy. *PLoS One.* 2017; 12(1): e0171157.

Llorens-Bobadilla E., Martin-Villalba, A. (2017). Adult NSC diversity and plasticity: the role of the niche. *Curr Opin Neurobiol.* 2017 Feb; 42:68-74.

Lodish H., Berk A., Zipursky S. L. (2000). Overview of Neuron Structure and Function. Section 21.1*Molecular Cell Biology 4th edition* (2000).

Louis D. N., Perry A., Reifenberger G., von Deimling A., Figarella-Branger D., Cavenee W. K., Ohgaki H., Wiestler O. D., Kleihues P., Ellison D. W. (2016). The 2016 World Health Organization Classification of Tumors of the Central Nervous System: a summary. *Acta Neuropathol.* 2016 Jun;131(6):803-20.

Ma K., Fox L., Shi G., Shen J., Liu Q., Pappas J. D., Cheng J., and Qu T. (2011). Generation of neural stem cell-like cells from bone marrow-derived human mesenchymal stem cells. *Neurol Res.* 2011 Dec; 33(10): 1083–1093.

Macchia G., Deodato F., Cilla S., Cammelli S., Guido A., Ferioli M., Siepe G., Valentini V., Morganti A. G., Ferrandina G. (2017). Volumetric modulated arc therapy for treatment of solid tumors: current insights. *Onco Targets Ther.* 2017; 10: 3755–3772.

Mak K. S., Agarwal A., Qureshi M. M., Truong M. T. (2017). Hypofractionated short-course radiotherapy in elderly patients with glioblastoma multiforme: an analysis of the National Cancer Database. *Cancer Med.* 2017 Jun;6(6):1192-1200.

Maltese W. A., Overmeyer J. H. (2014). Methuosis: nonapoptotic cell death associated with vacuolization of macropinosome and endosome compartments. *Am J Pathol.* 2014 Jun;184(6):1630-42.

Marcu J. P., Christian R. T., Lau D., Zielinski A. J., Horowitz M. P., Lee J., Pakdel A., Allison J., Limbad C., Moore D. H., Yount G. L., Desprez P. Y., McAllister S. D. (2011). Cannabidiol enhances the inhibitory effects of delta9-tetrahydrocannabinol on humanglioblastoma cell proliferation and survival. *Mol Cancer Ther.* 2010 Jan;9(1):180-9.

Martino G., Butti E., Bacigaluppi M. (2014). Neurogenesis or non-neurogenesis: that is the question. *J Clin Invest.* 2014 Mar 3; 124(3): 970–973.

Masilamani A. P., Ferrarese R., Kling E., Thudi N. K., Kim H., Scholtens D. M., Dai F., Hadler M., Unterkircher T., Platania L., Weyerbrock A., Prinz M., Gillespie G. Y., Harsh G. R. IV, Bredel M., Carro M. S. (2017). KLF6 depletion promotes NF-κB signaling in glioblastoma. *Oncogene.* 2017 Jun 22;36(25):3562-3575.

Massi P., Vaccani A., Ceruti S., Colombo A., Abbracchio M. P., Parolaro D. (2004). Antitumor effects of cannabidiol, a nonpsychoactive cannabinoid, on human glioma cell lines. *J Pharmacol Exp Ther.* 2004 Mar ;308(3):838-45.

Massi P., Solinas M., Cinquina V., Parolaro D. (2013). Cannabidiol as potential anticancer drug. *Br J Clin Pharmacol.* 2013 Feb;75(2):303-12.

McEntire D. M., Kirkpatrick D. R., Dueck N. P., Kerfeld M. J., Smith T. A., Nelson T. J., Reisbig M. D., Agrawal D. K. (2016). Pain Transduction: A Pharmacologic Perspective. *Expert Rev Clin Pharmacol.* 2016 Aug; 9(8): 1069–1080.

Meyer M., Reimand J., Lan X., Head R., Zhu X., Kushida M., Bayani J., Pressey J. C., Lionel A. C., Clarke I. D., Cusimano M., Squire J. A., Scherer S. W., Bernstein M., Woodin M. A., Bader G. D., Dirks P. B. (2015). Single cell-derived clonal analysis of human glioblastoma links functional and genomic heterogeneity. *Proc Natl Acad Sci U S A.* 2015 Jan 20;112(3):851-6.

Moloney J. N., Cotter T. G. (2017). ROS signalling in the biology of cancer. *Semin Cell Dev Biol.* 2017 Jun 3. pii: S1084-9521(16)30383-4.

Monticone M., Taherian R., Stigliani S., Carra E., Monteghirfo S., Longo L., Daga A., Dono M., Zupo S., Giaretti W., Castagnola P. (2014). NAC, tiron and trolox impair survival of cell cultures containing glioblastoma tumorigenic initiating cells by inhibition of cell cycle progression. *PLoS One.* 2014 Feb 28;9(2): e90085.

Morales P., Hurst D. P., Reggio P. H. (2017). Molecular Targets of the Phytocannabinoids: A Complex Picture. *Prog Chem Org Nat Prod.* 2017; 103:103-131.

Morales P., Reggio P. H., Jagerovic N. (2017). An Overview on Medicinal Chemistry of Synthetic and Natural Derivatives of Cannabidiol. *Front Pharmacol.* 2017 Jun 28; 8:422.

Morgan M. J., Liu Z. G. (2011). Crosstalk of reactive oxygen species and NF-κB signaling. *Cell Res.* 2011 Jan;21(1):103-15.

Moujalled D., Grubman A., Acevedo K., Yang S., Ke Y.D., Moujalled D. M., Duncan C., Caragounis A., Perera N. D., Turner B.J., Prudencio M., Petrucelli L., Blair I., Ittner L. M., Crouch P. J., Liddell J. R., WhiteA. R. (2017). TDP43 mutations causing amyotrophic lateral sclerosis are associated with altered expression of RNAbinding protein hnRNP K and affect the Nrf2 antioxidant pathway. *Hum Mol Genet*. 2017 May 1;26(9):1732-1746.

Mukhopadhyay P., Rajesh M., Yoshihiro K., Haskó G., and Pacher P. (2007). Simple quantitative detection of mitochondrial superoxide production in live cells. *Biochem Biophys Res Commun.* 2007 Jun 22; 358(1): 203–208.

Nabissi M., Morelli M. B., Santoni M., Santoni G. (2013). Triggering of the TRPV2 channel by cannabidiol sensitizes glioblastoma cells to cytotoxic chemotherapeutic agents. *Carcinogenesis.* 2013 Jan;34(1):48-57.

Nagel R., Semenova E. A., Berns A. (2016). Drugging the addict: non-oncogene addiction as a target for cancer therapy. *EMBO Rep.* 2016 Nov;17(11):1516-1531.

Nicolay J. P., Müller-Decker K., Schroeder A., Brechmann M., Möbs M., Géraud C., Assaf C., Goerdt S., Krammer P. H., Gülow K. (2016). Dimethyl fumarate restores apoptosis sensitivity and inhibits tumor growth and metastasis in CTCL by targeting NF-κB. *Blood.* 2016 Aug 11;128(6):805-15.

Nilius B., Mahieu F., Karashima Y., Voets T. (2007) Regulation of TRP channels: a voltage-lipid connection. *Biochem Soc Trans* 35:105–108.

Oka S., Kamata H., Kamata K., Yagisawa H., Hirata H. (2000). N-acetylcysteine suppresses TNF-induced NF-kappaB activation through inhibition of IkappaB kinases. *FEBS Lett.* 2000 Apr 28;472(2-3):196-202.

Oláh A., Tóth B. I., Borbíró I., Sugawara K., Szöllõs A. G.i, Czifra G., Pál B., Ambrus L., Kloepper J., Camera E., Ludovici M., Picardo M., Voets T., Zouboulis C. C., Paus R., Bíró T. (2014). *J Clin Invest.* 2014 Sep 2; 124(9): 3713–3724.

Olar A., Aldape K. D. (2014). Using the molecular classification of glioblastoma to inform personalized treatment. Cannabidiol exerts sebostatic and antiinflammatory effects on human sebocytes. *J Pathol.* 2014 Jan; 232(2): 165–177.

Olive K. P., Tuveson D. A., Ruhe Z. C., Yin B., Willis N. A., Bronson R. T., Crowley D., Jacks T. (2004). Mutant p53 gain of function in two mouse models of Li-Fraumeni syndrome. *Cell.* 2004 Dec 17;119(6):847-60.

Pecze L., Viskolcz B., Oláh Z. (2017). Molecular Surgery Concept from Bench to Bedside: A Focus on TRPV1+ Pain-Sensing Neurons. *Front Physiol.* 2017 Jun 2; 8:378.

Peñaranda Fajardo N. M., Meijer C., Kruyt F. A. (2016). The endoplasmic reticulum stress/unfolded protein response in gliomagenesis, tumor progression and as a therapeutic target in glioblastoma. *Biochem Pharmacol.* 2016 Oct 15; 118:1-8.

Pendergrass W., Wolf N., Poot M. (2004). Efficacy of MitoTracker Green and CMXrosamine to measure changes in mitochondrial membrane potentials in living cells and tissues. *Cytometry A.* 2004 Oct;61(2):162-9.

Perry L., Dickau R., Zarrillo S., Holst I., Pearsall D. M., Piperno D. R., Berman M. J., Cooke R. G., Rademaker K., Ranere A. J., Raymond J. S., Sandweiss D. H., Scaramelli F., Tarble K., Zeidler J. A. (2007) Starch fossils and the domestication and dispersal of chili peppers (Capsicum spp. L.) in the Americas. *Science* 315:986–988.

Pino A., Fumagalli G., Bifari F., Decimo I. (2017). New neurons in adult brain: distribution, molecular mechanisms and therapies. *Biochem Pharmacol.* 2017 Oct 1; 141:4-22.

Plaisier C. L., O'Brien S., Bernard B., Reynolds S., Simon Z., Toledo C. M., Ding Y., Reiss D. J., Paddison P. J., Baliga N. S. (2016). Causal Mechanistic Regulatory Network for Glioblastoma Deciphered Using Systems Genetics Network Analysis. *Cell Syst.* 2016 Aug;3(2):172-186.

Poligone B., Baldwin A. S. (2001). Positive and negative regulation of NF-kappaB by COX-2: roles of different prostaglandins. *J Biol Chem.* 2001 Oct 19;276(42):38658-64.

Purkait S., Mallick S., Sharma V., Kumar A., Pathak P., Jha P., Biswas A., Julka P. K., Gupta D., Suri A., Datt U. A., Suri V., Sharma M. C., Sarkar C. (2016). Prognostic Stratification of GBMs Using Combinatorial Assessment of IDH1 Mutation, MGMT promoter Methylation, and TERT Mutation Status: Experience from a Tertiary Care Center in India. *Transl Oncol.* 2016 Aug;9(4):371-6.

Prasad S., Gupta S. C., Tyagi A. K. (2017). Reactive oxygen species (ROS) and cancer: Role of antioxidative nutraceuticals. *Cancer Lett.* 2017 Feb 28; 387:95-105.

Qureshi M. A., Haynes C. M., Pellegrino M. W. (2017). The mitochondrial unfolded protein response: Signaling from the powerhouse. *J Biol Chem.* 2017 Aug 18;292(33):13500-13506.

Raza M. H., Siraj S., Arshad A., Waheed U., Aldakheel F., Alduraywish S., Arshad M. (2017). ROS-modulated therapeutic approaches in cancer treatment. *J Cancer Res Clin Oncol.* 2017 Jun 24.

Rimmerman N., Ben-Hail D., Porat Z., Juknat A., Kozela E., Daniels M. P., Connelly P. S., Leishman E., Bradshaw H. B., Shoshan-Barmatz V.& Vogel Z. (2013). Direct modulation of the outer mitochondrial membrane channel, voltage-dependent anion channel 1 (VDAC1) by cannabidiol: a novel mechanism for cannabinoid-induced cell death. *Cell Death and Disease* (2013) 4, e949.

Rinaldi M., Caffo M., Minutoli L., MariniL., Abbritti R. V., Squadrito F., Trichilo V., Valenti A., Barresi V., Altavilla D., Passalacqua M., and Caruso G. (2016). ROS and Brain Gliomas: An Overview of Potential and Innovative Therapeutic Strategies. *Int J Mol Sci.* 2016 Jun; 17(6): 984.

Ruggieri S., Tortorella C.,and Gasperini C. (2014). Pharmacology and clinical efficacy of dimethyl fumarate (BG-12) for treatment of relapsing–remitting multiple sclerosis. *Ther Clin Risk Manag.* 2014; 10: 229–239.

Ryan D., Drysdale A. J., Lafourcade C., Pertwee R. G., Platt B. (2009). Cannabidiol targets mitochondria to regulate intracellular Ca2+ levels. *J Neurosci.* 2009 Feb 18;29(7):2053-63.

Salazar-Ramiro A., Ramírez-Ortega D., Pérez de la Cruz V., Hérnandez-Pedro N. Y., González-Esquivel D. F., Sotelo J., Pineda B. (2016). Role of Redox Status in Development of Glioblastoma. *Front Immunol.* 2016 Apr 26; 7:156.

Scott K. A., Dennis J. L., Dalgleish A. G., Liu W. M. (2015). Inhibiting Heat Shock Proteins Can Potentiate the Cytotoxic Effect of Cannabidiol in Human Glioma Cells. *Anticancer Res.* 2015 Nov;35(11):5827-37.

Schagat T., Paguio A., Kopish K. (2007). Normalizing genetic reporter assays: approaches and considerations

for increasing consistency and statistical significance. *Cell notes* 9-12.

Scuderi C., Filippis D. D., Iuvone T., Blasio A., Steardo A., Esposito G. (2009). Cannabidiol in medicine: a review of its therapeutic potential in CNS disorders. *Phytother Res.* 2009 May;23(5):597-602.

Sevier C. S., Kaiser C. A. (2008). Ero1 and redox homeostasis in the endoplasmic reticulum. *Biochim Biophys Acta.* 2008 Apr;1783(4):549-56.

Shafer D. A., Chen Z-J., Harris T., Tombes M. B., Shrader E., Strickler K. Ryan A. A., Dent P., Malkin M. G. (2017). Phase I trial of dimethyl fumarate, temozolomide, and radiation therapy in glioblastoma multiforme. *J. Clin. Oncology* 2017 35:15_suppl, 2060-2060.

Shrivastava A., Kuzontkoski P. M., Groopman J. E., Prasad A. (2011). Cannabidiol induces programmed cell death in breast cancer cells by coordinating the cross-talk between apoptosis and autophagy. *Mol Cancer Ther.* 2011 Jul;10(7):1161-72.

Sin W. C., Aftab Q., Bechberger J. F., Leung J. H., Chen H., Naus C. C. (2016). Astrocytes promote glioma invasion via the gap junction protein connexin43. *Oncogene.* 2016 Mar 24;35(12):1504-16.

Singer E., Judkins J., Salomonis N., Matlaf L., Soteropoulos P., McAllister S., Soroceanu L. (2015). Reactive oxygen species-mediated therapeutic response and resistance in glioblastoma. *Cell Death Dis.* 2015 Jan 15;6: e1601.

Soldani C. & Scovassi A.I. (2002). Poly(ADP-ribose) polymerase-1 cleavage during apoptosis: An update. *Apoptosis* (2002) 7: 321.
Soubannier V. and Stifani S. (2017). NF-κB Signalling in Glioblastoma. *Biomedicines.* 2017 Jun; 5(2): 29.

Starowicz K., Nigam S., Di Marzo V. (2007). Biochemistry and pharmacology of endovanilloids. *Pharmacol Ther.* 2007 Apr 114(1):13-33.

Stock K., Kumar J., Synowitz M., Petrosino S., Imperatore R., Smith E. S., Wend P., Purfürst B., Nuber U. A., Gurok U., Matyash V., Wälzlein J. H., Chirasani S. R., Dittmar G., Cravatt B. F., Momma S., Lewin G. R., Ligresti A., De Petrocellis L., Cristino L., Di Marzo V., Kettenmann H., Glass R. (2012). *Nat Med.* 2012 Aug;18(8):1232-8.

Stupp R., Mason W. P., van den Bent M. J., Weller M., Fisher B., Taphoorn M. J., Belanger K., Brandes A. A., Marosi C., Bogdahn U., Curschmann J., Janzer R. C., Ludwin S. K., Gorlia T., Allgeier A., Lacombe D., Cairncross J. G., Eisenhauer E., Mirimanoff R. O.; European Organisation for Research and Treatment of Cancer Brain Tumor and Radiotherapy Groups; National Cancer Institute of Canada Clinical Trials Group. (2005). Radiotherapy plus concomitant and adjuvant temozolomide for glioblastoma. *N Engl J Med.* 2005 Mar 10;352(10):987-96.

Sun S., Hu F., Wu J., Zhang S. (2017). Cannabidiol attenuates OGD/R-induced damage by enhancing mitochondrial bioenergetics and modulating glucose metabolism via pentose-phosphate pathway in hippocampal neurons. *Redox Biol.* 2017 Apr; 11: 577–585.

Suzuki T., Yamamoto M. (2017), Stress-sensing mechanisms and the physiological roles of the Keap1-Nrf2 system during cellular stress. *J Biol Chem.* 2017 Oct 13;292(41):16817-16824.

Szallasi A. and Blumberg P. M. (1999). Vanilloid (Capsaicin) Receptors and Mechanisms. *Pharm Rev.* Jun 1999 51 (2) 159-212.

Szopa W., Thomas A. Burley T. A., Kramer-Marek G., Kaspera W. (2017). Diagnostic and Therapeutic Biomarkers in Glioblastoma: Current Status and Future Perspectives. *Biomed Res Int.* 2017; 2017: 8013575.

Talaverón R., Fernández P., Escamilla R., Pastor A. M., Matarredona E. R., and Sáez J. C. (2015). Neural progenitor cells isolated from the subventricular zone present hemichannel activity and form functional gap junctions with glial cells. *Front Cell Neurosci.* 2015 Oct 13; 9:411.

Tan Q., Yan X., Song L., Yi H., Li P., Sun G., Yu D., Li L., Zeng Z., Guo Z. (2017). Induction of Mitochondrial Dysfunction and Oxidative Damage by Antibiotic Drug Doxycycline Enhances the Responsiveness of Glioblastoma to Chemotherapy. *Med Sci Monit.* 2017 Aug 26; 23:4117-4125.

Taylor J. W., Schiff D. (2015). Treatment considerations for MGMT-unmethylated glioblastoma. *Curr Neurol Neurosci* Rep. 2015 Jan;15(1):507.

Torres S., Lorente M., Rodríguez-Fornés F., Hernández-Tiedra S., Salazar M., García-Taboada E., Barcia J., Guzmán M., Velasco G. (2011). A combined preclinical therapy of cannabinoids and temozolomide against glioma. *Mol Cancer Ther.* 2011 Jan;10(1):90-103.

Toyokuni S., Ito F., Yamashita K.,Yasumasa Okazaki Y., Akatsuka S. (2017). Iron and thiol redox signaling in cancer: An exquisite balance to escape ferroptosis. *Free Radical Biology and Medicine* 108 (2017) 610–626.

Treps L., Perret R., Edmond S., Ricard D., and Gavard J. (2017). Glioblastoma stem-like cells secrete the pro-angiogenic VEGF-A factor in extracellular vesicles. *J Extracell Vesicles.* 2017; 6(1): 1359479.

Tsatsanis C., Spandidos D. A. (2000). The role of oncogenic kinases in human cancer (Review). *Int J Mol Med.* 2000 Jun;5(6):583-90.

Turner S. E., Williams C. M., Iversen L., Whalley B. J. (2017). Molecular Pharmacology of Phytocannabinoids. *Prog Chem Org Nat Prod.* 2017; 103:61-10.

Tuveson D. A., Shaw A. T., Willis N. A., Silver D. P., Jackson E. L., Chang S., Mercer K. L., Grochow R., Hock H., Crowley D., Hingorani S. R., Zaks T., King C., Jacobetz M. A., Wang L., Bronson R. T., Orkin S. H., DePinho R. A., Jacks T. (2004). Endogenous oncogenic K-ras(G12D) stimulates proliferation and widespread neoplastic and developmental defects. *Cancer Cell.* 2004 Apr;5(4):375-87.

van Dam G. M., Themelis G., Crane L. M., Harlaar N. J., Pleijhuis R. G., Kelder W., Sarantopoulos A., de Jong J. S., Arts H. J., van der Zee A. G., Bart J., Low P. S., Ntziachristos V. (2011). Intraoperative tumor specific fluorescence imaging in ovarian cancer by folate receptor-α targeting: first in-human results. *Nat Med.* 2011 Sep 18;17(10):1315-9.

Villa G. R., Hulce J. J., Zanca C., Bi J., Ikegami S., Cahill G.L., Gu Y., Lum K.M., Masui K., Yang H., Rong X., Hong C., Turner K.M., Liu F., Hon G.C., Jenkins D., Martini M., Armando A.M., Quehenberger O., Cloughesy T.F., Furnari F.B., Cavenee W.K., Tontonoz P., Gahman T.C., Shiau A.K., Cravatt B.F., Mischel P.S. (2016). An LXR-Cholesterol Axis Creates a Metabolic Co-Dependency for Brain Cancers *Cancer Cell. 2016* Nov 14;30(5):683-693.

Vivanco I. (2014). Targeting molecular addictions in cancer. *British Journal of Cancer* (2014) 111, 2033–2038.

Wang J., Cazzato E., Ladewig E., Frattini V., Rosenbloom D. I., Zairis S., Abate F., Liu Z., Elliott O., Shin Y., Lee J. K., Lee I. H., Park W. Y., Eoli M., Blumberg A. J., Lasorella A., Nam D. H., Finocchiaro G., Iavarone A., Rabadan R. (2016). Clonal evolution of glioblastoma under therapy. *Nat Genet.* 2016 Jul;48(7):768-76.

Wang J., Liu P., Xin S., Wang Z., Li J. (2017). Nrf2 suppresses the function of dendritic cells to facilitate the immune escape of glioma cells. *Exp Cell Res.* 2017 Nov 15;360(2):66-73.

Wang Y., Xing D., Zhao M.,Wang J., Yang Y. (2016). The Role of a Single Angiogenesis Inhibitor in the Treatment of Recurrent Glioblastoma Multiforme: A Meta-Analysis and Systematic Review. *PLoS One.* 2016; 11(3): e0152170.

Wang Q., Chuikov S., Taitano S., Wu Q., Rastogi A., Tuck S. J., Corey J. M., Lundy S. K., and Mao-Draayer Y. (2015). Dimethyl Fumarate Protects Neural Stem/Progenitor Cells and Neurons from Oxidative Damage through Nrf2-ERK1/2 MAPK Pathway. *Int J Mol Sci.* 2015 Jun; 16(6): 13885–13907.

Wardyn J. D., Ponsford A. H., Sanderson C. M. (2015). Dissecting molecular cross-talk between Nrf2 and NF-κB response pathways. *Biochem Soc Trans.* 2015 Aug 1; 43(4): 621–626.

Widera D., Kaus A., Kaltschmidt C., Kaltschmidt B. (2008). Neural stem cells, inflammation and NF-κB: basic principle of maintenance and repair or origin of brain tumours? *J Cell Mol Med*. 2008 Apr; 12(2): 459–470.

Yamaguchi M., Tatsunori Seki T., Imayoshi I., Tamamaki N., Hayashi Y., Tatebayashi Y., Seiji Hitoshi S. (2016). Neural stem cells and neuro/gliogenesis in the central nervous system: understanding the structural and functional plasticity of the developing, mature, and diseased brain. *J Physiol Sci.* 2016; 66: 197–206.

Yee S. B., Baek S. J., Park H. T., Jeong S. H., Jeong J. H., Kim T. H., Kim J. M., Jeong B. K., Park B. S., Kwon T. K., Yoon I., Yoo Y. H. (2006). zVAD-fmk, unlike BocD-fmk, does not inhibit caspase-6 acting on 14-3-3/Bad pathway in apoptosis of p815 mastocytoma cells. *Exp Mol Med.* 2006 Dec 31;38(6):634-42.

Yoon S., Kovalenko A., Bogdanov K., Wallach D. (2017). MLKL, the Protein that Mediates Necroptosis, Also Regulates Endosomal Trafficking and Extracellular Vesicle Generation. *Immunity.* 2017 Jul 18;47(1):51-65. e7.

Yuan X., Curtin J, Xiong Y, Liu G, Waschsmann-Hogiu S, Farkas DL, Black KL, Yu JS. (2004). Isolation of cancer stem cells from adult glioblastoma multiforme. *Oncogene.* 2004 Dec 16;23(58):9392-400.

Zgair A., Wong J. C. M., Lee J. B., Mistry J., Sivak O., Wasan K. M., Hennig I. M., Barrett D. A., Constantinescu, C. S. Fischer P. M., Gershkovich P. (2016). Dietary fats and pharmaceutical lipid excipients increase systemic exposure to orally administered cannabis and cannabis-based medicines. *Am J Transl Res.* 2016; 8(8): 3448–3459.

Zhang J., Wang X., Vikash V., Ye Q., Wu D., Liu Y., Dong W. (2016). ROS and ROS-Mediated Cellular Signaling. *Oxid Med Cell Longev.* 2016; 2016: 4350965.

Zhang Q., Lenardo M. J., Baltimore D. (2017). 30 Years of NF-κB: A Blossoming of Relevance to Human Pathobiology. *Cell.* 2017 Jan 12;168(1-2):37-57.

Zhornitsky S. and Potvin S. (2012). Cannabidiol in Humans—The Quest for Therapeutic Targets. *Pharmaceuticals* 2012, 5, 529-552.

Zhou W. and Bao S. (2014). Reciprocal Supportive Interplay between Glioblastoma and Tumor-Associated Macrophages. *Cancers (Basel).* 2014 Jun; 6(2): 723–740.

Zhu J., Wang H., Fan Y., Lin Y., Zhang L., Ji X., Zhou M. (2014). Targeting the NF-E2-related factor 2 pathway: a novel strategy for glioblastoma (review). *Oncol Rep.* 2014 Aug;32(2):443-50.

Zygmunt P. M., Petersson J., Andersson D. A., Chuang H., Sorgard M., Di Marzo V., Julius D., Hogestatt E. D. (1999) Vanilloid receptors on sensory nerves mediate the vasodilator action of anandamide. *Nature* 400:452–457.

8. Acknowledgement

I would like to thank the whole team of neurosurgical research, especially Prof. Rainer Glass for supervision; Dr. Roland Kaelin for coordination of animal experiments; Yingxi Wu, Mengxhuo Hou and Linxhi Cai for *in vivo* GBM implantation; Sabrina Lakotta and Stefanie Lange for technical support around the laboratory. I am also thankful to all our collaborators:

- Prof. Gunter Schneider and Zonera Hassan at Klinikum Rechts der Isar for sharing with us pre-malignant mouse brains for our NFkB-p65 proneural glioma model and for the western blot and recombination PCRs.

- Prof. Reinhard Zeidler at the Helmholz Zentrum Munchen-Grosshadern for facilitating our access to the flow cytometry facility
- Dr. André Stiel and Dimitris Gorpas at the Helmholz Zentrum Munchen-Neuherberg and Klinikum Rechts der Isar for the detection of *ex vivo* ROS in the IOS and fluorescence spectroscopy.
- Dr. Franz Schilling and Dr. Geoff Topping for imaging of tumorigenesis by MRI at Klinikum Rechts der Isar
- Dr. Debora Paris and Dr. Dominique Melck for NMR analysis in Naples, Italy.

9. Appendix

9.1. Publications

Targeting APLN/APLNR improves anti-angiogenic efficiency and blunts pro-invasive side effects of VEGFA/VEGFR2-blockade in glioblastoma
Published in **Cancer Res. 2019 Feb 4. pii: canres.0881.2018**
Giorgia Mastrella, Mengzhuo Hou, Min Li, Veit M Stoecklein, Nina Zdouc, Marie N. M. Volmar, Hrvoje Miletic, Sören Reinhard, Christel C Herold Mende, Susanne Kleber, Katharina Eisenhut, Gaetano Gargiulo, Michael Synowitz, Angelo Luigi Vescovi, Patrick N Harter, Josef M Penninger, Ernst Wagner, Michel Mittelbronn, Rolf Bjerkvig, Dolores Hambardzumyan, Ulrich Schüller, Jörg Christian Tonn, Josefine Radke, Rainer Glass and Roland Eugen Kälin

Wittig derivatization of sesquiterpenoid polygodial leads to cytostatic agents with activity against drug resistant cancer cells and capable of pyrrolylation of primary amines
Published in European Journal of Medicinal Chemistry 103 (2015) 226 e 237
Ramesh Dasari, Annelise De Carvalho, Derek C. Medellin, Kelsey N. Middleton, Frederic Hague, Marie N. M. Volmar, Liliya V. Frolova, Mateus F. Rossato, Jorge J. De La Chapa, Nicholas F. Dybdal-Hargreaves, Akshita Pillai, Roland E. Kaelin, Veronique Mathieu, Snezna Rogel, Cara B. Gonzales, Jorge B. Calixto, Antonio Evidente, Mathieu Gautier, Gnanasekar Munirathinam, Rainer Glass, Patricia Burth, Stephen C. Pelly, Willem A.L. van Otterlo, Robert Kiss, Alexander Kornienko

Synthetic and biological studies of sesquiterpene polygodial: activity of 9-Epipolygodial against drug-resistant cancer Cells
Published in ChemMedChem 2015, 10, 2014 – 2026
Ramesh Dasari, Annelise De Carvalho, Derek C. Medellin, Kelsey N. Middleton, Frédéric Hague, Marie N. M. Volmar, Liliya V. Frolova, Mateus F. Rossato, Jorge J. De La Chapa, Nicholas F. Dybdal-Hargreaves, Akshita Pillai, Véronique Mathieu, Snezna Rogelj, Cara B. Gonzales, Jorge B. Calixto, Antonio Evidente, Mathieu Gautier, Gnanasekar Munirathinam, Rainer Glass, Patricia Burth, Stephen C. Pelly, Willem, A. L. van Otterlo, Robert Kiss, and Alexander Kornienko

9.2. Affidavit

LMU LUDWIG-MAXIMILIANS-UNIVERSITÄT MÜNCHEN | Dean's Office Medical Faculty | MMRS

Affidavit

Volmar, Marie Nhery Murielle

Surname, first name

Marchioninistr. 27

Street

81377 Munich

Zip code, town

Germany

Country

I hereby declare, that the submitted thesis entitled

Cannabidiol for glioblastoma therapy:
models, molecular pathways, and predictive markers

is my own work. I have only used the sources indicated and have not made unauthorised use of services of a third party. Where the work of others has been quoted or reproduced, the source is always given.

I further declare that the submitted thesis or parts thereof have not been presented as part of an examination degree to any other university.

New York, 10/04/2019

Place, date

Marie Nhery Murielle Volmar

Signature doctoral candidate

9.3. Confirmation of congruency

LMU LUDWIG-MAXIMILIANS-UNIVERSITÄT MÜNCHEN

Dean's Office
Medical Faculty

MMRS

Confirmation of congruency between printed and electronic version of the doctoral thesis

Volmar, Marie Nhery Murielle

Surname, first name

Marchioninistr. 27

Street

81377 Munich

Zip code, town

Germany

Country

I hereby declare that the electronic version of the submitted thesis, entitled

Cannabidiol for glioblastoma therapy:
models, molecular pathways, and predictive markers

is congruent with the printed version both in content and format.

New York, 10/04/2019

Place, date

Marie Nhery Murielle Volmar

Signature doctoral candidate